KU Leuven
Group Biomedical Sciences
Faculty of Medicine
Department of Development & Regeneration
Skeletal Biology and Engineering Research Center
Laboratory for Developmental and Stem Cell Biology

Functional analysis of SMOC2 using developmental models

Hendrik Mommaerts

Promotor: Dr. Przemko Tylzanowski
Co-promotor: Prof. Dr. Frank P. Luyten

Doctoral thesis in Biomedical Sciences
Leuven, October 2014

Table of contents

Abbreviations

ActR	Activin receptor
AER	Apical Ectodermal Ridge
AGM	Aorta-Gonad-Mesonephros
ALK	Activin-Like receptor Kinase
ALPM	Anterior Lateral Plate Mesoderm
AML	Acute Myeloid Leukemia
AP	Anterior-Posterior
APC	Adenomatous Polyposis Coli
as	anterior somites
AVE	Anterior Visceral Endoderm
BAMBI	BMP and Activin Membrane-Bound Inhibitor
BMP	Bone Morphogenetic Protein
BMPR	Bone Morphogenetic Protein Receptor
c-myb	Myb proto-oncogene protein
c/ebp	CCAAT/enhancer binding protein
caAlk	constitutively active Activin-Like receptor Kinase
CaMKII	Ca2+/calModulin-dependent protein Kinase II
CD1	Cluster of Differentiation 1
Cdc42	Cell Division Control protein 42
cDNA	Complementary DeoxyriboNucleic Acid
CE	Convergent extension
chd	Chordin
CHT	Caudal Hematopoietic Tissue
CK1	Casein Kinase 1
Col2	Collagen type II
CRISPR	Clustered Regularly Interspaced Short Palindromic Repeats
CRP	C-Reactive Protein
csf1ra	Colony Stimulating Factor 1 Receptor
CTRL	Control
ctsk	Cathepsin K
Cvl2	Crossveinless 2
d	Dorsal diencephalon
D. rerio	Danio Rerio
DAAM	Disheveled-associated activator of morphogenesis
DAB	3,3'-diaminobenzidine
Dag1	Dystroglycan
ddx18	DEAD-box 18
dHAND	Hand2, heart and neural crest derivatives expressed 2
Dkk	Dickkopf
dm	Dorsal midbrain
DMSO	DiMethyl SulfOxide
DNA	DeoxyriboNucleic Acid
dpc	Days Post Coitus
dpf	Days Post Fertilization
Dpp	Decapentaplegic
Dsh	Dishevelled
DV	Dorso-ventral
EC	Exctracellular Calcium binding domain
ECM	Extracellular Matrix
EGF	Epidermal Growth Factor
EGTA	Ethylene Glycol Tetraacetic Acid
EMP	Erythroid-Myeloid Progenitors
EN-1	Engrailed-1
ENU	N-ethyl-N-nitrosourea
env	viral envelop gene
ERK	extracellular-signal-regulated kinases
EST	Expressed Sequence Tags

ets1	V-Ets Erythroblastosis Virus E26 Oncogene Homolog 1
etsrp	V-Ets Erythroblastosis Virus E26 Oncogene Homolog 1b
Fgf	Fibroblast Growth Factor
fli1	Friend Leukemia Integration 1a
FRZB	Frizzled-related protein
FS	Follistatin-like domain
Fsrp	Follistatin-related protein
Fzd	Frizzled
G. gallus	Gallus Gallus
GAG	Glycosaminoglycan
gag	Viral Group-specific Antigen
gata	GATA binding protein
GDF	Growth Differentiation Factor
GFP	Green Fluorescent Protein
GOF	Gain of Function
GSK3β	Glycogen Synthase Kinase 3β
GTP	Guanosine triphosphate
H. sapiens	Homo Sapiens
H&E	Haematoxylin & Eosin
hbbe1.1	Hemoglobin Beta Embryonic
HH	Hamburger-Hamilton
HOX	Homeobox containing gene
hpf	Hours Post Fertilization
Hprt1	Hypoxanthine phosphoribosyltransferase 1
HSC	Hematopoietic stem cell
hspa	Heat Shock Protein
HSPG	Heparan Sulphate Proteoglycan
IBP	Insulin-like Growth Factor-binding Protein
ICM	Intermediate Cell Mass
Id	Inhibitor of Differentiation gene
IHC	Immunhistochemistry
ILK	Integrin-like kinase
IP3	Inositol 1,4,5-trisphosphate
irf8	Interferon Regulatory Factor 8
JNK	c-Jun N-terminal Kinases
kb	kilobase
kDa	kilodalton
KI67	Antigen KI-67
KOH	Potassium Hydroxide
LEF1/TCF	Lymphoid enhancer-binding factor 1/T-cell Factor
lh	Lateral hindbrain
lmo2	LIM domain only 2
LOF	Loss of Function
LRP	Low density lipoprotein Receptor-related Protein
M. musculus	Mus Musculus
MAPK	Mitogen-activated protein kinase
MBT	Mid-Blastula Transition
mg	Milligram
MHC	Myosin Heavy Chain
ml	Milliliter
mM	millimolar
MO	Morpholino
mpx	myeloid-specific peroxidase
MQ	MilliQ
MRF	Myogenic Regulatory Factor
mRNA	Messenger Ribonucleic Acid
Msx	Msh homeobox
Myf	Myogenic Factor gene
myoD	Myogenic Differentiation gene

n	Notochord
NDS	Normal Donkey Serum
NFAT	Nuclear factor of activated T-cells
NGS	Normal Goat Serum
NHEJ	Non-homologuous End Joining
nkx2.5	NK2 transcription factor related gene
nl	nanoliter
NPM1	Nucleophosmin
O/N	Overnight
OA	Osteoarthritis
ORF	Open Reading Frame
P-SMAD	Phosporylated MAD homolog
p300/CBp	E1A binding protein/ CREB-binding protein
Pax	Paired Box gene
PBI	Posterior Blood Islands
PBS	Phosphate Buffered Saline
PBST	PBS + Tween20
PCP	Planar Cell Polarity
PCR	Polymerase Chain Reaction
Pent	Pentagone
PFA	Paraformaldehyde
pg	picogram
PKC	Protein Kinase C
PLPM	Posterior Lateral Plate Mesoderm
pol	viral polymerase gene
ppt	pipetail
qPCR	Quantitative Polymerase Chain Reaction
RA	Retinoic Acid
RAC1	Ras-related C3 botulinum toxin substrate 1
rag2	Recombination activating gene 2
RBI	Rostral Blood Islands
RCASBP	Replication Competent ALV LTR with a Splice acceptor (Bryan high-titer Polymerase)
RhoA	Ras homolog gene family gene
Rock1	Rho-associated, coiled-coil-containing protein kinase 1
rRNA	Ribosomal Ribonucleic Acid
runx1	Runt-related transcription factor 1
SEM	Standard Error of Means
SFRP	secreted Frizzled-related protein
SHH	Sonic Hegdehog
SIP1	Smad Interacting Protein 1
six3b	Sine culis homeobox homolog 3b
slb	Silberblick
SMAD	MAD homolog
SMO	Spemann-Mangold Organizer
SMOC	SMOC domain
smoc1/2	Secreted Modular Calcium-binding Protein 1/2
Smurf	SMAD specific E3 ubiquitin protein ligase
snb	Somitabun
snh	Snailhouse
SP	Signal peptide
Sparc	Secreted Protein Acidic and Rich in Cysteine
spi1B	spleen focus forming virus proviral integration oncogene
SPOCK	Sparc/Osteonectin, Cwcv and Kazal-Like Domains Proteoglycan
ss	Somite Stage
Stat	signal transduction and activation of transcription
swr	swirl
t	Telencephalon
T-ALL	T-cell acute lymphoblastic leukemia

tal1	T-cell acute lymphocytic leukemia 1
TALEN	Transcription activator-like effector nucleases
TBX	T-box gene
TCA	Trichloroacetic acid
TGFβ	Transforming Growth Factor β
TIGM	Texas Institute for Genomic Medicine
TILLING	Targeting Induced Local Lesions in Genomes
TMEFF	Transmembrane protein with EGF-like and two follistatin-like domains
TREAT-OA	Translational Research in Europe Applied Technologies forOsteoarthritis
Tsg	Twisted Gastrulation
TY	Thyroglobulin domain
UA	Umbilical artery
UAS	Upstream activation sequence
UTR	Untranslated Region
VA	Vitelline artery
VDA	Ventral Dorsal Aorta
ved	Ventrally expressed dharma/bozozok antagonist
vent	Ventral expressed homeobox
vox	Ventral homeobox
vWC	von Willebrand factor type C
WIF	Wnt Inhibitory Factor
WISH	Wholemount In-Situ hybridization
Wnt	Wingless-type MMTV integration site family
X. laevis	Xenopus laevis
YSE	Yolk Sac Extension
ZFN	Zinc-finger nuclease
ZPA	Zone of Polarizing Activity
μm	Micrometer

In this manuscript standard nomenclature guidelines were used:

	Gene/mRNA	**Protein**
D. rerio	*smoc2*	Smoc2
H. sapiens / G. gallus	*SMOC2*	SMOC2
M. musculus	*Smoc2*	SMOC2

Chapter 1:

Introduction

1.1 Background and rationale

How many times do we use our joints throughout the day? How many joints do we use while walking, typing, or working out? How many times do we stretch our neck, flex our knee, elbow or fingers? You only notice the importance of your joints when you suffer from an injury induced by sport, trauma or ageing. Joints can get damaged in many ways and the most common joint condition leading to chronic disability is osteoarthritis (OA). During OA the articular cartilage is progressively lost in combination with a mild chronic non-specific joint inflammation, a thickening of the subchondral bone and the presence of osteophytes at the joint margins. This results in joint pain, swelling around the joint, inflammation, crepitus, and limited joint functionality with pain at the end of the range (Dal-Pra et al., 2006). While some therapies are available, they focus on either drastic steps like the entire joint replacement or a host of pain relief therapies offering a "supervised neglect" to the patient instead of a control of disease progression or cure.

Increasing evidence indicates that the onset and progression of a condition in the joint, like OA, is regulated by the same signaling pathways involved in the development of cartilage and bone (Lories, 2008). Investigation of these pathways with all its ligands, receptors, positive and negative regulators and the interaction between all of these is crucial to understand the homeostasis and the associated disabling conditions of the joint. Therefore, a highly purified protein extract from bovine articular cartilage was analyzed by direct protein sequencing and assessed for its chondrogenic activity in an *in-vivo* ectopic chrondrogenic assay. This screen resulted in the identification of several proteins including GDF5 (Chang et al., 1994) and FRZB1 (Hoang et al., 1996). Both proteins were already shown to be associated with joint development and joint disease (Lories and Luyten, 2005; Lories et al., 2007). The third protein was identified as the extracellular protein SMOC2 (Secreted Modular Calcium-binding Protein 2). Importantly, genetic analysis revealed a statistically significant association between *SMOC2* and hip OA in selected patient populations (TREAT-OA; unpublished data). For *SMOC2*, no function in the developing joint or the damaged joint has been described.

As embryonic pathways were shown to be reactivated during disease processes, the study of developmental pathways regulated by genes of interest is important for the understanding of the molecular basis of postnatal disease processes (Lappin et al., 2002; Lees et al., 2005; Roxburgh et al., 2006). The conservation of signaling events across species and organs permits us to study some mechanistic aspects of a disease using developmental models. The advantage of the developmental over the clinical models in unraveling the molecular basis of a disease lies in the speed (much faster), the cost (significantly lower), the ethical issues (no human subjects or postnatal animal models) and the possibility to carry out complex genetic experiments, to mention a few. Arthritic diseases and disorders, such as OA, could be at least partially associated by such a reactivation of the developmental program (Luyten et al., 2006; Lories, 2008). Therefore, we used developing zebrafish, chicken and mice embryos to model the network of a newly identified OA associated gene and its connection with the disease process.

1.2 SMOC2, an extracellular matrix protein

1.2.1 Extracellular matrix

One of the factors that allows for the transition from a single cell to a multicellular organism was the emergence of secreted structural proteins. They created an environment where many cells could stay for an extended period of time in physical proximity. This permitted for cell-cell communication, cellular differentiation and eventually the formation of complex multicellular organisms. The structural function of the ECM is at the level of cells (formation of a micro-environment), organs (shape and boundaries) or organisms (tissue elasticity, shock absorption). The composition of the extracellular matrix is complex, organism-, organ- and time-dependent and may include proteoglycans and fibrous proteins like collagens, fibronectin, elastins, laminins and many others (Frantz et al., 2010). Proteoglycans are secreted glycoproteins containing hydrophilic glycosaminoglycans (GAGs) that can absorb many water molecules, leading to the swelling of the proteins into a gel-like structure. They are essential for shock absorption (e.g. knee cartilage). The fibrous proteins are structural elements, which contribute to the elasticity of the tissue and regulate cell

migration by modulating cell interaction and adhesion. Additionally, the ECM participates in signaling processes by regulating the distribution of morphogens, the storage of ligands and interacting directly with secreted ligands and their receptors (Frantz et al., 2010).

1.2.2 Matricellular proteins

Only in the past two decades, the matrix surrounding the cells has been recognized as more than just a structural mesh holding cells together. Next to proteoglycans and fibrous proteins, the ECM harbors matricellular proteins that do not contribute to the structural aspect of the matrix. These proteins are defined as secreted proteins that regulate the interaction of the cells with the structural components, secreted growth factors, proteases, hormones, or cytokines among others (Bornstein and Sage, 2002). As the composition of the ECM is tissue dependent, the function of matricellular proteins differs depending on the type of tissue and the specific micro-environment.

A secreted protein must meet several conditions to qualify as matricellular protein, including: a) high expression levels during development and upon injury; b) binding to many cell surface receptors, ECM components, growth factors, cytokines or proteases; c) de-adhesive properties; d) no structural role; and e) a discrete phenotype when targeted for gene disruption in mouse models (Bornstein, 2009). The prototypical matricellular proteins are SPARC, tenascin-C and thrombospondin-1, but close family members and thrombospondin-2, osteopontin, CCN, and tenascin-X have been added to this family over the years (Bornstein, 2000; Bornstein and Sage, 2002; Bornstein, 2009).

1.2.3 SPARC

The SPARC family of matricellular proteins includes SPARC/BM-40/osteonectin, hevin, SMOC proteins SMOC1 and SMOC2, testican1, 2 and 3 (SPOCK) and Fstl-1 (Fig 1.1) (Bradshaw, 2012).

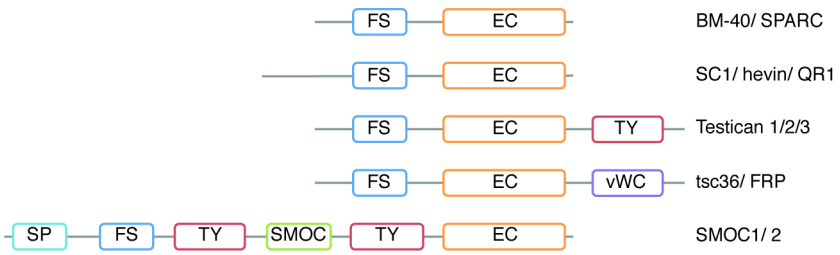

Figure 1.1: Domain organization of the SPARC family of matricellular proteins

The Follistatin-like domain (FS), the Extracellular Calcium binding domain (EC), the Thyroglobulin domain (TY), the domain with a high similarity to the von Willebrand factor type C (vWC), the Signal peptide (SP) and the Smoc domain (SMOC). All members of the family contain the FS and the EC domain. (Adapted from (Vannahme et al., 2003)

All members contain a common domain organization with an Extracellular calcium-binding domain (EC domain) and a Follistatin-like domain (FS domain). SPARC additionally contained an N-terminal acidic region, which was shown to interact with Ca^{2+} ions and hydroxiapatite.

SPARC is widely expressed during embryonic development in mice, but loss of SPARC only results in mild, non-lethal phenotypes such as early onset of cataract, increased adipogenesis, osteopenia and lax skin to mention a few (Delany et al., 2000; Bradshaw and Sage, 2001; Brekken and Sage, 2001; Bradshaw et al., 2002; Bradshaw, 2009). As these defects were suggestive of a defective extracellular matrix, it was shown that many of these defects could be attributed to the altered synthesis/assembly of major structural basal lamina components like fibrillar collagen. Next to the role in ECM assembly, SPARC was shown to regulate the activity of matrix metalloproteinases and to modulate different signaling pathways by interfering with the ligand-receptor interaction of the PDGF, VEGF, bFGF and TGFβ1 signaling (Tremble et al., 1993; Gilles et al., 1998; Brekken and Sage, 2001; Nischt et al., 2001; Wakefield and Roberts, 2002; McClung et al., 2007). Recently, Sparc was shown to be downstream of Fgf21 and to specifically mediate the development of erythroid progenitor cells during the primitive hematopoiesis in zebrafish embryos (Ceinos et al., 2013).

1.2.4 SMOC2

SMOC2, discovered independently in several laboratories including ours, was characterized as a secreted modular protein with high expression levels throughout development in many different tissues (Vannahme et al., 2003; Maier

et al., 2008). In mice, the onset of *Smoc2* expression was reported in the Reichert's membrane at E8.5. At E12.5 *Smoc2* transcripts could also be detected in the face prominences, limbs and somites and at E14.5 additional expression was detected in the heart, lungs and kidneys (Maier et al., 2008). In adult mice, SMOC2 was detected in the spleen, thymus, ovaries, cartilage, muscle, hippocampus and skin. Although some reports indicated a similar expression pattern of *Smoc1* and *Smoc2*, other studies reported on a more mutually exclusive expression pattern of *Smoc1* and *Smoc2* in the brain and gonads (Pazin and Albrecht, 2009; Okada et al., 2011; Rainger et al., 2011). Nevertheless, *Smoc1* expression was shown to be restricted to the basement membranes, whereas *Smoc2* was predominantly found in the non-basement membranes (Vannahme et al., 2002; Vannahme et al., 2003; Maier et al., 2008). Just like other members of the SPARC family, SMOC2 contains a FS and an EC domain. In addition, SMOC1 and SMOC2 proteins have an extra putative SMOC domain, flanked by two thyroglobulin domains (TY) that separate the FS and the EC domain (Fig 1.1).

The SMOC2 EC domain consists of 2 EF-hand motifs that are able to interact with Ca^{2+} ions changing the conformation of the protein as shown by circular dichroism spectroscopy (Vannahme et al., 2003). The FS domain is present in proteins like Follistatin, TMEFF1 and TMEFF2 among others and consists of a N-terminal EGF like domain and a C-terminal Kazal domain (Esch et al., 1987; Eib and Martens, 1996; Hohenester et al., 1997; Horie et al., 2000). In contrast to SPARC, the FS domain of SMOC2 only contains the C-terminal part (Vannahme et al., 2003). Kazal domains were described to inhibit the activity of multiple proteinases such as trypsin and elastase by directly interacting with the enzyme. Although similar to the Kazal proteinase inhibitors, no FS domains have been shown to inhibit proteinase activity. The TY domains are mainly present in SPARC family members (testicans and SMOC proteins), different cell surface antigens and insulin-like growth factor-binding protein (IBP) (Vannahme et al., 2003; Sala et al., 2005). The domain is assumed to be involved in the proteolytic degradation of the protein although other functions like modulating the interaction with binding partners, or influencing the conformation of the protein, have been suggested as well (Molina et al., 1996). Finally, the 60 amino acids long SMOC domain is a specific domain for the SMOC1 and SMOC2 proteins.

Computer modeling suggests that this peptide folds into a random coil separating the two TY domains. No similarity has been found between this putative domain and any other known protein or peptide.

In all SPARC family members, except for the SMOC subfamily, the FS domain is immediately followed by the EC domain (Vannahme et al., 2002; Vannahme et al., 2003). In SPARC an interaction was described between the FS and the EC domain that resulted in a stabilized Ca^{2+} affinity (Hohenester et al., 1997; Busch et al., 2000). In the SMOC proteins however, a TY-SMOC-TY module is inserted that separates the FS and EC domain by more than 220 amino acids. Furthermore, the FS-EC interaction was shown to involve the β5 sheet and its preceding loop of the FS domain and the proline-rich loop (helix E) connecting the two EF-hand motifs of the EC domain. In SMOC proteins, this β5 sheet of the FS domain and the helix E of the EC domain are preserved, whereas the loop preceding the β5 sheet is not (Vannahme et al., 2003). The effect of the insertion of the TY-SMOC-TY module and the loss of the β5 sheet-preceding loop on the interaction of the FS and EC domain is unknown.

Despite many studies performed on SMOC2, its molecular function and mechanism of action is not clear. It has been shown that, in endothelial cells, SMOC2 stimulates mitogenesis and potentiates angiogenic activity induced by growth factors like bFGF and VEGF (Rocnik et al., 2006). In addition, SMOC2 was shown to be upregulated in tubulating endothelial cells and therefore suggested to play a role in the angiogenic switch in tumors. In human keratinocytes, SMOC2 was shown to interact with Integrin α5β1 and α5β6 and to promote their migration (Maier et al., 2008). Furthermore, SMOC2 was shown to be downstream of BMP signaling in C2C12 myoblasts and downstream of Hedgehog signaling in mouse testis, mesonephros and kidney (Korchynskyi et al., 2003; Pazin and Albrecht, 2009). SMOC2 was also shown to be important for serum-induced entry into the S phase of the cell cycle and the growth factor induced DNA synthesis (Liu et al., 2008). This appears to be mediated via the induction of cyclin D1, which is dependent on integrin-linked kinase activity. Just as the EC domain of SPARC, the EC domain of SMOC2 mediates the conformation of the protein by binding to Ca^{2+} ions (Vannahme et al., 2003). Furthermore, SMOC2 was reported to interact with CRP and vitronectin (Novinec et al., 2008). Next,

SMOC2 also appeared to be associated with vitiligo, although this depended on the population investigated (Alkhateeb et al., 2010; Birlea et al., 2010; Alkhateeb et al., 2013). Finally, *SMOC2* was reported to be associated with craniofacial and dental defects that could be phenocopied in the zebrafish by using *smoc2* specific morpholinos (Bloch-Zupan et al., 2011; Melvin et al., 2013).

Recent studies have shown that the *SMOC2* candidate orthologue in D. melanogaster, *pentagone* (*pent*), regulates the life span and the fecundity of the fly and regulates the generation of a BMP signaling gradient (Li and Tower, 2009). Mechanistically, Pent interacts with Dally, a heparan sulphate proteoglycan and also a binding partner of Dpp, a BMP orthologue. By doing so, Pent was suggested to either promote the distribution of Dpp, or antagonize the co-receptor function of Dally or to regulate the interaction of Dpp and Dally (Vuilleumier et al., 2010; Vuilleumier et al., 2011).

1.3 Gastrulation

1.3.1 Introduction

After fertilization, cells undergo rapid mitotic divisions resulting in the formation of number of blastomers. Once the rate of cell division slows down, these blastomers undergo intense migration and change their relative position during the process of gastrulation (Greek gaster: stomach, gut). As a result, the embryo becomes organized into three germ layers (endoderm, ectoderm and mesoderm), from which all further structures and organs develop. The endoderm gives rise to epithelial tissues of the gut, the ectoderm to skin and neural tissue and mesoderm to muscles, connective tissues, organs and gonads. This process requires coordinated changes in cell shape, movements and adhesion. The subsequent directional migration of cells of the different germ layers results in the establishment of the primary body axes. Although gastrulation is a universal process and most of the cellular processes are common, the regulation of the process differs widely across species.

1.3.2 Zebrafish gastrulation

A fertilized oocyte undergoes discoidal meroblastic cleavages leading to the formation of a number of blastomeres on one side of the yolk (Fig 1.2A). Cleavage continues until around the tenth cell division (Kane and Kimmel, 1993; Langdon and Mullins, 2011), the mid-blastula transition (MBT), when zygotic transcription starts, cell cycle slows down and cell motility increases. At this stage the embryo forms a blastula and three different cell types can be distinguished: the cells located closest to and fused with the yolk (the yolk syncytial layer), the most superficial epithelial cells (the enveloping layer) and the blastomeres in between (the deep cells) (Fig 1.2B). At 5 hpf, gastrulation is initiated with the migration of the blastoderm towards the vegetal pole (epiboly). Radial intercalation by changes in cell shape, microtubule length and actin distribution was suggested to be the driving force resulting in a thinning blastoderm stretching over the yolk surface (Fig 1.2C). Around 6 hpf, when half of the yolk is covered with cells, the epiblast at the edges of the cellular front starts migrating inwards and upwards back towards the animal pole (involution). This results in a thickening along the ridge of the cellular layer, the germ ring, which consists of an epiblastic ectodermal layer and internal hypoblastic mesendodermal cells (Fig 1.2D) (Langdon and Mullins, 2011; Solnica-Krezel and Sepich, 2012).

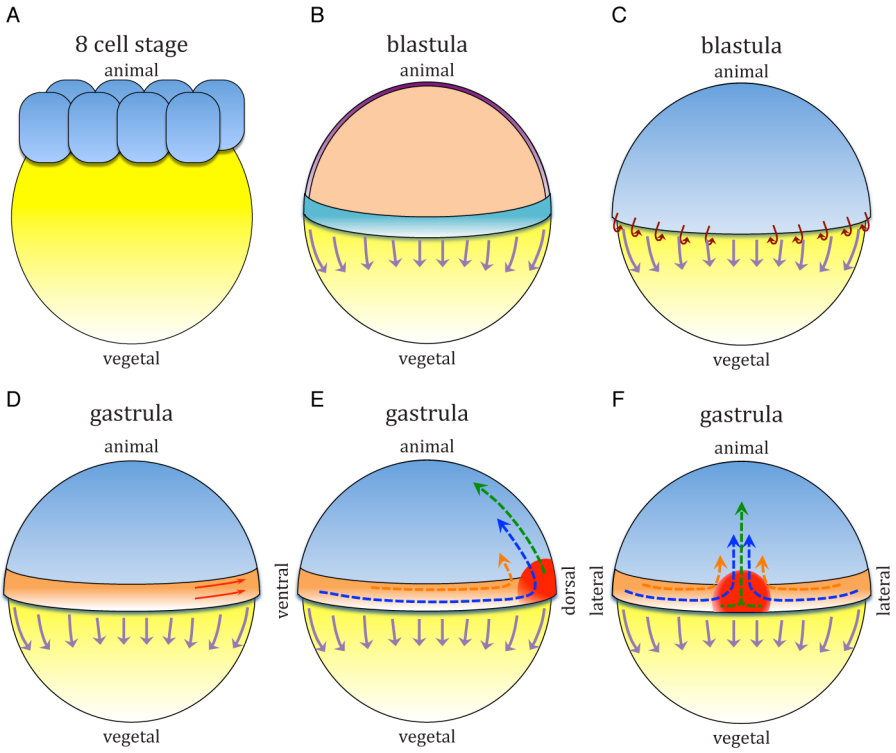

Figure 1.2: Cell migration during early zebrafish development

A-F. Schematic representation of different embryonic stages of zebrafish development: 8 cell stage (A), blastula stage (B-C: lateral view) and gastrula stage (D-E: lateral view and F: dorsal view). Initially, cells accumulate on top of the yolk (A). Later, these cells spread out over the surface of the yolk (epiboly: purple arrows) and become organized in three cell layers: the enveloping layer (purple), the deep cells (orange), and the yolk syncytial layer (turquiose) (B). When the cells have covered 50% of the yolk, involuting cells (red arrows in C) at the cellular front develop a ring of mesodermal tissue (germ ring: orange in D-F). At the dorsal side, mesodermal cells start accumulating (red arrows) to form the shield and hence the dorso-ventral axis (D). Subsequently, the mesodermal cells organize themselves in axial, adaxial and paraxial mesoderm by converging towards the dorsal side and extending towards the animal pole (convergence and extension). This also results in the formation of the anterior-posterior axis (E-F: orange, blue and green arrow). Based on (Gilbert, 2006; Slack, 2013).

At the same time, the epiblastic and hypoblastic cells start to develop a localized thickening on the future dorsal side of the embryo (convergence). This temporary structure is called the embryonic organizer or shield and is the hallmark of the establishment of the dorso-ventral axis (Fig 1.2E). From the shield and while epiboly continues, cells migrate towards the animal pole (extension) thereby establishing the anterior-posterior axis (Fig 1.2F). Cells located adjacent to the shield will also migrate towards the dorsal side and follow the extension along the newly formed anterior-posterior axis. During the convergence and extension process, the mesendodermal progenitors undergo

medio-lateral elongation and intercalation, and/or directed migration dependent on their dorso-ventral location. As a result, by the end of gastrulation all cells are repositioned to the proper location along the anterior-posterior and dorso-ventral axis. During the following developmental stages, the embryo will grow further, as tissues develop and organs mature. Although cells continue extensive migration and their fate is not fully determined, lineage-tracing experiments have shown what tissues can develop from each segment of this early gastrula embryo (Fig 1.3) (Gilbert, 2006; Slack, 2013).

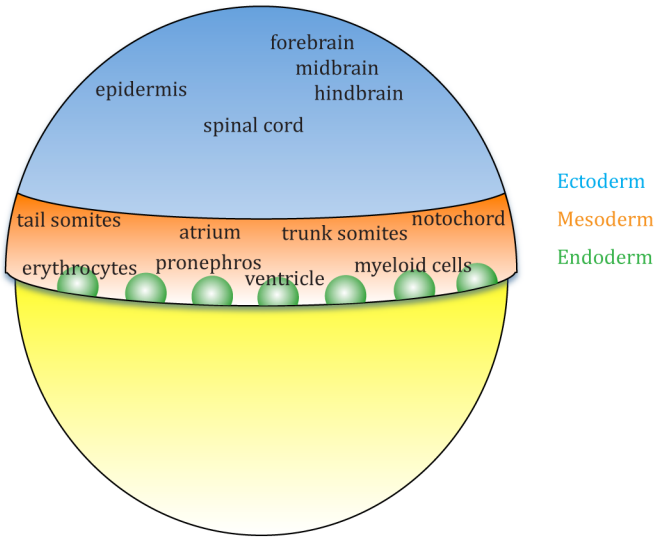

Figure 1.3: Fate map of the early zebrafish gastrula

Lateral view, dorsal to the right. Ectoderm, mesoderm and endoderm are indicated in blue, orange and green respectively. Not all organ fates are indicated. Adapted from (Gilbert, 2006; Kimelman, 2006).

When comparing the overall processes involved during vertebrate gastrulation across species, the same principle applies: cells organize themselves to form the blueprint of the future body plan. When comparing the early and late gastrula embryos of animal models like D. rerio, X. laevis, G. gallus and M. musculus, a great similarity in tissue organization is apparent, despite the difference in morphology (Fig 1.4). All these embryos develop three germ layers, three body axes, (pre-) specified cell populations, and an equivalent of the Spemann-Mangold Organizer (SMO). These structures and cell populations are the result of conserved changes at the cellular level where cells undergo changes in shape, direction, adhesion and migration properties. Although in general the cellular changes are similar in all of these organisms, the regulation and the timing is

species dependent. This results in the different morphology that can already be seen at these early stages of development (Fig 1.4).

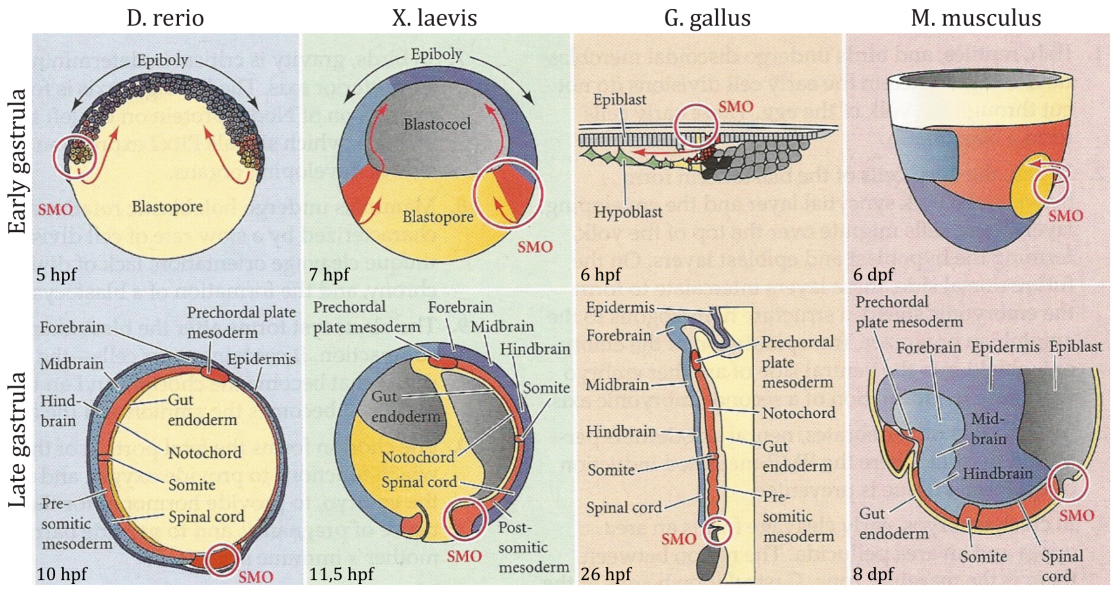

Figure 1.4: Comparison of gastrula stage embryos

As gastrulation starts, each of the embryos has a group of cells functioning as an equivalent of the Spemann-Mangold organizer (SMO). By the end of gastrulation, the three germ layers have formed and migrated relatively to each other resulting in an internal endodermal layer (yellow), an external ectodermal layer (blue) and the mesodermal layer in between (red). Adapted from (Gilbert, 2006)

The most obvious difference is the ex utero development of the zebrafish, frog and chicken embryos while mouse embryos develop in utero. Furthermore, the cleavage pattern of the embryos differs greatly. Zebrafish and chicken embryos undergo discoidal telolecithal meroblastic cleavage, while amphibians like X. laevis undergo displaced radial mesolecithal holoblastic cleavage and mammals, like M. musculus and H. sapiens undergo rotational isolecithal holoblastic cleavage. At later stages, chicken and mouse embryos develop a condensation of cells along the anterior-posterior axis that results in the development the primitive streak. The anterior most part of the primitive streak develops into the organizer or node (Hensen's node in chicken embryos and the node in mouse embryos). This organizing center later regresses posteriorly and secretes various transcription factors that pattern the embryo along the anterior-posterior axis. This is in contrast with the organizer in X. laevis and D. rerio, where the organizer is specified at the dorsal side and does not migrate. In X. laevis and D.

rerio embryos the cells migrate towards the organizer, while in G. gallus and M. musculus the organizer migrates while patterning the surrounding tissue. In addition, G. gallus and M. musculus embryos have secondary organizing centers, the hypoblast and the anterior visceral endoderm (AVE) respectively. The AVE, blocks the mesoderm inducing signals from the node, whereas the chicken hypoblast gives rise to extra-embryonic tissues (Gilbert, 2006; Slack, 2013).

The induction of the dorso-ventral axis and the different early structures in the gastrulating embryo requires a tight spatiotemporal control of the changes in cell shape, migration, adhesion and differentiation. The ECM is ideally suited to provide the environment that allows a homogenous mass of cells to develop different characteristics. Structural components like Fibronectin were shown to bind to one of its Integrin receptors, Integrin α5β1 and α5β3, resulting in the contraction of actin filaments thereby changing the shape of the cell (Danen et al., 2002; Mao and Schwarzbauer, 2005; Davidson et al., 2006). Furthermore, the differential development of tissues and cells is also a result from the tightly regulated balance of signaling pathways like BMP, WNT, Nodal and FGF to mention a few. It is their specific interaction that balances the expression of target genes required for the changes in cell shape, adhesion and motility, and their differentiation.

1.3.3 Regulation of gastrulation: BMP & WNT

1.3.3.1 BMP signaling

BMP signaling is initiated by the binding of BMP ligands (BMP2, 4, 7) to both type I and type II serine/threonine kinase receptors as a dimer (Fig 1.5). The type I receptors that can interact with BMP ligands are ActRIa (ALK2), BMPRIa (Alk3) and BMPRIb (ALK6) while the type II receptors include BMPRII (TβRII), ActRII and ActRIIb. When BMP ligand dimers interact with the type II receptors, the latter phosphorylates the type I receptor, thereby initiating the formation of a receptor complex. In the canonical BMP signaling pathway, the activated type I receptor will phosphorylate the receptor-SMAD proteins (SMAD1, 5, 8) that will interact with the co-SMAD (SMAD4) and as a complex translocate to the nucleus,

bind to the target sequences and influence the transcription of BMP target genes. In parallel, the non-canonical BMP signaling pathway, the BMP-MAPK pathway can also mediate BMP signals (Balemans and Van Hul, 2002; Ramel and Hill, 2012). Whether BMP ligands signal through the canonical or the non-canonical pathway depends on the composition of the receptors. In case of a preformed complex or type I and type II receptors, it was shown canonical BMP signaling was favored. In case of ligand binding induced receptor complex formation, signaling through the BMP-MAPK pathway was initiated. Other receptors of the TGFβ superfamily bind TGFβ, Activin and Nodal ligands and signaling by these ligands is mediated by the R-SMAD proteins SMAD2 and 3 and the co-SMAD protein SMAD4 (Gilboa et al., 2000; Nohe et al., 2002).

BMP signaling is modulated in the extracellular compartment by soluble BMP antagonists, like NOGGIN, CHORDIN, FOLLISTATIN among others, that bind the ligand and prevent ligand-receptor interaction. BAMBI, a dominant negative receptor prevents the formation of the receptor complex by sequestering the receptors. Intracellularly, inhibitory-SMAD proteins (SMAD6, 7) antagonize the activation of SMAD1, 5, 8. SMAD6 was also shown to compete with SMAD1, 5, 8 for SMAD4 (Balemans and Van Hul, 2002). Smurf-1 interacts with SMAD1 and 8 pushing them towards ubiquitination-mediated degradation. In the nucleus, negative cofactors like SIP1 and positive cofactors like p300/CBp affect target gene expression by changing the chromatin structure and affecting the binding of the SMAD complex to the DNA target sequence. Furthermore, BMP signaling is also affected by the crosstalk with other signaling pathways like TGFβ, Wnt and ERK-MAPK signaling adding to the complexity of the pathways and permitting a tight spatiotemporal regulation of target gene expression (Massague and Chen, 2000).

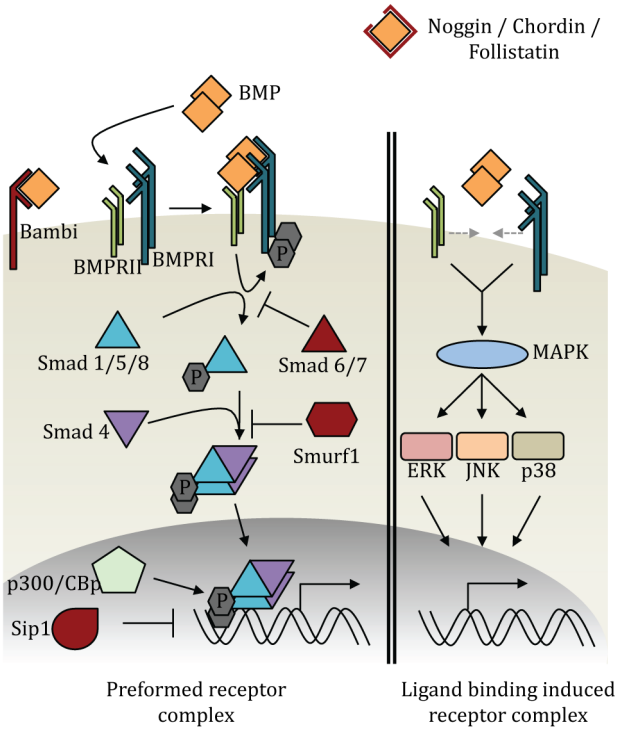

Figure 1.5: Schematic overview of SMAD dependent BMP signaling

Ligand binding to receptor dimers induces the phosphorylation of type 1 receptors and SMAD1/5/8 proteins, which interact with co-SMAD proteins and translocate to the nucleus to activate target gene transcription.

1.3.3.2 Function of Bmp signaling during zebrafish gastrulation

Bmp family members play an essential role in generating a dorso-ventral pattern as zebrafish mutants like *swirl (bmp2b), snailhouse (bmp7), somitabun (smad5), lost-a*-fin *(alk8), mini fin (alk2), chordino (chordin),* and *ogon (sizzled)* present defects in dorso-ventral development (Langdon and Mullins, 2011).

Prior to gastrulation Bmp mRNA is expressed uniformly throughout the embryo. Yet, the early dorsal specific expression of Bozozok inhibits the expression of Bmp ligands from initial stages onwards. Subsequently, the development of the shield and the secretion of inhibitory dorsal factors (Chordin, Noggin1, Follistatin-like2) from this organizing center, results in blocking Bmp ligand-receptor interactions. Further fine-tuning of the Bmp signal is controlled by additional regulators like Tolloid, Sizzled, Twisted gastrulation and Crossveinless-2, as all these factors affect the maturation and function of Chordin (Schier and Talbot, 2005; Langdon and Mullins, 2011).

These opposing actions of the ventral Bmps and the dorsal Bmp antagonists create a gradient of Bmp signaling from the ventral to the dorsal side, allowing

differential differentiation and cell fate specification along this axis. In addition, it was shown that this Bmp gradient also regulates cell movements as it establishes a reverse gradient of Cadherin-mediated cell adhesion (Von der Hardt 2007). Bmp mutant zebrafish, like *snailhouse, swirl*, and *somitabun* do not only present dorso-ventral patterning defects but also the migration of the ventrolateral cells is compromised (Mullins et al., 1996; Schmid et al., 2000; Mintzer et al., 2001; Little and Mullins, 2004). As expression of non-canonical Wnt ligands was shown to be altered when levels of Bmp signaling are manipulated, it was suggested that Bmp signaling modulates the cell movements by regulating the expression of non-canonical Wnt ligands like Wnt5b and Wnt11 (Myers et al., 2002).

Wnt signaling also regulates the gradient of Bmp signaling. During early stages of embryonic development, canonical Wnt signaling plays a dual role dependent on the stage of the embryo. Initially, β-catenin induces the dorsal organizer specific expression of *bozozok*, thereby negatively regulating Bmp signaling at this location. During later stages Wnt8 was shown to induce ventral genes like *vox/vent/ved*, thereby promoting Bmp signaling and thus ventral fates. Furthermore, Fgf signaling also affects dorso-ventral patterning of the early gastrula embryo by repressing the expression of Bmp ligands Bmp2b and Bmp7 in the dorsal cells, independent of Chordin (Fig 1.6) (Schier and Talbot, 2005; Langdon and Mullins, 2011).

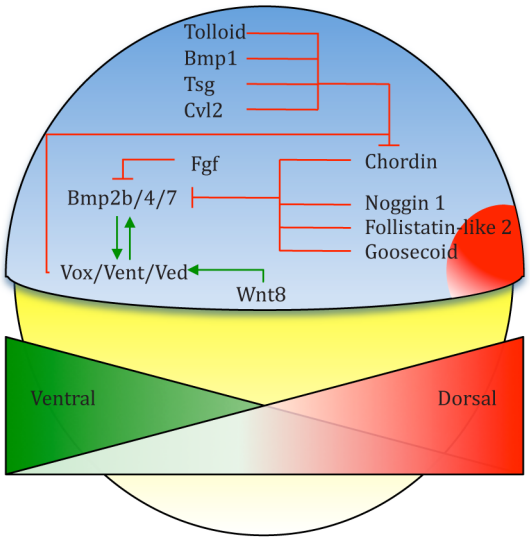

Figure 1.6: Bmp mediates the patterning of the zebrafish early gastrula

A gradient of Bmp signaling is maintained by the balance of Bmp ligands on the ventral side and Bmp antagonists produced at the dorsal side of the embryo. At this stage Bmp mediated signaling is induced by Wnt8 and its own target genes vox/vent/ved and repressed by Chordin, Noggin1, Follistatin-like 2, Goosecoid and FGF. Chordin is further regulated by Tolloid, Bmp1, Tsg, Cvl2 and the Bmp target genes *vox/vent/ved*. Adapted from (Langdon and Mullins, 2011).

1.3.3.3 Wnt signaling

There are several pathways transducing Wnt signaling (Rao and Kuhl, 2010). The canonical Wnt signaling pathway is dependent on β–catenin (Fig 1.7). In the OFF state, β–catenin is captured and phosphorylated by a destruction complex composed of APC, CK1, Axin and GSK3β. This results in the ubiquitination of β–catenin and the subsequent degradation by the proteasome. Upon Wnt binding to the FRIZZLED receptor and the coreceptor LRP6/5, DISHEVELLED (dsh) is recruited to the ligand receptor complex, which results in the phosphorylation of dsh. Subsequently, CK1 is recruited leading to the phosphorylation of the LRP5/6 coreceptor by CK1 and GSK3β. This then serves as a docking site for the binding of Axin, resulting in the release of β–catenin into the cytoplasm leading to the cytoplasmic accumulation and the eventual translocation to the nucleus. There, β–catenin displaces the repressor groucho from the LEF1/TCF regulatory complex and regulates the activation of canonical Wnt target genes (Clevers, 2006). The non-canonical Wnt pathways is β–catenin independent and the two most studied pathways are the planar cell polarity pathway (PCP) and the Ca^{2+} pathway (Fig 1.7). The PCP pathway affects cell migration and contraction by regulating cell polarity and cytoskeletal organization. Upon ligand binging, DISHEVELLED can either activate ROCK1, in a RHOA/DAAM dependent manner or JNK in a RAC1 dependent manner. The Ca^{2+} pathway is activated by Wnt ligand-receptor interaction inducing the release of Ca^{2+} ions from the endoplasmatic reticulum through the induction of IP3 via a trimeric G-protein. The Ca^{2+} ions will then activate Ca^{2+} sensitive enzymes like PKC, CaMKII and NFAT (Logan and Nusse, 2004; Gao and Chen, 2010; Sugimura and Li, 2010; De, 2011).

Wnt signaling involves 19 different ligands identified so far binding to several different receptors making it one of the most complex signaling cascades. In

addition, Wnt signaling is modulated by the extracellular inhibitors (SFRP1-5, WIF and Cerberus) that can bind directly to the Wnt ligands and prevent them to bind to the receptors. Another class of factors that modulate Wnt signaling interfere with the LRP5/6 coreceptor, like DICKOPF, WISE and SCLEROSTIN and are therefore specific for the canonical pathway (Kawano and Kypta, 2003).

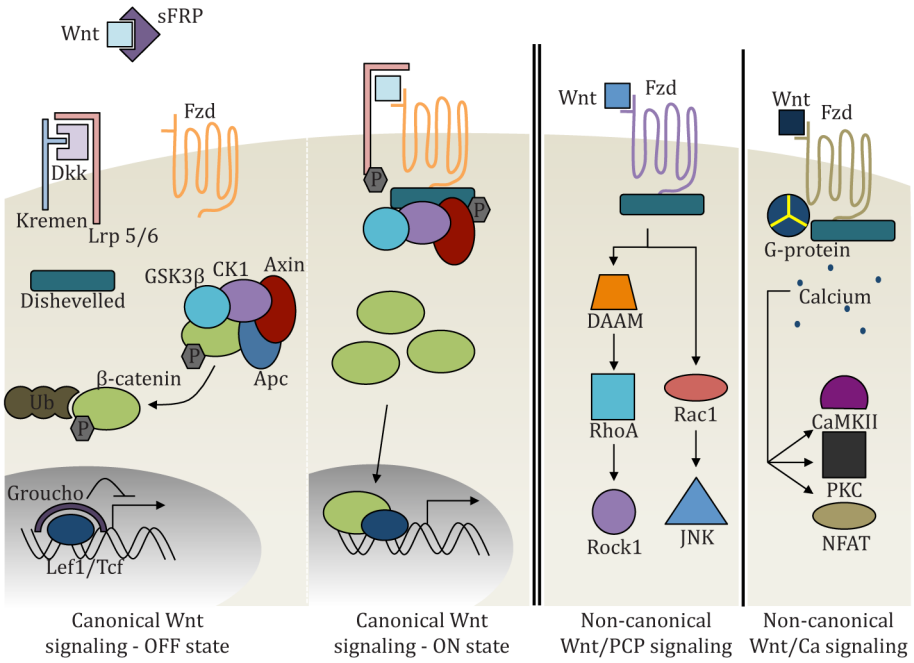

Figure 1.7: Schematic overview of canonical and non-canonical Wnt signaling

In the OFF-state, the canonical Wnt signaling represses target gene activation by the degradation of β–catenin mediated by the destruction complex. Upon ligand binding, this destruction complex dissociates due to the recruitment of these factors to the receptor complex and allows β–catenin to accumulate in the cytoplasm and translocate to the nucleus where it activates target gene transcription. In the non-canonical Wnt/PCP signaling, Dsh activates Rock1 and JNK mediated signaling resulting in cytoskeletal rearrangements. Non-canonical Wnt/Ca^{2+} signaling is dependent on the release of Ca^{2+} to activate CaMKII, PKC or NFAT.

1.3.3.4 Function of Wnt during zebrafish gastrulation

The specification of the dorsal axis preludes the initiation of extensive cell migration and changes in cell shape and adhesion properties. Just like the specification of the dorso-ventral axis, all cellular movements, from epiboly, to involution, intercalation, extension and conversion are tightly regulated in space and time by a number of signaling pathways. In zebrafish, the non-canonical Wnt signaling was shown to be the main signaling pathway involved as this pathway

regulates cytoskeletal organization by modulating actin and microtubules, and cellular adhesion by regulating Cadherin localization and turnover.

The involvement of non-canonical Wnt/PCP signaling during gastrulation is illustrated by the zebrafish mutants *ppt (wnt5b)*, *slb (wnt11)*, *knypek (glypican 4)* and *trilobite (strabismus)* which present cell movements defects. Furthermore, the Wnt/Ca^{2+} pathway also regulates gastrulation as the release of Ca^{2+} ions appeared to activate enzymes like PKC and CamKII that control cell adhesion and movement. In addition, Disheveled, Fz7, and Flamingo, the small GTPases Rho, Rac and Cdc42, and Jun-N-terminal kinase (JNK) are other core component of the non-canonical Wnt pathways that affect gastrulation by regulating polarized cell movements, and the actin and myosin cytoskeleton. Interestingly, in the absence of non-canonical Wnt signaling convergence and extension movements are impaired, but they are not absent, indicating other regulatory mechanisms contribute to this process. This is illustrated by the conversion and extension defects when the levels of the Wnt signaling independent factors Stat3, Slit2, Sprouty and Protocadherin 8 among others are altered (Heisenberg and Tada, 2002; Rohde and Heisenberg, 2007).

1.4 Hematopoiesis

1.4.1 Introduction

Hematopoiesis (from αἷμα: blood and ποιεῖν: to make) refers the process of the generation of blood cells. Hematopoietic development starts right after gastrulation and continues throughout adult life to produce and replenish blood cells. In vertebrates, the different progenitors are induced in multiple hematopoietic waves in anatomically distinct domains. During the initial or primitive hematopoietic wave the hemangioblasts generate the first erythrocytes and macrophages to provide the rapidly developing embryo with oxygen and the first line of defense against pathogens. This hemangioblast was defined as a common precursor for both endothelial and hematopoietic cells that retain the ability to give rise to new primitive erythroblasts (Jagannathan-Bogdan and Zon, 2013). Over the years, some controversy has arisen over the term hemangioblast as a bipotential precursor. It appears that these precursor cells represent a state

of competence rather than a precursor state. *In vitro* these cells are capable of differentiating into endothelial cells, whereas *in vivo* evidence of endothelial differentiation is absent (Amaya, 2013). Hemangioblasts are not hematopoietic stem cells, as the latter can give rise to all blood cells (erythrocytes, megakaryocytes, myeloid cells and lymphocytes) during the definitive wave of hematopoiesis. The development of the hematopoietic system has been of great interest as the study of this system can help researchers understand blood disorders and cancers. In particular, research for the regulation and the behavior of hematopoietic stem cells within their niche gained more interest over the years, especially since hematopoieisis is an evolutionary conserved process allowing the use of different animal models. When comparing hematopoietic processes in different animal models, species dependent differences in location and timing can be seen (Fig 1.8).

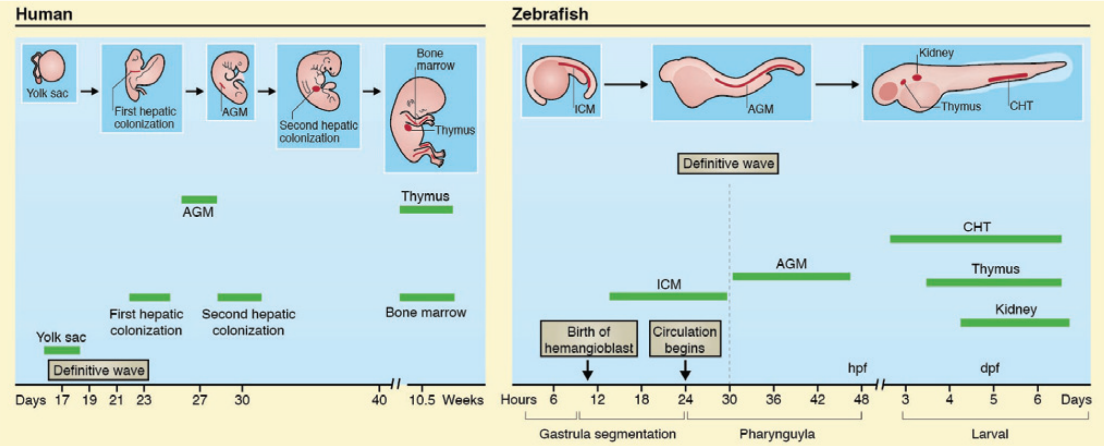

Figure 1.8: Comparison of locations of hematopoiesis in M. musculus, H. sapiens and D. rerio

In mouse and humans, embryonic hematopoiesis takes place in the yolk sac. From there and together with precursors derived from AGM, umbilical artery (UA), vitelline artery (VA) and placenta for mouse, these precursors migrate into the fetal liver. Hematopoiesis then proceeds by colonizing thymus, and bone marrow, the two main hematopoietic niches. In zebrafish, similar migratory processes take place with precursors deriving from an initial wave and a definitive wave that later migrate to the thymus, the kidney marrow (analogous to the bone marrow in mammals) and the caudal hematopoietic tissue (CHT). Timing of the different event differs greatly across species: conclusion of hematopoiesis in the thymus or bone marrow (or kidney marrow in zebrafish) starts around 4 dpf in zebrafish, 15 dpf in mice and 70 days in humans. Adapted from (Cumano and Godin, 2007; Jagannathan-Bogdan and Zon, 2013).

Yet, the genetic regulation and the molecular program of the different blood cell lineages is highly identical, which allows us to use the best suited animal model to investigate a particular aspect of blood cell development.

1.4.2 Zebrafish hematopoiesis

Similar to other vertebrates, zebrafish hematopoiesis occurs in multiple successive waves in anatomically distinct sites (Davidson and Zon, 2004; Ellett and Lieschke, 2010; Jagannathan-Bogdan and Zon, 2013). The primitive hematopoietic wave (10hpf - 1dpf) initiates in both the anterior and the posterior lateral plate mesoderm (ALPM and PLPM) (Fig 1.9A). Anteriorly, the mesoderm differentiates into the rostral blood islands (RBI, most rostral ALPM) and cardiac progenitors (most caudal ALPM). Posteriorly, the bilaterally organized mesoderm fuses at the midline and develops into the intermediate cell mass (ICM). Both the RBI and the ICM harbor bipotent hemangioblasts. In the RBI, these hemangioblasts will give rise to precursors of myeloid cells and endothelial cells, while the ICM will produce erythrocytes and endothelial cells (Fig 1.9B). During the next wave, or intermediate hematopoiesis (>30hpf), erythroid-myeloid progenitors (EMP) are formed in the posterior blood islands (PBI), the most caudal part of the ICM (Fig 1.9B). These EMPs can differentiate into both erythroid and myeloid cells. At the same time, the anterior myeloid precursors differentiate into macrophages or neutrophils. At 30 hpf, multipotent hematopoietic stem cells appear in the ventral dorsal aorta. Eventually, these HSCs will migrate out of the VDA and populate the kidney, the thymus and the caudal hematopoietic tissue (CHT) (Fig 1.9B-C). Around 4-5 dpf and after further migration into the kidney and the thymus, their final location, they are able to give rise to all hematopoetic lineages during the further development of the zebrafish.

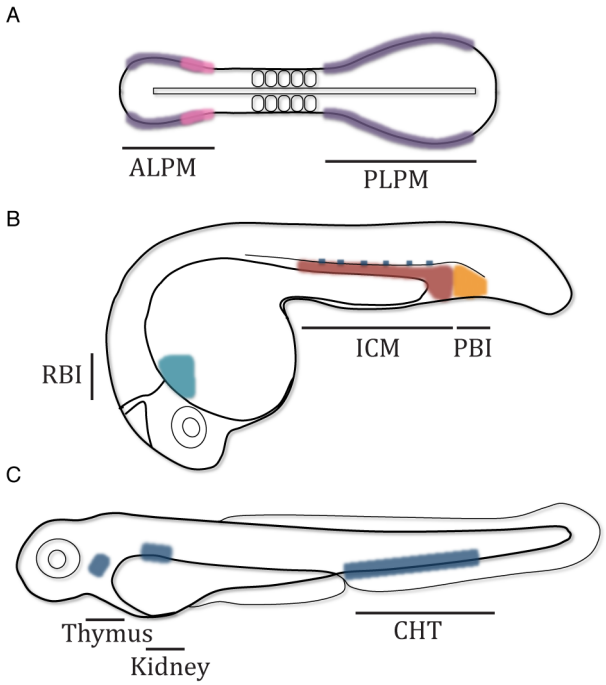

Figure 1.9: Mapping the different sites of hematopoeisis at different stages of zebrafish development
A-C: Anterior to the left A: dorsal view B-C: lateral view dorsal to the top. A. A 5ss embryo with hematopoietic precursors located in the anterior lateral plate mesoderm (ALPM) and the posterior lateral plate mesoderm (PLPM) (purple). Cardiac progenitors are located posteriorly of the hematopoietic precursors in the ALPM (pink). B. 24-30 hpf embryo with myeloid precursors (green) in the rostral blood islands (RBI), erythroid precursors (red) in the inner cell mass of the PLPM, and erythro-myeloid precursors (orange) in the posterior blood islands (PBI). Along the ventral wall of the dorsal aorta, hematopoietic stem cells are formed that migrate later into the thymus, kidney and CHT (blue zones in C). Adapted from (Monteiro et al., 2011)).

1.4.3 Transcriptional regulation of embryonic hematopoiesis in zebrafish

The location and time specific generation of cells of the different hematopoietic lineages requires tight control by regulatory factors (Fig 1.10).

In the ALPM, mesoderm specific transcription factors like *gata4-6* are expressed during initial stages of somitogenesis. It was shown that the loss of these factors resulted in a reduction or even a loss of myeloid cells in the ALPM at 24 hpf and cardiac migration defects at 22-24 hpf. These Gata transcription factors were shown to be essential for the specification of the anterior hemangioblast as the markers *scl, lmo2, gata2, fli1,* and *etsrp* were absent or reduced in *gata5-6* double morphants (Peterkin et al., 2009).

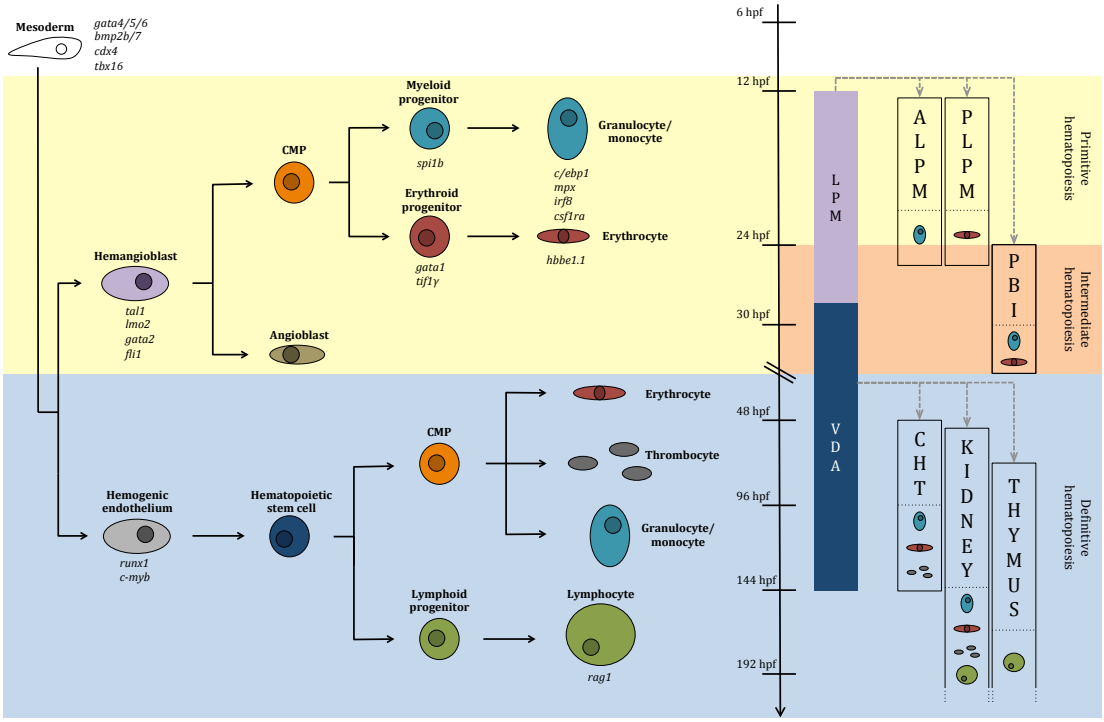

Figure 1.10: Ontogeny of hematopoiesis in zebrafish

Zebrafish hematopoiesis occurs in different consecutive waves. The primitive wave initiates in the anterior and posterior lateral plate mesoderm (ALPM and PLPM) generating erythrocytes and macrophages to provide the rapidly developing embryo with oxygen and a first line of defense (yellow). Around 24 hpf an intermediate wave in the posterior blood islands generates erythrocytes and myeloid cells (orange). During primitive and intermediate hematopoiesis, cells are derived from the hemangioblast. This bipotent precursor can give rise to both angioblasts and common myeloid precursors. The latter can develop into myeloid and erythroid precursors. From 26 hpf, the definitive wave starts with the development of hematopoietic stem cells from the hemaogenic endothelium of the ventral dorsal aorta (VDA). These stem cells subsequently colonize the caudal hematopoietic tissue, the kidney marrow and the thymus to generate all blood cell lineages (blue). Adapted from (Jing and Zon, 2011).

Loss of any of the hemangioblast marker genes resulted in defects in hematopoiesis and/or vasculogenesis. Dependent on the anatomical site, the hemangioblasts further differentiate along the hematopoietic lineage into either erythroid (*gata1*) or myeloid (*spi1b*) cells or along the vascular lineage into endothelial cells (*fli1*). The differentiation along the erythroid or the myeloid lineage is determined by the stage and population dependent cross-antagonism of *spi1b* and *gata1* (Fig 1.11) (Monteiro et al., 2011).

In the ICM and the PBI, the erythroid-myeloid fate decision is further determined by *tif1γ* (Monteiro et al., 2011; Xu and Orkin, 2011). During later stages of

myeloid development, further differentiation of the myeloid lineage is regulated by the level of *spi1b* expression that was shown to be regulated by its own transcriptional target, *runx1*, thereby establishing a negative feedback loop. Low levels of *spi1b* were shown to induce neutrophils, whereas high levels induced macrophages (Fig 1.11) (Jin et al., 2012).

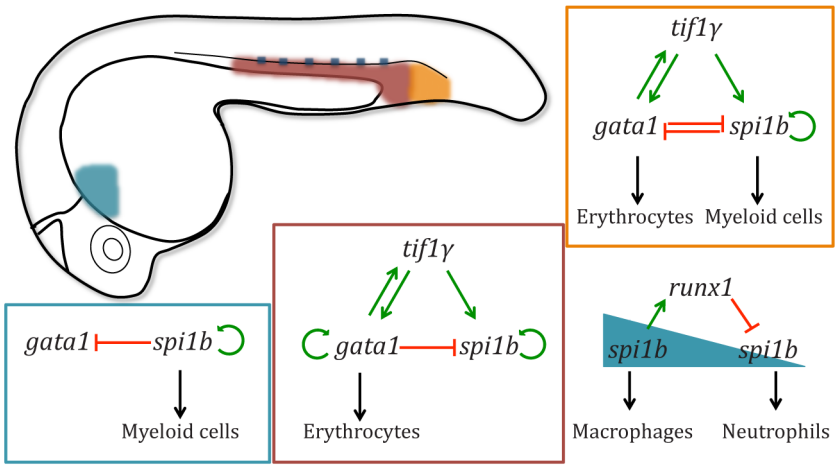

Figure 1.11: Differential regulation of erythroid versus myeloid cell fate during primitive and intermediate hematopoiesis

Genetic interactions between *gata1*, *spi1b* and *tif1γ* determine the fate of the precursors. In the RBI (green) spi1b blocks the expression of gata1, thereby promoting myeloid fates. In the PLPM derivered cell populations, *tif1γ* enters the play by regulating *gata1* and *spi1b* positively. In the ICM (red), *gata1* blocks the expression of *spi1b*, thereby promoting erythroid cell fate. In the PBI (orange) however, *spi1b* and *gata1* block each other's expression resulting in the generation of both erthrocytes and myeloid cells. Further specification of the myeloid lineage is determined by the level of *spi1b*, and its transcriptional target *runx1.* High levels promote macrophage fates whereas lower levels induce neutrophils. Adapted from (Monteiro et al., 2011; Xu et al., 2012).

1.4.4 Zebrafish as a model for hematopoietic conditions

The regulatory cascade directing hematopoiesis in humans is highly conserved in zebrafish. Consequently, the contribution of the studies in zebrafish to the understanding of hematopoiesis, the development and behaviour of the HSC and the hematopoietic malignancies is not to be underestimated (Table 1.1).

Forward genetic screens resulted in the identification of new regulatory genes associated with hematopoietic development and disease. For example, the analysis of the *weissherbst* mutant resulted in the identification of a new iron transporter *ferroportin1*, associated with human hemochromatosis type 4.

Similarly, *hspa9b*, related to myelodysplastic syndrome and *ddx18*, related to acute myeloid leukemia were discovered (Donovan et al., 2000; Craven et al., 2005; Payne et al., 2011).

The analysis of the function of a candidate gene has been limited to the injection of mRNA or a morpholino into a one-cell stage embryo resulting in a transient gain- or loss-of-function. Despite the transient nature of these experiments, this has led to many important observations and it still is a powerful tool to analyze in a relatively fast way the function of a gene compared to the more traditional murine knockout. However, many efforts have been done to improve the generation of zebrafish transgenics in order to be able to perform reverse genetic screens in zebrafish. Using ENU screening, TILLING (targeted induced local lesions in genome), zinc-finger nucleases (ZFNs) or CRISPR/Cas9 specific defects in targeted loci can be generated yielding new mutants to analyze gene function. This resulted in the identification of genes like *NPM1* in acute myeloid leukemia, *RPS19* in Diamond-Blackfan anemia and *VHL* in Chuvash polycytemia (Danilova et al., 2008; Uechi et al., 2008; van Rooijen et al., 2009; Bolli et al., 2010). Furthermore, the recent application of the Tol2 transposons, Cre-*loxP* and Gal4-*UAS* systems allowed the generation of stable transgenic hematopoietic cancer models like for T cell acute lymphoblastic leukemia (T-ALL), where mouse *Myc* was driven by the zebrafish *rag2* promotor or for AML1-ETO, the most common chromosomal rearrangement in AML (Langenau et al., 2003; Yeh et al., 2008).

Zebrafish, is a very efficient platform to screen chemical compounds and assess their effect on hematopoiesis (Yeh et al., 2009; Ridges et al., 2012). The development of transgenic reporter lines and mutants zebrafish will only contribute further to the elucidation of the role of certain players during the process of hematopoiesis. This was already illustrated with the discovery of prostaglandin E2 as a HSC inducing factor (North et al., 2007)

Finally, transplantation based xenografts in zebrafish were also established to investigate hematopoiesis associated cancers (ie. erythroleukemia and acute promyelocytic leukemia) and assess the efficacy of small molecules on tumor progression (Corkery et al., 2011; Pruvot et al., 2011).

Zebrafish mutant	Gene	Human disease	Reference
weissherbst	*Ferroportin*	Hemochromatosis	(Donovan et al., 2000)
frascati	*Mitoferrin*	Hypochromic anemia	(Shaw et al., 2006)
shiraz	*Glutaredoxin 5*	Hypochromic anemia	(Wingert et al., 2005)
dracula	*Ferrochelatase*	Erythropoietic protoporhyria	(Childs et al., 2000)
merlot	*Protein 4.1r*	Hemolytic anemia	(Shafizadeh et al., 2002)
retsina	*Solute carrier family 4, anion exchanger 1*	Congenital dyserythropoietic anemia type II	(Paw et al., 2003)
riersling	*Beta-spectrin*	Hereditary spherocytosis	(Liao et al., 2000)
sauternes	*Gamma-aminolevulinate synthetase*	Congenital sideroblastic anemia	(Brownlie et al., 1998)
vlad tepes	*Gata1*	Familial dyserythropoietic anemia & thrombocytopenia	(Del Vecchio et al., 2005)
yquem	*Uroporphyrinogen decarboxylase*	Porphyria tarda & hepatoerythropoietic porphyria	(Wang et al., 1998)
zinfandel	*Globin locus*	Hypochromic anemia	(Brownlie et al., 2003)

Table 1.1: The zebrafish embryo as a model for human blood disorders

Based on (Jing and Zon, 2011; Martin et al., 2011; Kulkeaw and Sugiyama, 2012).

1.5 Chicken limb development

The development of the limbs initiates with the emergence of the limb buds from the lateral plate mesoderm in the flank of the body. At specific locations along the anterior-posterior axis limb fields are specified upon condensation of ectodermal and underlaying mesodermal cells. The lateral plate mesoderm and the adaxial mesoderm (somites) will later develop into muscle, cartilage, bone, tendons and vasculature. The ectoderm however will give rise to the skin and its derivatives like hair and nails (Gilbert, 2006). The specification of the position of the limb fields was shown to depend on the combined action of retinoic acid (RA), T-Box (TBX4 and 5), Homeobox (HOX), Fibroblast Growth Factor (FGF8 and 10) and WNT (WNT2b and WNT8c) signaling (Lewandoski et al., 2000; Kawakami et al., 2001). Once specified, the outgrowth of the limb is further regulated by the distal most cells of the limb, the apical ectodermal ridge (AER) (Fig 1.12A). This ectodermal thickening is induced by mesenchymal BMP4 and FGF10 signals, and by secreting FGF4 and FGF8 itself, it maintains the proliferation of the underlying mesenchymal cells (Niswander et al., 1993; Ohuchi et al., 1997; Saunders, 1998). The identity of the digits along the anterior-posterior axis (AP) is determined by a group of Sonic Hedgehog (SHH) producing

cells localized in the posterior mesenchyme, the Zone of Polarizing Activity (ZPA) (Riddle et al., 1993). The exact localization of this ZPA is dependent on the interactions of RA, dHAND and HOX factors. The specification of the dorso-ventral axis is dependent on the dorsal expression of *WNT7a*, and the ventral repressor activity of EN-1 on the expression of *WNT7a* in the ventral ectoderm (Fig 1.12B) (Niswander, 2003).

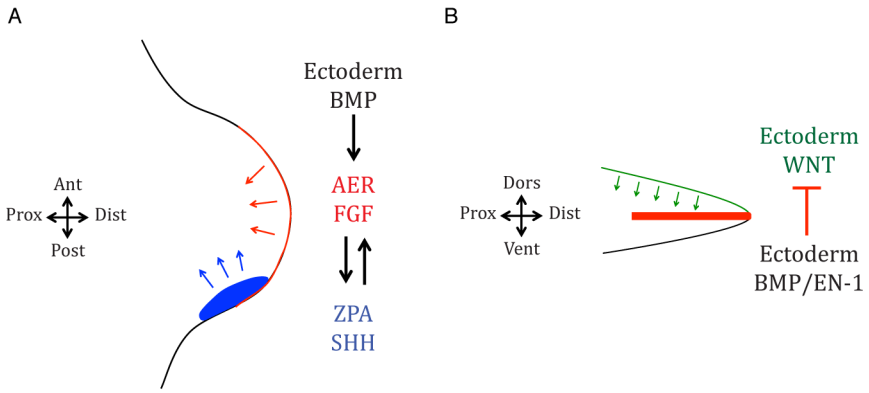

Figure 1.12: Molecular regulation of the outgrowth and patterning of the chicken limb bud

A-B. Schematic representation of an outgrowing limb bud with the different organizing centers: the apical ectodermal ridge (AER), the zone of polarizing activity (ZPA) and the ectoderm that regulate the proximo-distal outgrowth (A), the anterio-posterior (A) and the dorso-ventral differentiation (B), respectively. A. Dorsal view, anterior to the top. B. Posterior view, dorsal to the top.

Chapter 2:

Aims of the study

2.1 General objective

SMOC2 was extracted from bovine articular cartilage 20 years ago by our laboratory together with GDF5 (Chang et al., 1994) and FRZB1 (Hoang et al., 1996) and showed a potent osteo-chondrogenic acitivity *in vivo*. Over the years, research has shown SMOC2 is involved in many different processes and had been associated with many conditions. However, the role of SMOC2 in the cartilage and bone is still unknown. At the beginning of this project, there was no evidence for an interaction of SMOC2 with any known signaling cascade. With this project we aimed at the identification of a SMOC2-associated pathway and the investigation of the function of Smoc2 in that pathway.

2.2 Specific aims

2.2.1 Identification of the Smoc2-associated signaling cascade in zebrafish embryos

To understand the molecular events regulated by Smoc2, the Smoc2 associated signaling pathway needs to be identified. Currently one of the most robust, *in vivo*, methods for pathway identification is based on the zebrafish model organism. Therefore, we will carry out gain and loss of function experiments by injecting *smoc2* morpholino and *smoc2* mRNA in the one-cell stage embryos respectively. Subsequently we will perform a molecular analysis to assign those genes to signaling pathways as well as developmental processes such as cell migration and/or differentiation.

2.2.2 Generation of tools to investigate the role of SMOC2 in the chicken developing limb

Zebrafish is very useful in pathway identification projects but is inadequate to study the function of genes in the endochondral bone formation and joint induction since in the fish they occur in a very different way than in higher

vertebrates. To address the function of SMOC2 during those processes we will use the *in ovo* developing chick embryo. Therefore, *SMOC2* will be cloned in the RCAS viral vector and locally injected in the chicken limb bud. Using histological techniques and WISH analysis we will perform a preliminary analysis of the induced phenotype.

2.2.3 Analysis of the *Smoc2*$^{-/-}$ phenotype in mice.

Up to date, no description of the murine *Smoc2*$^{-/-}$ phenotype was published. Therefore, using histological stainings and morphological observations we performed a preliminary analysis of the function of SMOC2 in the mouse model.

Chapter 3:

Materials & methods

3.1 Model systems

3.1.1 The zebrafish model system.

The zebrafish is a relatively new model system that was first used during the 1930s for the investigation of karyokinesis and the mechanism of cell division. Already at that point it was suggested the zebrafish was a favorable laboratory subject not just to be used in ornamental aquaria. From the 1950 onwards, the appreciation for the zebrafish as a laboratory animal only increased. Zebrafish were primarily used for anatomical studies and toxicity assays. Already then, the potential of the zebrafish as a model was recognized: 1) zebrafish females produce hundreds of eggs weekly that are fertilized externally; 2) the development of the embryo and larvae is extremely quick compared to other animal models; 3) embryos are transparent allowing visualization of developing organs and structures; 4) they are small, and can be housed in a small space compared to other models; 5) embryos can be systemically manipulated by injection at the one-cell stage. Recently, much attention has gone to the development of transgenic reporters and tissue specific knock-outs, and the induction of targeted mutations. Using ENU screening, TILLING (targeted induced local lesions in genome), zinc-finger nucleases (ZFNs), TALEN, Crispr/Cas9, Tol2 transposons, Cre-*loxP* and Gal4-*UAS* systems stable transgenic models can be generated to investigate gene function and to model diseases.

3.1.2 The chicken model system

To investigate the function of SMOC2 it is required to assess it in its specific environment, the articular joint. Although perfectly suited for the identification of the pathway associated with SMOC2, the zebrafish model cannot be used for these functional studies, as zebrafish do not have human-like joints. However, the chicken limb model provides the environment, similar to human joints, that is needed to assess the function of SMOC2.

The chicken embryo is probably one of the oldest animal models used to study the development of an embryo (Stern, 2004). This model allows the study of many organs, including limbs in an *in vivo* setting (Tickle, 2003). The chicken embryo has been successfully used to study various aspects of human diseases,

including skeletal defects (Simmons and Gilliam, 1981; Brown et al., 2003; Tickle, 2004). The use of chicken embryos resulted in many important discoveries such as the molecular basis of anterio-posterior and proximo-distal axis formation, the first cellular oncogene, and the oscillating gene expression during somitogenesis as well as articular cartilage development (Rosier and O'Keefe, 1998; Rosier et al., 1998; Stern, 2005). The main advantages of the chicken embryo are the availablility, the low cost and the ease of manipulation. Although the embryo develops *in ovo*, this does not prevent experiments where cells are tracked, beads are implanted or tissues are grafted. In addition, it allows for the screening of chemicals and gene delivery by electroporation or viral infection.

The RCAS virus is derived from the avian Rous Sarcoma Virus that contains 4 genes: gag, pol, env and the src oncogene. In the RCAS viruses the latter is replaced by an expression cassette that contains a ClaI restriction site, which allowed the cloning of the open reading frame (ORF) of the gene of interest downstream of the env gene (Morgan and Fekete, 1996; Gordon et al., 2009). The gag, pol and env genes encode structural components (viral coats) and enzymes for replication (Fig 3.1). The viral coat proteins are of critical importance for the infection, as they have to interact with their corresponding cellular receptor. A series of RCAS subfamilies have been developed, all with different viral coat proteins. Once a cell is infected with a virus of a certain subtype, further infection of the cell by cells with the same viral coats is prevented. Infection with viruses of a different subclass is however still possible, which allows multiple viruses with different coats to infect the same cell. Furthermore a more efficient polymerase, the Bryan high-titer (BP) was introduced into the RCAS vector to increase the viral titer (RCASBP).

In order to monitor the efficiency of our viral injections we developed a system based on viruses with different coats. These viral coat proteins are of critical importance for the infection as they are responsible for the interaction with the cellular receptors. Importantly, two different viruses with the same coat protein cannot infect the same cell. However, two viruses with different viral coat proteins van bind to different cellular receptors and therefore infect the same cell. Currently, we use two subtypes of the RCAS virus: RCASBPA and RCASBPB. With a RCASBPB-GFP virus present in the lab, this allows us to co-inject the

RCASBPA viruses with the RCASBPB-GFP virus in order to control for the injection efficacy. Importantly, the cloning of the gene of interest in the RCAS vector must be in frame with the open reading frame of the viral genes. Therefore, a shuttle vector, pSLAX12, is used. This is a small, high copy number plasmid that provides ClaI restriction sites to use for cloning into RCAS. To ensure the ORF of the gene of interest is similar to the ORF of the virus, the ORF has to be subcloned in the NcoI site of the multiple cloning site of the pSLAX12 vector (Fig 3.1).

Figure 3.1: Schematic representation of the cloning strategy and multiple cloning site of pSLAX12
Downstream of the gag, pol, env, the gene of interest can be cloned in to the RCAS vector using the ClaI site. The pSLAX vector permits cloning of the gene of interest in between two ClaI sites. Ideally the translation start site of the gene of interest uses the ATG of the NcoI restriction site. Alternatively, the ATG of the gene must be in frame with the ATG of the NcoI site.

3.1.3 The mouse model

As the favorite model for over 100 years the mouse model has proven to be of great importance in the field of biomedical research. Just like humans, mice are mammals, in contrast to yeast, worms, fruitflies, zebrafish and frogs. With their physiology closely resembling that of humans, they make excellent models to study different processes of the immune, nervous and skeletal system to mention a few. In addition, mice also develop diseases relevant to humans like atherosclerosis, diabetes, osteoporosis and cancer. Furthermore, other

conditions like Alzheimer's disease can be induced in mice in order to study its onset and progression. Before, mice were (exposed to DNA damaging chemicals and) bred in order to generate offspring with a particular trait. Later however, innovative genetic techniques were used to generate a genetically modified mouse model that can be used to study the function of a gene or a specific condition. Currently, with the international research community using the mouse as a model for their research, over 1000 transgenic mouse models are available world-wide.

3.2 Experimental procedures

3.2.1 Zebrafish care & manipulations

Adult zebrafish (Danio rerio) were maintained at 28°C, on a 14/10 hour, light/dark cycle under standard aquaculture conditions as described (www.zfin.org). All experiments were performed using embryos obtained from random matings of the wild type AB strain, the *Tg(mpx:GFP)*^{i114}, the *Tg(fli:eGFP)*^{y1} or the *Tg(myl7:GFP)* transgenic line (Lawson and Weinstein, 2002; Huang et al., 2003; Gray et al., 2011). Embryos were kept in embryo medium and staged by hours post-fertilization, the number of somites (somite stage or ss) or the onset of circulation according to defined criteria.

An ATG and a SPLICE morpholino (MO) against *smoc2* were designed and purchased from GeneTools (ATG-MO: 5'-CGCATCCTCGCAGCTCCCCAGAAGC-3'; SPLICE-MO: 5'-AAGGTGTTGTGACCCACCGTGAGCG-3'). MOs were resuspended at a stock concentration of 2mM. The working solution consists of 0.4 mM (3.5 ng) and 0.05 mM p53 MO (0.39 ng; p53 MO: 5'-GCGCCATTGCTTTGCAAGAATTG-3'). RT-PCR as a control for the splicing of the first exon was performed with the primers indicated in Figure 4.7 (primer F: 5'-GATGCGCGTATCGGTGCTG-3'; primer R: 5'- CTCTGCAACACACTTGGGG-3').

EST analysis for determination of the ORF of *smoc2* was performed using the primers in Table 3.1.

Clone	Forward primer (5' - 3')	Reverse primer (5' - 3')
O-Smoc2	ATGCGCGTATCGGTGCTG	GAATTCAGGGGGGTTTTTGGTGAT
B-Smoc2		GCCTTGTTTCTTTGACAGGTTCAGTTTAC
N-Smoc2 1		GGCCTTGACAAATGCAACATGTAATAC
N-Smoc2 2		CCCGTTCCATGTGTGGTACAGG

Table 3.1: Primer sequences used for cloning.

The full-length ORF of *smoc2* was cloned in the pCS2+ expression vector (smoc2 ORF-F: 5'-TATATAATCGATATGCGCGTATCGGTG-3'; smoc2 ORF-R: 5'-CTAGCCTTGTTTCTTTGACAGGTTCAG-3'). Capped mRNA was generated using the mMESSAGE mMACHINE SP6 Kit (Ambion) according to manufacturer's protocol. Diluted MO or diluted mRNA was injected in one-cell stage embryos in a volume of 1 nl. Injected embryos were maintained at 28.5 °C and analyzed at the appropriate stage. Images were acquired with DMR Leica and Stereo Discovery V8 (Zeiss) microscopes.

3.2.2 Chicken care & manipulations

Fertilized White Leghorn eggs (Poel-Houben, Halle, Belgium) were incubated in a humidified incubator at 38°C for approximately 48 hours. Staging was performed according to the criteria of Hamburger-Hamilton (Hamburger and Hamilton, 1992). 2-3 ml of albumin was removed to lower the embryo from the upper surface and prevent damaging of the embryo during the manipulations. By cutting a 'window' in the upper surface of the shell the embryo was accessed. The lateral plate mesoderm of the right hindlimb was targeted by injecting multiple times with high-titer viral supernatans suplemented with 1/40 1% Fast Greeen solution (Sigma-Aldrich) in PBS. After adding an antibiotic/antimycotic solution, the eggs were sealed with clear tape and incubated until the stage required.

3.2.3 Mouse care

Smoc2 heterozygote mice were purchased from TIGM and crossed into the CD1 background. Mouse colonies were housed in a conventional animal facility and maintained according to Animal Welfare Guidelines.

3.2.4 Whole-mount in situ hybridization (WISH)

All whole-mount in situ hybridization (WISH) analyses were performed using digoxygenin-labelled anti-sense RNA probes, that were generated from linearized plasmids using SP6, T3 or T7 polymerase and a DIG RNA labeling mix (Roche Applied Science, manufacturers protocol). Subsequently the probes were purified using the microspin columns P-30 (Bio-Rad). All but the *smoc1* and *smoc2* probes were generous gifts from other labs (Table 3.2).

Probe	Source	Probe	Source
ntl	C. Houart (London)	*flt4*	S. Schulte-Merker (Leiden)
pcdh8		*dll4*	
myod		*vegfc*	
chd		*draculin*	T. Takahashi (Manchester)
gata2		*hbbe1.1*	
runx1	K. Crosier (Auckland)	*gata1*	C. Esguerra (Leuven)
ikaros	R. Patient (Oxford)	*nkx2.5*	
c-myb		*vox*	
lmo2		*vent*	
irf8	Z. Wen (Hong Kong)	*krox20*	W. Annaert (Leuven)
csf1ra		*chd*	C. Houart (London)
c/ebp1		*pcdh8*	
tal1	T. Evans (New York)	*myod*	
gata2		*ntl*	
spi1b	N. Itoh (Kyoto)	*dHAND*	V. Zappavigna (Modena)
mpx		*SHH*	M. Logan (London)
flk1	M. Dewerchin (Leuven)	*BMP2*	
fli1		*FGF8*	

Table 3.2: Probes used in this study and their sources
Zebrafish probes in blue and chicken probes in yellow

For *smoc2*, the ORF and the 3' UTR was cloned in the pCR-Script vector using the following primers:

- smoc2 probe S: 5' – GATGCGCGTATCGGTGCTG – 3'
- smoc2 probe AS: 5' – GGCCTTGACAAATGCAACATGTAATAC – 3'

Dependent on the orientation of the amplified fragment, either a probe of the 5' coding sequence or a probe of the 3' UTR was generated.

For *smoc1,* the following primers were used to clone the 3' coding sequence:

- smoc1 probe S: 5' – ATGATGGTTCCAAGCCCACACC – 3'

- smoc1 probe AS: 5’ – GCGACCTTAACAAGGACAAGACCATC – 3’

3.2.4.1 Zebrafish

WISH was performed as described by the group of Thisse (Thisse and Thisse, 2008).

3.2.4.2 Chicken

WISH was performed according to (Salsi et al., 2008)

3.2.5 Skeletal staining

Skeletal staining was performed using Alcian Blue (8GX, Sigma-Aldrich) and Alizarin Red (Sigma-Aldrich) to stain cartilage and bone respectively. Embryos were collected and the limbs were isolated, fixed and dehydrated in 95% ethanol for 3-5 days. First the limbs were stained with Alcian Blue solution (20% glacial acetic acid, 80% ethanol and 150 mg/ml Alcian Blue) for 24 hours. After two consecutive washes with 95% ethanol for 2 days, the limbs were cleared in 1% KOH for 30-60 minutes. Next, all mineralized tissue, like the bone, was stained with Alizarin Red solution (1% KOH with 50 mg/ml) for 4-5 hours. After additional clearing in 1% KOH for 12 hours at 4°C, they were passed every 24 hours to a solution with increasing ratios of 1% KOH and glycerol (80:20, 60:40, 40:60, 20:80).

3.2.6 Immunohistochemistry P-SMAD

Embryonic zebrafish were fixed O/N in 4% PFA and washed multiple times in PBST supplemented with 1% DMSO. After blocking in blocking buffer (10% Normal Donkey Serum in PBST) for 1 hour, the embryos are incubated O/N on the rocking plate in the antibody solution (1/300 diluted P-SMAD 1/5/8 antibody (Cell Signaling, 9511S) in blocking solution). Subsequently, the embryos are washed three times for an hour on the rocking plate and blocked again in blocking buffer for 1 hour. The secondary antibody is applied O/N at 4°C (1/500 donkey anti rabbit Alexa 488/555 (Invitrogen). Finally, unbound secondary antibodies are removed by washing three times for 1 hour in 0.3% Triton-100 in PBS.

3.2.7 RNA extraction cDNA synthesis qPCR

Embryos at 12 or 20 ss were fixed gently with 1% trichloroacetic acid (TCA) on ice for 10 min, followed by dissection of the anterior part of the fish by cutting at the level of the most anterior somites (Law and Sargent, 2013). Older embryos were clipped at the most rostral part of the yolk sac extension. Total RNA was isolated from 10-15 dissected stage-matched pooled embryos using the High Pure RNA Tissue Kit (Roche Applied Science; manufacturers protocol). At least four RNA isolations were performed per condition and subsequently reverse transcribed using Primescript RT Reagent (Takara; manufacturers protocol). Real-time PCR was performed in duplicate with gene specific primers (Table 3.3) with SYBR Premix Ex Taq II (Takara; manufacturers protocol) using Rotor-gene 6000 detection system (Corbett Research, Westburg). Samples were confirmed to be anterior by checking anterior *six3b* expression and posterior *charon* expression. Gene expression was normalized to the housekeeping gene *β-actin* and presented as a ratio to control embryos. The significance of the difference in expression was analyzed using the Student's T-test.

Gene	Forward primer (5' - 3')	Reverse primer (5' - 3')
β-actin	TGCCCCTCGTGCTGTTTT	TCCCATGCCAACCATCACT
alk8	GCATTGCAGCTAAAGGATCCAA	TCCTCAAGTGACTCTCAGCG
bmp2b	CGACTCTCTGTCGTGGGATA	TGATCAGTCAGTTCCGGAGG
bmp4	GGCCTGCAAAGGCGTCCCAG	CAGCTCCTCCAGGTGCTCTTCAT
c/ebpα	GAGTACAGGCTGAGGAGGGA	ACATTGCGCATTTTCGCCTT
c/ebp1	TGCACATACACAGGATTTTGCT	CCGGTACTCAGCACTGTCTT
c-fos	CAACTGTCACGGCGATCTCT	GCCACAGAGGAGATCATGGG
charon	AAAGTGGTGCACAAAAGCGA	CGTTATGCGCTGTGTAAAGGG
chd	GCTGTCCCATCTGTGAAGAGAA	GTTCCAGGTGCGTGCATTTT
ctsk	AGGCCATCGACCGTTTCAAT	CCCATTCTGACCTGAGCGAT
ets1	ACAGCGGATCTTGTTGAGGG	TGTCCTCAAAGAATAGACGCCA
gata1	GACTGACCTACTGCCATCGT	AGACTTGGCGAACTGGACTG
gata2	AAACTCCACAACGTCAACAGG	CGAAACCCTCACCAGATCGT
gata4	CACTTCGACAGCTCCGTACT	CCTCGCAGATCATCAAAAACTCTAA
gata5	CTGCCTGTGTCAGAAAACGC	AACTGTGTCGATGCCTGTGT
gata6	ACACTTTCTCTGCAACGCCT	GAGGAAGACATGCGCTTCTG
ikaros	CACAGAGGTTTGTGGGAGAGA	ATTGCACTGTTGATGGCCTG
irf8	TCCATTTTCAAAGCGTGGGC	AGCGCAATCTGGTCTTCCAT
lmo2	GGGACGCAGGCTTTACTACA	CGTCCTGACCAAACAGTCTGA
mpx	TTGTGCTCTTTCAGTGGGGG	ACTTGTAAGCAGCGTCCACTA
nfatc	ACCTGCCCACAAATGTTCCA	TGAAGAGGCGCACATACCTG
rRNA (18S)	CCTGCGGCTTAATTTGACTC	GACAAATCGCTCCACCAACT
runx1	AATCCTACCCTGCACCAACG	CCTTCGCTCTGATTGGGGAG
six3b	GCTGCCAAAAACAGGCTTCAG	CAGCCCGATTCTGACATGGAG
spi1b	AGTCAGAACGATCACTCTTGGG	GTGACTGCACGCTTTGTAGC
tal1	AAATCAACGATGGTTCGCAGC	GTTCACATTCTGCTGTCGCC
ved	CACACACACGAGTCTGGCTTCAG	CGCCGGCCACTAGAGGGAGA
vox	CTCGGCCTGTCGGAAACACAGATCA	GGGAACGGGAGCCGCTGTCT

Table 3.3: Primer sequences used for qPCR

Chapter 4:

The role of *smoc2* during zebrafish development

4.1 Cloning of the zebrafish *smoc2* sequence

We cloned zebrafish *smoc2* by analyzing available EST sequences and designing primers flanking the ORF. The complete ORF was then cloned into the pCS2+ expression vector, which allows for the *in vitro* synthesis of polyadenylated mRNA. The sequence of this clone was compared to the online available data in order to detect potential point mutations introduced during PCR or cloning. Despite the fully sequenced zebrafish genome, the annotation of the genes in the database was and still is incomplete. Abnormalities in our clone were left undetected until April 2012, with the publication of Bloch-Zupan on craniofacial defects in *smoc2* morphants and the submission of the *smoc2* mRNA sequence on the NCBI website (Thisse, 2001; Bloch-Zupan et al., 2011). Comparison of the amino acid sequence of our clone (O-Smoc2) with the clone of Bloch-Zupan (B-Smoc2) resulted in the identification of six point mutations of which five were located within the different domains of Smoc2. An additional stretch of 37 amino acids was found at the 3' end of the gene, downstream of exon 11, resulting in a sequence difference of over 9% (Fig 4.1).

```
O-Smoc2  MRVSVLLLLCALYAGNVHKLSALTFLRVEQDKECNTDCSGAPRKPLCASDGRTFSSRCEFLRAKCRDPQL
B-Smoc2  MRVSVLLLLCALYAGNAHKLSALTFLRVEQDKECNTDCSGAPRKPLCASDGRTFSSRCEFLRAKCRDPQL
N-Smoc2  MRVSVLLLLCALYAGNAHKLSALTFLRVEQDKECNTDCSGAPRKPLCASDGRTFSSRCEFLRAKCRDPQL
         ------ SP -------               ----------------------- FS -----------

O-Smoc2  AVSRGQCKDTPKCVAEKKYTEQQAKKLFPQVFVPVCNPDGTYSEVQCHSYTGYCWCVMPNGRPISGSAVA
B-Smoc2  AVSRGQCKDTPKCVAEKKYTEQQAKKLFPQVFVPVCNPDGTYSEVQCHSYTGYCWCVMPNGRPISGSAVA
N-Smoc2  AVSRGQCKDTPKCVAEKKYTEQQAKKLFPQVFVPVCNPDGTYSEVQCHSYTGYCWCVMPNGRPISGSAVA
         ----- ---------------------------------------- TY1 --------------------

O-Smoc2  NKKPQCQGSKNSKVNLKEPGKSDPSTVLVVESQPSVDEEDIISQYPTLWSEQVRSRQNRTRTQSTSCDQE
B-Smoc2  NKKPQCQGSKNSKVNPKEPGKSDPSTVLVVESQPSVDEEDIISQYPTLWSEQVRSRQNRTRTQSTSCDQE
N-Smoc2  NKKPQCQGSKNSKVNPKEPGKSDPSTVLVVESQPSVDEEDIISQYPTLWSEQVRSRQNRTRTQSTSCDQE
         ------          ---------------------- SMOC ------------------- ----

O-Smoc2  QLSAQGEARQHKNEAVFVPDCASGGLYKPVQCHPSTGYCWCVLVDTGRPIPGTSTRHEQPKCDGNARAHP
B-Smoc2  QLSAQEEARQHKNEAVFVPDCASGGLYKPVQCHPSTGYCWCVLVDTGRPIPGTSTRHEQPKCDGNARAHP
N-Smoc2  QLSAQEEARQHKNEAVFVPDCASGGLYKPVQCHPSTGYCWCVLVDTGRPIPGTSTRHEQPKCDGNARAHP
         ---------------- TY2 ------------------------------------------

O-Smoc2  NKPKDHYRSRHLQGCPGEKKTEFLTSVLDALSTDMVHAVTDPAAGGRMLEPDPSHALEERVVHWFFSQLD
B-Smoc2  NKPKDHYRSRHLQGCPGEKKTEFLTSVLDALSTDMVHAVTDPAAGGRMLEPDPSHTLEERVVHWYFSQLD
N-Smoc2  NKPKDHYRSRHLQGCPGEKKTEFLTSVLDALSTDMVHAVTDPAAGGRMLEPDPSHTLEERVVHWYFSQLD
                    ------------------------------- EC --------------------

O-Smoc2  KNSSGDIGKKEIKPFKRLLRKKSKPKKCVKKFVEYCDISSDKALSLQELMGCLGVTKEEGESHCFLRCTS
B-Smoc2  KNSSGDIGKKEIKPFKRLLRKKSKPKKCVKKFVEYCDISNDKALSLQELMGCLGVTKEEGESHCFLRWAK
N-Smoc2  KNSSGDIGKKEIKPFKRLLRKKSKPKKCVKKFVEYCDISNDKALSLQELMGCLGVTKEEG--------AK
         -- EF1 ----------------------------- EF2 ---------

O-Smoc2  KKSRHLHTRLKVITKNPPEFKASRASRTIVSRIT*
B-Smoc2  TGDGTTSSKLNLSKKQG*-----------------
N-Smoc2  TGDGTTSSKLNLSKKQG*-----------------
```

Figure 4.1: Sequence alignment of different zebrafish Smoc2 clones

Comparison of the O-Smoc2 and B-Smoc2 clone indicated over 9% difference in amino acid identity. Indicated in red are the residues that are different: six point mutations of which five are located in the SP, TY2 and EC domain; a stretch of 37 amino acids at the 3' end of the ORF.

In-depth analysis of this alternative 3' end, revealed that it partially consisted of a pCS2+ sequence (orange), and two *smoc2* genomic DNA fragments (blue and purple) (Fig 4.2).

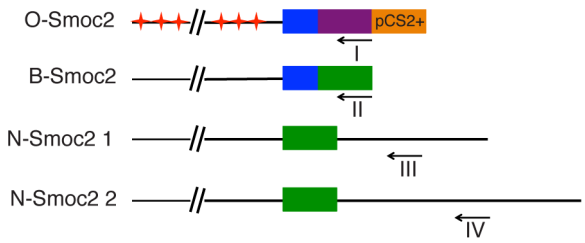

Figure 4.2: Schematic representation of the different Smoc2 clones

The lab clone contained six point mutations dispersed throughout the gene. Four different stretches of amino acids were identified (blue, purple, orange and green). A new EST assembly resulted in the identification of two overlapping contigs that did not contain any point mutation, nor the blue, purple or orange stretch of amino acids. Based on the contigs, new primers (I-IV) were designed.

The blue domain was also found in the publically available clone (accession number: JQ085591) and in the genomic DNA database (accession number: FR649726.1). The purple domain however was only found in the genomic sequence. The integration of these domains could be due to an alternative splicing event. Therefore, we used online available tools like Netgene2, ASSP and Human Splicing Finder, to analyze the splicing events of exon 11 (Brunak et al., 1991; Wang and Marin, 2006; Desmet et al., 2009). Our analysis indicated that the blue domain was flanked by two splice donor sites, whereas the purple domain was not (Fig 4.3A). So indeed, the integration of the blue domain in the *smoc2* ORF could be due to an alternative splicing event. This domain was also picked up by the group of Dolfus (Bloch-Zupan et al., 2011). Interestingly, this group submitted this clone to the NCBI website, but published and designed a MO in the same area based on the clone without the blue domain (Bloch-Zupan et al., 2011). Using the online splicing analysis tools, a score was generated for the two splice donor sites of exon 11. As the score for splice donor site A (red) was higher than the score for site B (yellow), it is therefore more likely to be the

primary splice donor site (Fig 4.3B). Yet it is important to mention that the score for site B is comparable to the score of other *smoc2* exon splice donor sites, which suggests that it can not be excluded that the splicosoom uses site B instead of site A.

A

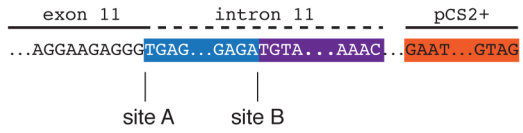

B

Splice donor position	Splice site	Consensus value (0-100)
Exon 1	ACGgtgggt	84.8
Exon 2	AAGgtcaga	91.69
Exon 3	GAGgtaaga	95.9
Exon 4	AAGgtacca	75.89
Exon 5	CAGgtaaat	87.83
Exon 6	AAGgtgagt	97.89
Exon 7	AATgtgagt	87.02
Exon 8	AAGgtaatg	84.8
Exon 9	AGGgtgagc	90.86
Exon 10	GAGgtaaac	83.9
Exon 11 site A	AGGgtgagt	93.03
Exon 11 site B	GATgtacga	76.23
Exon 12	CTGgtgagt	94.09
Exon 13	AAAgtggga	76.63

Figure 4.3 Splice donor site analysis

A. Schematic representation of the genomic sequence of exon 11 with its blue domain, intron 11 and the green exon 12. 2 splice donor sites were detected for exon 11. B. Using the Human Splicing Finder, we analyzed the donor splice sites for all exons.

Tracing back the cloning strategy of previous lab members, an antisense primer was found that complemented the 3' end of the purple domain. So we conclude that the integration of the purple domain in the ORF of *smoc2* is due to an incorrect primer design. The integration of the orange domain, which was part of the pCS2+ multiple cloning site, was most likely due to incorrect use of restriction enzymes and ligases.

The biological consequences of these sequence alterations are unknown but could potentially influence, positively or negatively, the function of the protein by causing different folding properties, hence changing the interaction with other proteins or with its own domains. Furthermore, these mutations could affect the stability of the mRNA and therefore the amount of protein generated. Therefore we decided to reanalyze the ESTs and design different new primers (I-IV) to reclone zebrafish *smoc2* in order to ensure that we were working with the correct and biologically relevant ORF (Fig 4.2).

Our newly generated contigs did not contain point mutations or any of the domains indicated in blue, purple or orange (Fig 4.2). Using the primer sets II-IV, amplicons were generated, whereas the use of primer set I did not result in an amplified fragment, suggesting that this sequence information was incorrect. Cloning of this new *smoc2* ORF in pCS2+ (N-Smoc2) and subsequent sequencing indicated that no more point mutations were present. As anticipated, the blue domain, found in the O-Smoc2 protein and the B-Smoc2 protein, was not found in the N-Smoc2 protein.

Unfortunately, the ENSEMBL database is not 100% complete and correct. For zebrafish *smoc2*, two different transcripts were found. Each of them matches with either the 5' or the 3' end of our clone. Our newly generated clone could therefore not be compared to the database, not could the splicing events be assessed. In addition, the annotation of the different exons of *smoc2* is incomplete. Further optimization of the publically available zebrafish data is required to prevent problems like encountered during this project.

Remark:
The identification of the point mutations and the difference in the 3' end of the ORF was done after a number of experiments were performed with this O-Smoc2 clone. After cloning the N-Smoc2 clone, these experiments were repeated. Despite the 9% difference in amino acid identity, no different overexpression phenotypes could be detected with this correct N-Smoc2 clone. Therefore, the overexpression data obtained with the O-Smoc2 clone were still included and are still considered to be relevant. Yet, we are aware of the fact that the data on the O-Smoc2 clone could be biased due to the change in sequence. For the sequence analysis, the expression analysis, the domain study and the rescue of the morpholino phenotypes, the N-Smoc2 clone was used.

4.2 Sequence and expression analysis during zebrafish development

Alignment of the protein sequence of zebrafish Smoc2 revealed an identical organization of the different domains across species. Within the FS, TY, SMOC, EC domains the conservation is very high (55-80% identity to human SMOC2), while in the SP domain and the C terminal part the conservation is much lower (Fig 4.4).

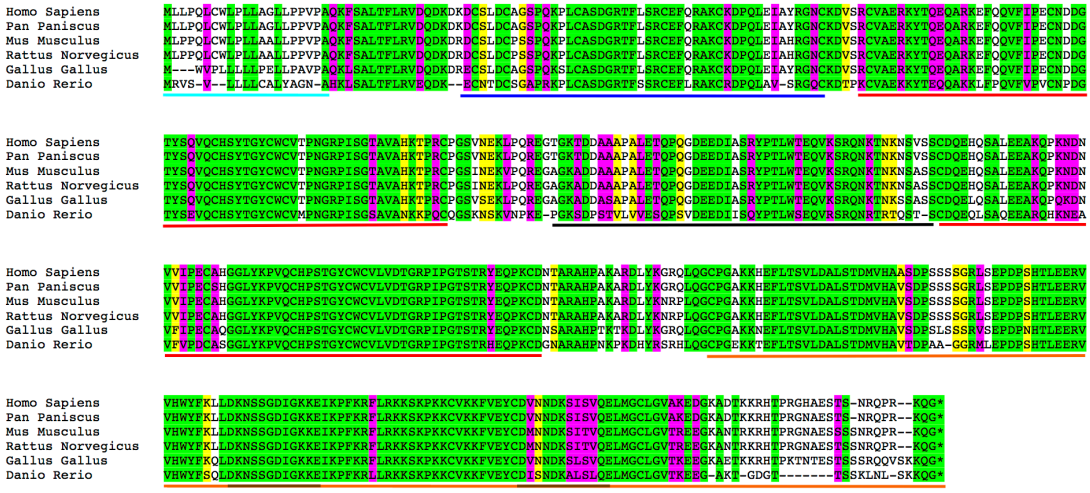

Figure 4.4: Sequence alignment of Smoc2

Amino acid sequence alignment (ClustalW) of Smoc2 homologs reveals a high degree of sequence conservation and similar domain organization (green: identical residue; purple: conserved residue; yellow: similar residue). The signal peptide is indicated in light blue, the Follistatin-like domain in dark blue, two Thyroglobulin domains flanking the putative SMOC domain in red and the extracellular calcium binding domain in orange, with the EF-hand motifs in brown.

To determine the spatiotemporal pattern of *smoc2* mRNA expression during zebrafish development, we performed whole mount in-situ hybridization (WISH) using two non-overlapping probes. During pregastrulation stages, *smoc2* expression was not spatially restricted (Fig 4.5). During segmentation and later stages of development however, the expression pattern became restricted to anterior structures, with a predominant expression in the retina, notochord, anterior somites, lateral hindbrain, lateral epidermis, cerebellum, dorsal midbrain, telencephalon, and diencephalon. Furthermore, an additional expression pattern can be seen at later stages in the epidermis of the tail (see inset at 30 hpf). This *smoc2* expression pattern is in accordance with the available online data (www.zfin.org) (Thisse, 2001).

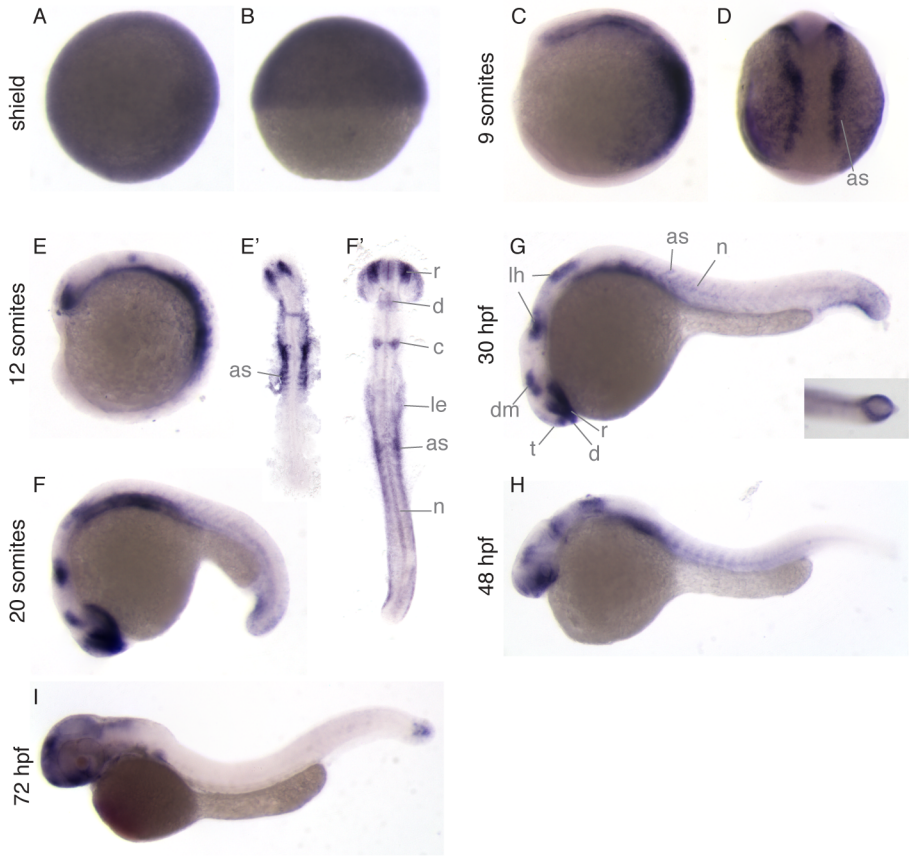

Figure 4.5: Expression analysis of *smoc2*

A-I. Expression pattern of *smoc2* during the indicated stages of zebrafish development. The initial ubiquitous expression pattern becomes more anteriorly restricted as development progresses, although a caudal epidermal expression appears at later stages (see inset). From somitogenesis onwards, transcripts are detected in anterior somites (as), anterior and ventral retina (r), dorsal diencephalon (d), telencephalon (t), dorsal midbrain (dm), lateral hindbrain (lh), cerebellum (c) and the notochord (n).

To ensure the expression pattern that is shown in Fig 4.5 was specific for *smoc2* and not *smoc1* transcripts, the expression patterns of both genes were compared (Fig 4.6). At the onset of blood cell circulation, the expression pattern of *smoc1* mRNA didn't overlap with the expression pattern of *smoc2* mRNA. These expression domains were in line with the online available data and allowed us to conclude that the *smoc2* probe is specific for the detection of the *smoc2* transcripts (Thisse, 2001).

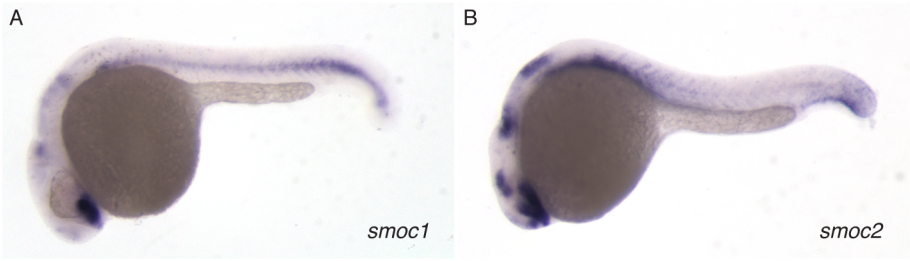

Figure 4.6: Differential expression of *smoc1* and *smoc2*

27 hpf; lateral view, anterior to the left. *smoc1* (A) and *smoc2* (B) transcripts were found in different tissues

Additionally, we performed RT-PCR analysis with *smoc2* specific primers at different developmental stages. Prior mid-blastula stage, we could detect *smoc2* mRNA indicating that maternal *smoc2* mRNA was present in the early embryo. After zygotic transcription was initiated, *smoc2* mRNA continued to be expressed throughout all further stages analyzed (Fig 4.7).

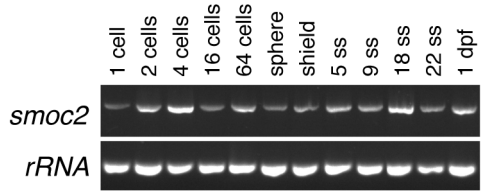

Figure 4.7: *smoc2* is expressed throughout all stages of zebrafish development

RT-PCR indicated *smoc2* mRNA is present in the embryo from early stages onwards and continues to be expressed after the mid-blastula transition.

Based on the sequence and expression analysis, we conclude that the *smoc2* sequence is evolutionary conserved with an identical domain organization across species and a high degree of amino acid sequence conservation. In addition, maternal *smoc2* mRNA is present before mid-blastula transition. During later stages of development, *smoc2* is expressed in a ubiquitous way. From mid-segmentation stages onwards, the expression becomes anteriorly restricted. Further experiments are required to determine the function of Smoc2 during zebrafish development.

4.3 *smoc2* loss of function

Two different morpholinos (MO) were used to perform the loss-of-function experiments. An ATG-MO, targeting the translation start site and a SPLICE-MO, targeting the first exon-intron boundary, prevents proper splicing of the pre-mRNA (Fig 4.8A). As a control for the splicing of intron 1, an RT-PCR analysis was performed 24 hours after injection with the SPLICE-MO (Fig 4.8B). With the first intron of *smoc2* spanning over 50 kb, no amplicon could be generated, using the primers F and R annotated in blue in Fig 4.8A. Co-injection with *smoc2* mRNA, where splicing already occurred, did allow for the amplification of the fragment as in the control conditions (Fig 4.8B). The morpholinos were co-injected with a *p53*-MO to prevent off-targeting effects and the associated activation of p53-mediated apoptosis (Robu et al., 2007). Both the injection of 1 nl of ATG- (0.4 mM, 3.5 ng) or the SPLICE-MO (0.4 mM, 3.6 ng) resulted in the same phenotype. For all subsequent experiments, the ATG-MO was used.

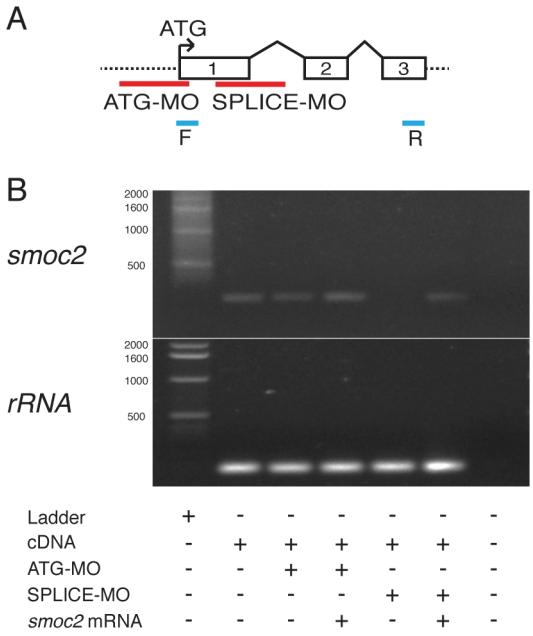

Figure 4.8: *smoc2* loss-of-function strategy

A. Diagram illustrating the MO and primer design. B. RT-PCR using primers F and R indicated in A to analyze the splicing of intron 1.

4.3.1 *smoc2* knock down results in a mild ventralization

Morphological analysis of morphant embryos at bud stage did not reveal apparent phenotypic abnormalities (Fig 4.9A-B). The first observable phenotypes in the morphants were detected during somitogenesis. At 15 ss, the posterior structures appeared compressed and reduced in length, and also the

somites lost their typical chevron pattern (Fig 4.9C-D). In general, the development of the morphants was delayed as compared to the control embryos. The time point when the first blood cells entered the circulation and started flowing through the dorsal aorta and the posterior cardinal vein was delayed by 2-3 hours (around 29-30 hpf in the morphants versus 26-28 hpf in the control embryos). At that moment, the location of the heart, development of the ear and initiation of the pigmentation of the eye were the same in control and morphant embryos. Therefore, and to correct for heterochronicity, the time point when the first blood cells started circulating was chosen to be a proper landmark for staging the embryos and comparing their phenotypes.

At the onset of blood cell circulation, the yolk sac extension (YSE) of the ATG-MO or SPLICE-MO injected embryos appeared reduced in length (Fig 4.9E-G: colored lines) and the tail was kinked (Fig 4.9E-G). Posterior from the YSE, the posterior blood islands (PBI) appeared to be enlarged and denser in the morphants as compared to the control embryos (Fig 4.9E-G). Closer investigation and measurement of the surface area of the PBI indicated a significant increase in their size in morphant embryos (Fig 4.9H-J). As development progressed, the morphant defects became more pronounced with heart and yolk sac edema, heart defects similar to the *heartstring* phenotype (Garrity et al., 2002) and a compression of the anterior head structures along the anterior posterior axis (data not shown).

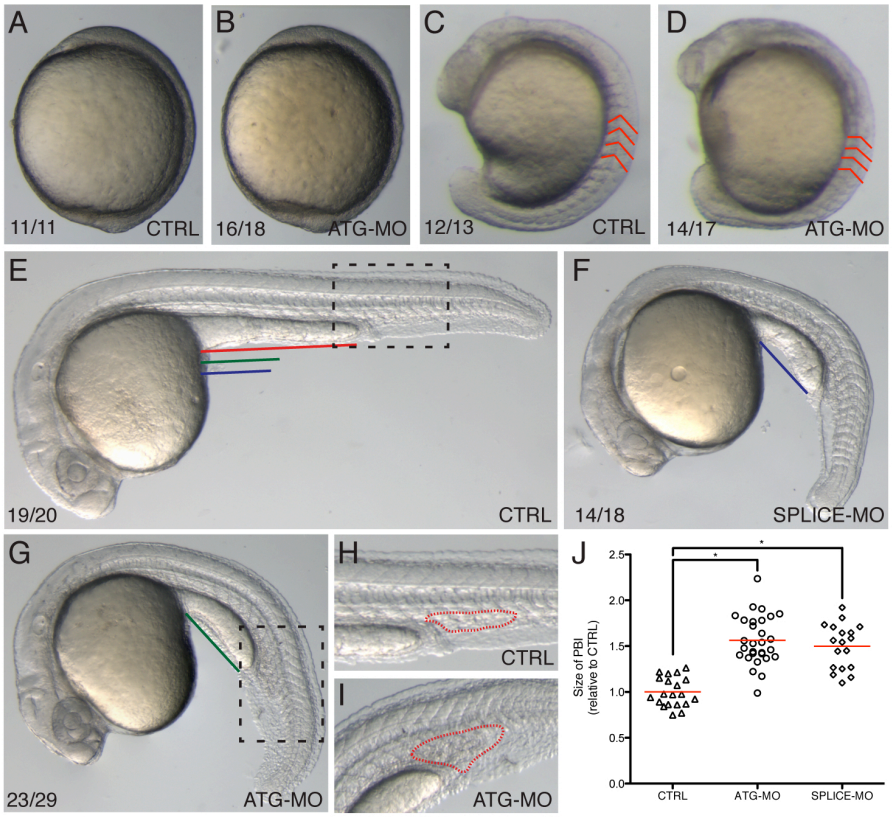

Figure 4.9: *smoc2* morphants present a mild ventralization defect

A-I. Lateral view of control embryos (A, C, E, H) and *smoc2* morphants (B, D, F, G, I) at bud stage (A-B; anterior to the top), 15 ss (C-D; anterior to the top) and the onset of circulation (E-I; anterior to the left). *smoc2* morphants presented anterior-posterior outgrowth defects (C-I), loss of 'v-shaped' somites (compare red lines in C-D), shortened yolk extension (compare colored lines in E-G), a downward curvature of the tail and denser and expanded blood islands (delineated with black dotted lines in E,G and magnification of the dotted region in H and I). J. Quantification of the surface of the PBI of control embryos (n=20), ATG morphants (n=29; * $p<0.05$) and SPLICE morphants (n=18; * $p<0.05$).

To analyze the specificity of the MO, we performed a rescue experiment with *smoc2* mRNA. As our ATG-MO only binds to the first five bases of the ORF, and is therefore unable to block translation of the in vitro synthesized mRNA, we could use the latter to restore the levels of *smoc2* (Fig4.10A-D). Co-injection of the *smoc2* ATG-MO with *smoc2* mRNA at the one-cell stage embryo resulted in a dose dependent rescue of the morphant phenotype at the onset of blood cell circulation. Up to 63% of the embryos lacked morphant specific defects after injection with 200 pg of *smoc2* mRNA (Fig 4.10E). Attempts to obtain a 100% rescue, with a higher concentration of *smoc2* mRNA, were unsuccessful due to the high number of early gastrulation defects induced by the *smoc2* mRNA (Fig 4.10C-D) (Vuilleumier et al., 2010). Co-injection of the SPLICE-MO with *smoc2*

mRNA resulted in a similar trend, although more embryos presented early gastrulation defects (data not shown). This was probably due to the late action of the SPLICE-MO and the presence of the maternal *smoc2* mRNA. Therefore the amount of functional Smoc2 accumulates, which results in more dorsalized defects.

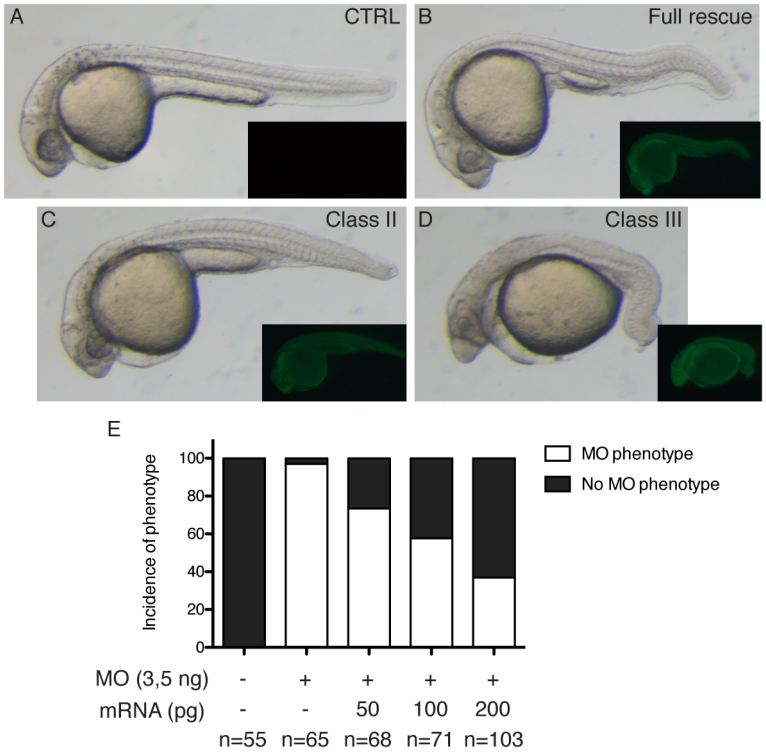

Figure 4.10: Co-injection of *smoc2* ATG-morphants with *smoc2* mRNA rescues the MO phenotypes
A-D. Different phenotypes after co-injection of *smoc2* ATG-MO (0.4mM) and *smoc2* mRNA (200 pg). A subset of embryos presented dorsalized phenotypes (C-D). Success of injection is monitored in insets. E. Injection of increasing concentrations of *smoc2* mRNA resulted in a higher percentage of embryos without the morphant phenotype.

Together, we showed that *smoc2* morphants displayed a mild ventralization defect with an apparent increase in the size of the PBI. This defect was shown to be specifically induced by the silencing of *smoc2*.

4.3.2 Molecular analysis of the PBI defect in the *smoc2* morphants

To confirm our morphological observation that the morphants had an expanded PBI, we performed WISH analysis using several PBI markers (*gata1, ikaros, draculin* (Fig 4.11A-F) and *hbbe1.1* (data not shown)) at the time point when the

first blood cells started flowing and could show that the transcription of these markers was apparently upregulated in the morphants and confirmed the morphological observation of the increase in the size of the PBI (Fig 4.11A-F). Interestingly, *mpx*, a marker for both the posterior and the anterior or rostral blood islands (RBI), appeared downregulated in *smoc2* ATG morphants in both populations of blood cell progenitors (Fig 4.11G-H) and co-injection with *smoc2* mRNA rescued the loss of *mpx* transcripts in both the RBI and the PBI (Fig 4.11J). This loss and rescue of *mpx* expression was also seen in the SPLICE morphants (Fig 4.11I, K) indicating that both *smoc2* morpholinos act specifically on the same transcript resulting in similar morphological and molecular phenotypes.

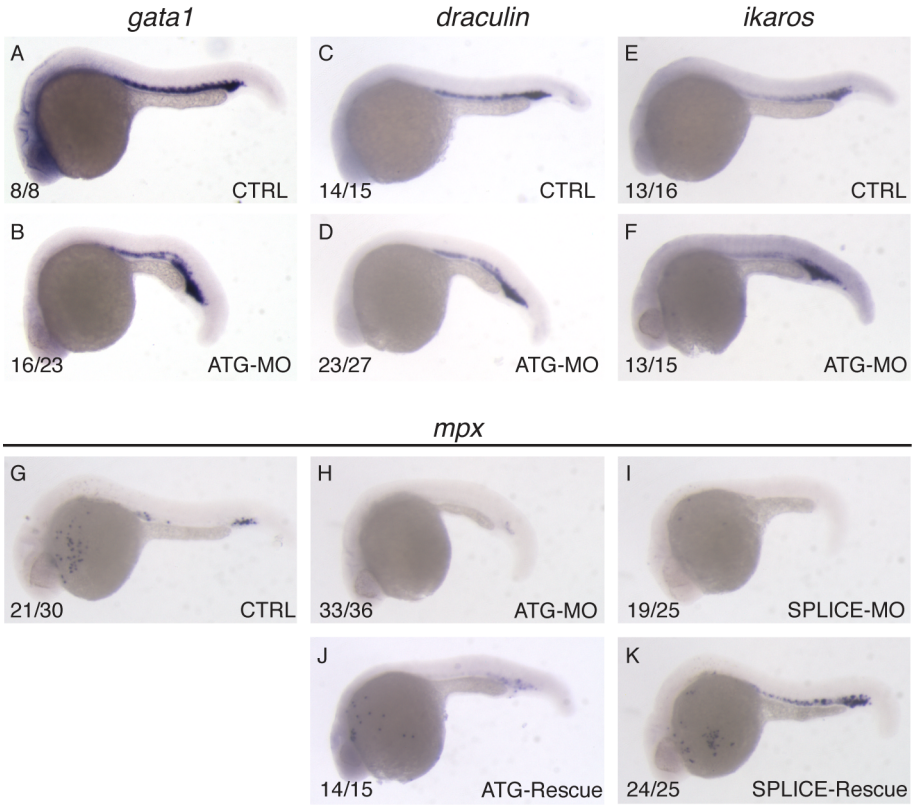

Figure 4.11: *smoc2* morphants display an enlarged PBI and a reduced expression of *mpx*.
Lateral view of control embryos (A, C, E, G), *smoc2* morphants (B, D, F, H, I), and rescued morphants ((J, K) at the onset of blood cell circulation. Analysis of the expression pattern of the PBI markers *gata1* (A-B), *draculin* (C-D) and *ikaros* (E-F). The neutrophil specific marker *mpx* (G-K) indicates an enlarged PBI with a reduction in *mpx* expression in both the PBI and the RBI. This signal was restored upon co-injection with *smoc2* mRNA.

The apparent morphological enlargement of the PBI is therefore supported by the results of the WISH analysis. Similar PBI phenotypes were seen in zebrafish

embryos where the levels of Bmp signaling were altered (Dal-Pra et al., 2006). Therefore, we investigated whether an early defect in dorso-ventral patterning caused this phenotype by analyzing the expression of *chordin*, at this stage the dominant Bmp antagonist, *vox* and *vent*, two Bmp target genes, and the phosphorylation status of the Smad1/5/8 proteins, the intracellular mediators of Bmp signaling (Imai et al., 2001; Gilardelli et al., 2004). Detecting a change in the *smoc2* morphants could provide us with a molecular mechanism that is needed to determine the function of Smoc2. Yet, when comparing the control embryos to the *smoc2* morphants, no change could be detected in either the expression domains or levels of *chordin*, *vox* or *vent*, or the activation of the Smad1/5/8 proteins (Fig 4.12).

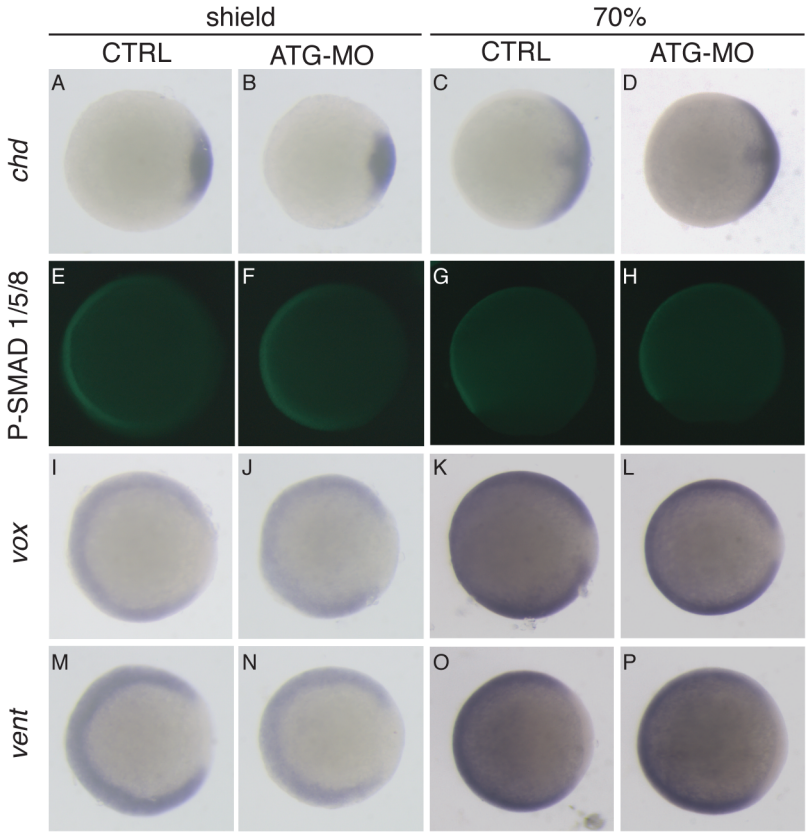

Figure 4.12: *smoc2* knockdown does not result in early dorso-ventral patterning defects.
A-D, E, F, I-L, M-P. Animal view, dorsal to the right. G, H. Lateral view, dorsal to the right. A-D, I-P. WISH analysis for the extracellular Bmp inhibitor chd (A-D) and the Bmp target genes *vox* (I-L) and *vent* (M-P) (n≥19). E-H. Immunostaining for phosphorylated Smad1/5/8 proteins (n≥23).

The enlargement of the PBI could not be attributed to a change in early Bmp signaling. However, this defect could be caused by the impaired axial outgrowth,

meaning this could be a secondary defect. Therefore, and as *smoc2* was predominantly expressed in the anterior half of the zebrafish and as there appears to be a defect in the RBI, next to the defect in the PBI, we focused our attention on the anterior domain.

The anterior lateral plate mesoderm is the primary site for embryonic myelopoiesis. As *smoc2* dependent regulation of these myeloid cells is only possible when *smoc2* is expressed in the proximity of myeloid regulatory genes, we analyzed the expression pattern of *smoc2* in relation to the expression pattern of *tal1* and *spi1b*, two regulatory genes required for the induction and differentiation of the myeloid lineage. As the protocol for dual colored WISH analysis was not optimized in the lab, we performed this expression analysis in relation to *krox20,* the marker for rhombomere 3 and 5 (Fig 4.13) (Thisse, 2001). At the 5 ss, a weak but apparent *smoc2* expression in the anterior lateral domain could be detected in proximity of *tal1* and *spi1b* expression (arrow in Fig 4.13C). According to the publically available data of Thisse, this anterior expression of *smoc2* is restricted to the epidermis (Thisse, 2001). Additional marker analysis is required to confirm this.

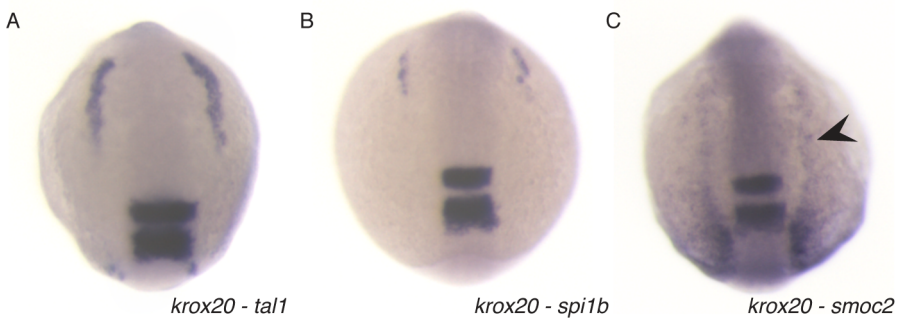

Figure 4.13: *smoc2* is expressed in the proximity of *tal1* and *spi1b* expressing cells.
Dorsal views, anterior to the top of uninjected embryos at 5 ss. Analysis of the expression pattern of *tal1* (A), *spi1b* (B) and *smoc2* (C) in relation to *krox20* (rhombomere 3 and 5) (n≥20).

Together, we have shown that our morphological observation of an enlarged PBI was confirmed by the molecular analysis of PBI markers. These defects were shown not to be induced by a defective DV patterning at earlier stages of development. In addition, we detected an additional defect for the myeloid marker *mpx* in both the RBI as the PBI and we showed that *smoc2* was expressed

in close proximity of the hematopoietic regulatory genes *tal1* and *spi1b* in the ALPM, which suggests that *smoc2* could affect their function.

4.3.3 *smoc2* modulates early embryonic myelopoiesis

To further explore the anterior myeloid defect, we investigated the status of the hemangioblast in *smoc2* morphants by analyzing the expression of *tal1*, *lmo2* and *gata2*, the molecular markers for these precursor cells (Fig 4.14A-L) in the ALPM. At 12 ss, WISH analysis indicated a reduced expression level without an apparent change in the size of the domain of *tal1*. The qPCR analysis on RNA isolated from the anterior tissues confirmed the reduction in the expression level of *tal1* mRNA. This reduction could be rescued by co-injection with *smoc2* mRNA supporting the notion that the *tal1* phenotype was specifically induced upon knockdown of *smoc2* (Fig 4.14A-D). The expression of *lmo2* was also significantly reduced upon reduction of the levels of *smoc2* (Fig 4.14E-H). However, no significant change in expression levels of *gata2* could be detected (Fig 4.14I-L). Nevertheless, the significant reduction in *tal1* and *lmo2* expression in *smoc2* morphants supports the requirement for Smoc2 during hemangioblast development in the ALPM.

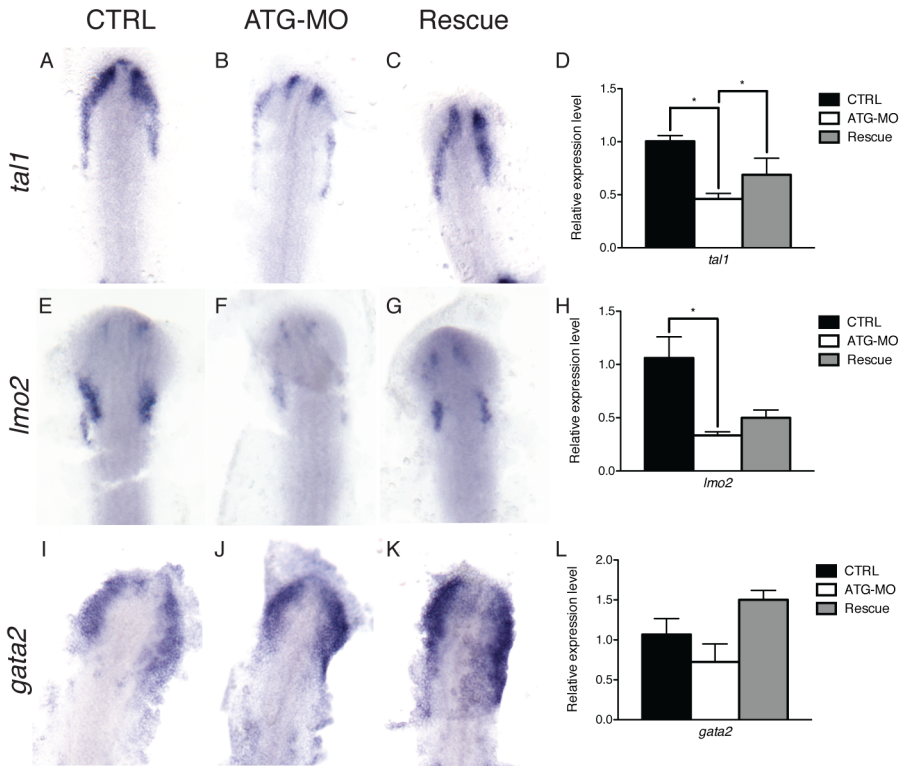

Figure 4.14: *smoc2* morphants display hemangioblast defects at 12 ss

A-C, E-G, I-K. Dorsal view of anterior lateral plate mesoderm; anterior to the top. WISH analysis for *tal1* (A-C), *lmo2* (E-G), *gata2* (I-K) of control embryos, ATG morphants and rescue embryos at 12 ss (n≥12).. D, H, L. Quantification of changes in expression levels by qPCR. Values plotted as mean ± SEM; n≥4; * p<0.05.

Within the myelopoietic lineage, the hemangioblasts develop into *spi1b* positive granulocyte-myeloid progenitors. In the ALPM, *spi1b* induces its own repressor, *runx1*, thereby creating a negative regulatory loop (Jin et al., 2012). WISH and qPCR analysis for *spi1b* and *runx1* at 12 ss showed a reduction in the expression domain and levels of both markers upon injection with *smoc2* MO (Fig 4.15A-H). For *spi1b and runx1*, the expression could be restored by co-injecting *smoc2* mRNA. The expression of another early myeloid marker, *c-myb*, apparently changed when analyzed by WISH but the quantification by qPCR did not support that observation (Fig 4.15I-L).

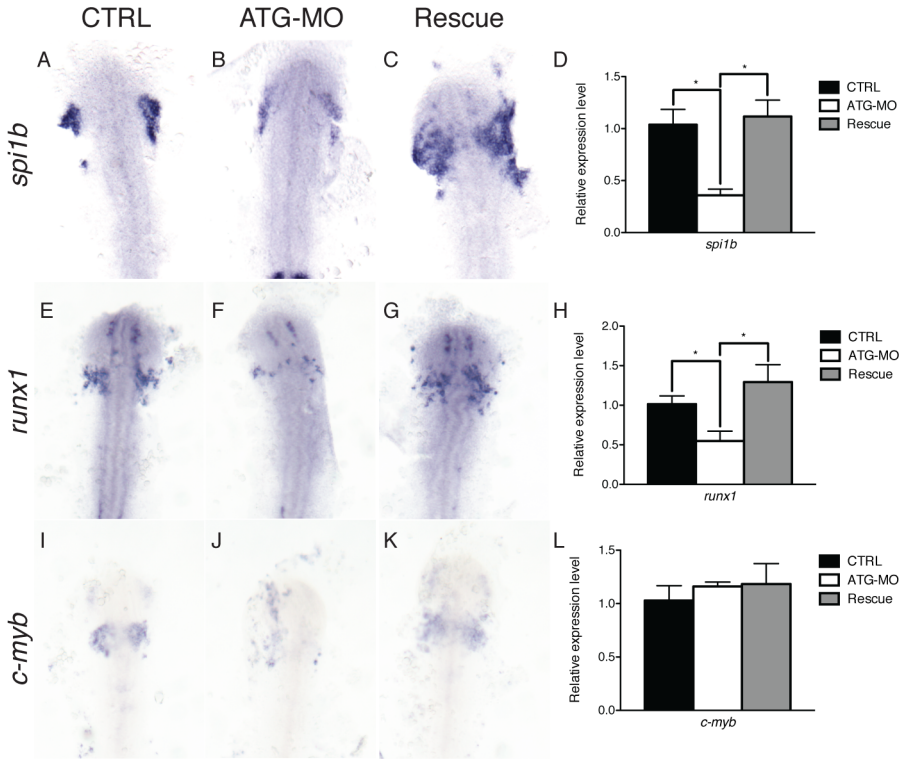

Figure 4.15: *smoc2* morphants display defects in embryonic hematopoiesis at 12 ss

A-C, E-G, I-K. Dorsal view of anterior lateral plate mesoderm; anterior to the top. WISH analysis for *spi1b* (A-C), *runx1* (E-G), *c-myb* (I-K) of control embryos, ATG morphants and rescue embryos at 12 ss (n≥12). D, H, L. Quantification of changes in expression levels by qPCR. Values plotted as mean ± SEM; n≥4; * p<0.05.

At 18 ss, the hemangioblast marker *tal1* did not change anymore, whereas *lmo2* still did significantly (Fig 4.16A-H). Similarly, the granulocyte-macrophage progenitor specific *spi1b* expression was still downregulated in the *smoc2* morphants (Fig 4.16I-L). In addition, *runx1* and *c-myb* showed a significant reduction in their expression in the *smoc2* morphants both by WISH and qPCR (Fig 4.16M-T). Co-injection with *smoc2* mRNA resulted in a significant restoration of the expression levels of all markers, except *lmo2* (Fig 4.16D, H, L, P, T).

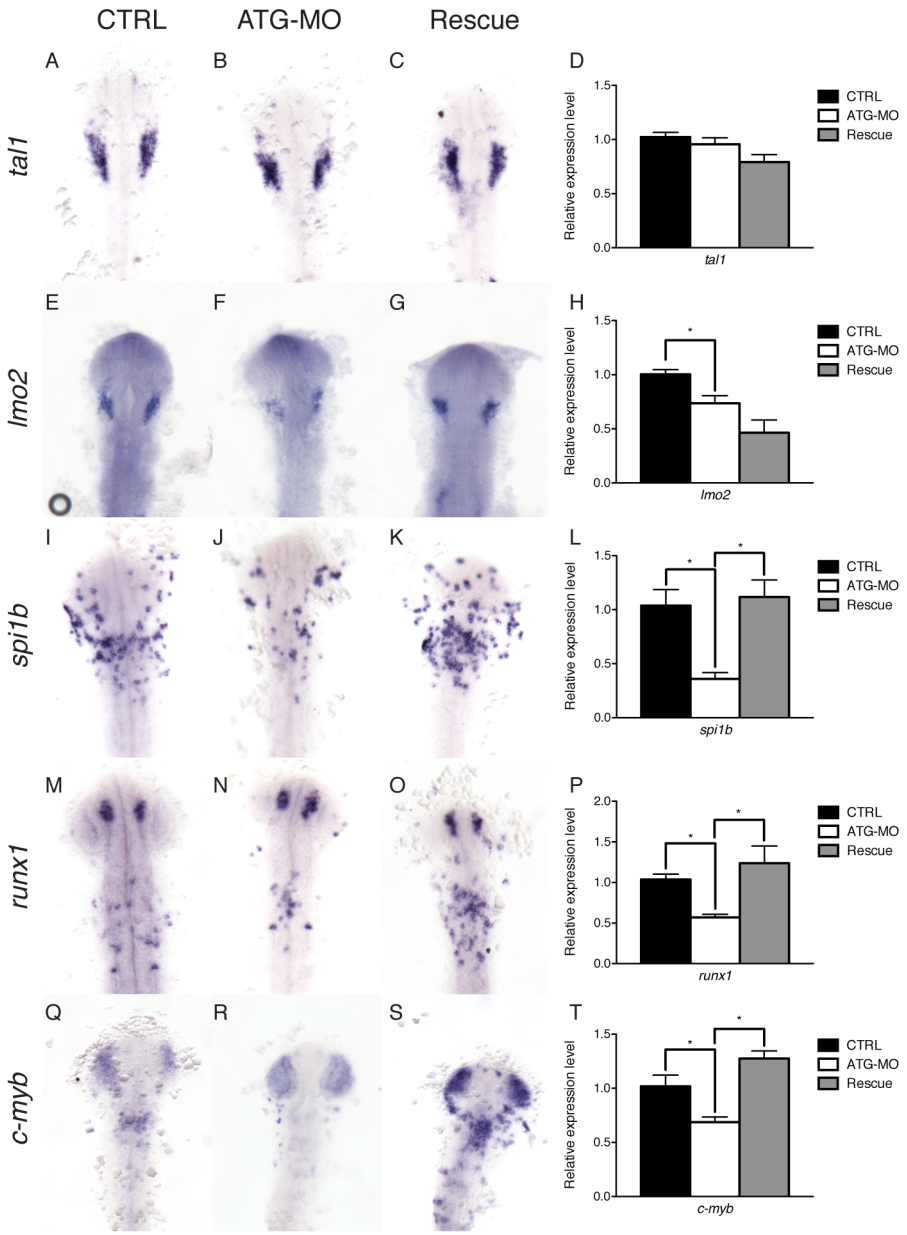

Figure 4.16: *smoc2* morphants display defects in embryonic hematopoiesis at 20 ss

A-C, E-G, I-K, M-O, Q-S. Dorsal view of anterior lateral plate mesoderm; anterior to the top. WISH analysis for *tal1* (A-C), *lmo2* (E-G), *spi1b* (I-K), *runx1* (M-O), *c-myb* (Q-S) of control embryos, ATG morphants and rescue embryos at 20 ss (n≥11). D, H, L, P, T. Quantification of changes in expression levels by qPCR. Values plotted as mean ± SEM; n≥4; * p<0.05.

spi1b was shown previously to downregulate the expression of the erythroid specific gene *gata1.* Hence, a reduction of Spi1b levels induced ectopic *gata1* expression in the ALPM at 24 hpf (Rhodes et al., 2005; Monteiro et al., 2011). However, our WISH and qPCR analysis did not indicate an ectopic expression of this erythroid marker at the onset of blood cell circulation (Fig 4.11A-B and data not shown).

In summary, during the initial stages of hematopoietic development, the knockdown of *smoc2* resulted in defective hemangioblast and myeloid progenitor development in the ALPM.

4.3.4 The myelopoietic defect induced by *smoc2* knockdown persists until the onset of circulation

At the end of segmentation, *spi1b* positive progenitors give rise to *irf8* and *csf1ra* expressing macrophages and *c/ebp1* and *mpx* expressing neutrophils. To investigate the effect of the early defects in *smoc2* morphants on myeloid development, we performed WISH and qPCR analysis for these marker genes. The earliest myeloid marker, *irf8*, specific for developing macrophages, was significantly downregulated in morphants at 18 ss (Fig 4.17A-D) (Li et al., 2011).
At the moment when the first blood cells start circulating, the macrophage defect persisted, as the number of *csf1ra* positive cells was reduced in the morphants compared to the control or the rescue condition (Fig 4.17E). Similar results were found when analyzing the *irf8*, *c/ebp1* or the *mpx* positive cells (Fig 4.17F-H).

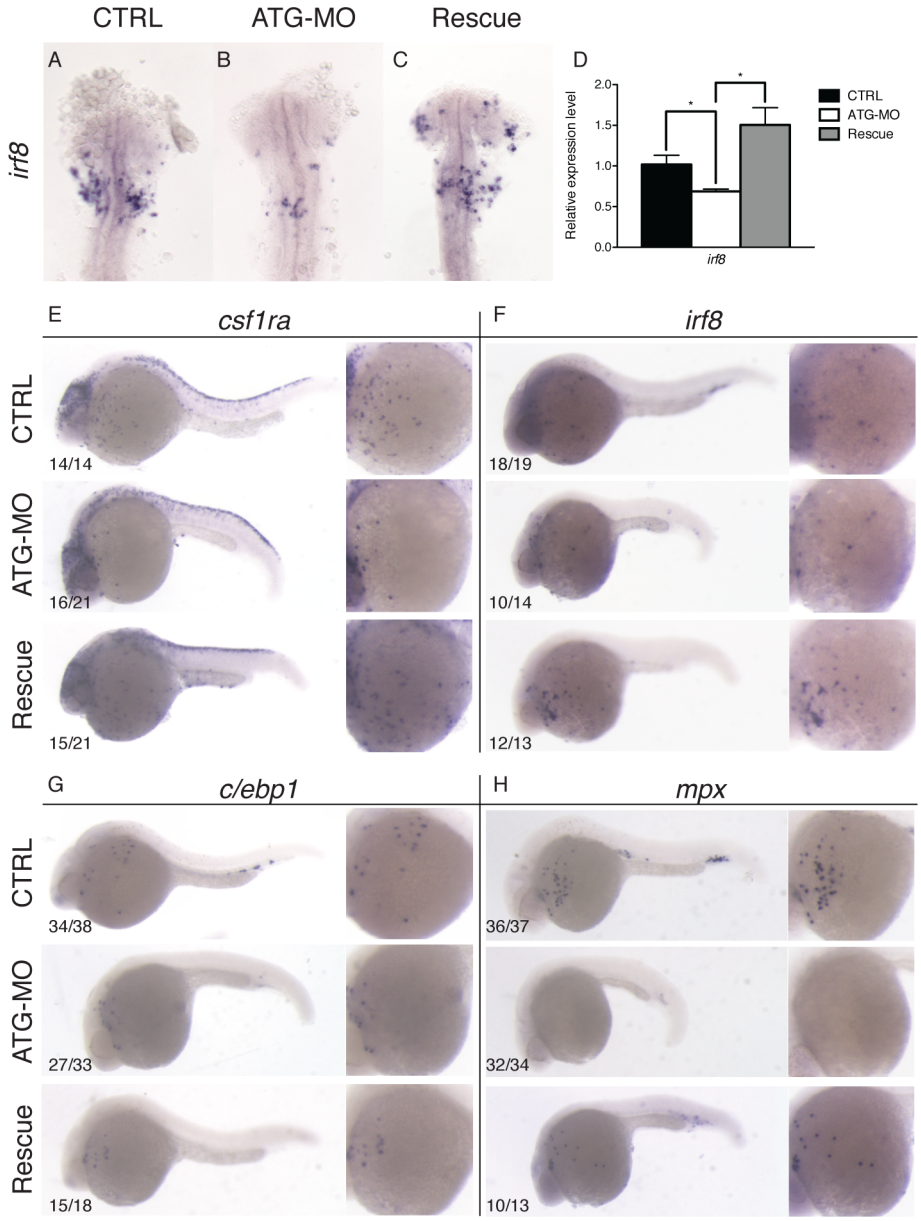

Figure 4.17: The early *smoc2* morphant defects result in defective myeloid development

A-C. Dorsal view of anterior lateral plate mesoderm; anterior to the top. WISH analysis for *irf8* (A-C) of control embryos, ATG morphants and rescue embryos at 20 ss (n≥11). D. Quantification of changes in expression levels by qPCR. Values plotted as mean ± SEM; n≥4; * p<0.05. E-H. Lateral views of the embryos, anterior to the left, dorsal to the top, at the onset of blood cell circulation. Analysis of the expression pattern of the macrophage marker *csf1ra* (E) and the early macrophage marker *irf8* (F), the early neutrophil marker *c/ebp1* (G), and the late neutrophil marker *mpx* (H).

To confirm the anterior myeloid defect at this late stage, qPCR analysis was performed on the anterior part of the embryo at the onset of blood cell circulation. For *csf1ra*, no quantitative analysis was performed, as *csf1ra* at this stage also marks the neural crest-derived pigment cells, masking the macrophage defect (Parichy et al., 2000). Although the WISH indicates a

decrease in the number of *irf8* positive cells, this could not be reproduced by the qPCR (Fig 4.18A). However, for *c/ebp1* and *mpx* a significant decrease in their expression levels could be detected (Fig 4.18B-C). This neutrophil defect persisted until later stages of development as the *Tg(mpx:GFP)*^{i114} transgenic reporter fish, used to study neutrophilic inflammation, still showed a significant reduction in the number of GFP positive cells as compared to the control embryos at 3 dpf (Fig 4.18D-E) (Gray et al., 2011).

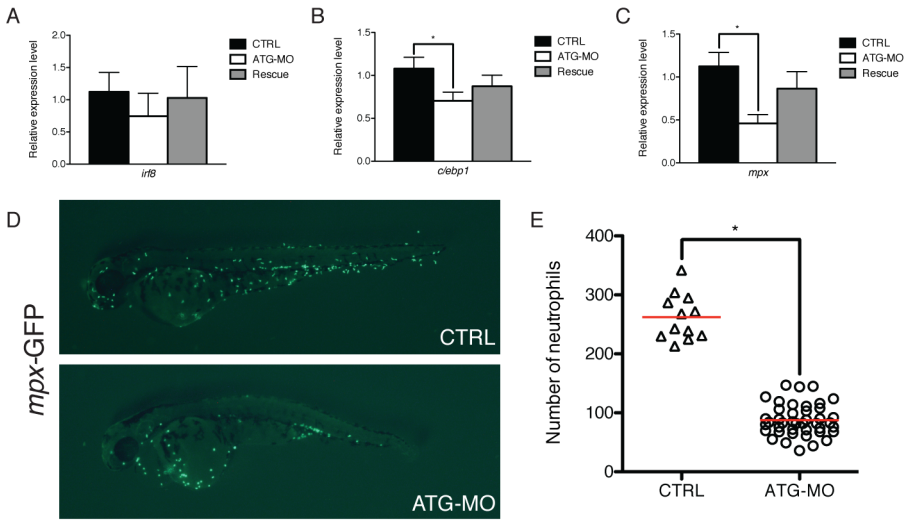

Figure 4.18: Quantification of neutrophil defect.

qPCR analysis of the early macrophage marker *irf8* (A), the early neutrophil marker *c/ebp1* (B), and the late neutrophil marker *mpx* (C). Values plotted as mean ± SEM; n=4; * p<0.05. D-E. Visualization and quantification of the *mpx*-positive cells using the mpx reporter embryos (Tg(*mpx*:GFP)^{i114}) at 3 dpf and the quantification of the number of neutrophils in the ATG morphants (n=42) as compared to the control embryos (n=12; * p<0.05).

In summary, the defect in hemangioblast and myeloid progenitor development resulted in a loss of neutrophils and macrophages at later stages of development.

4.3.5 *smoc2* does not modulate early cardiovascular development

During gastrulation, the interaction of multiple transcription factors (*gata4*, *gata5*, *gata6*, *tal1*, *nkx2.5* and *fli1*, among others) induces differentiation of the ALPM into hematopoietic, vascular and cardiac progenitors (Peterkin et al., 2009). qPCR analysis of the *smoc2* morphants for the mesodermal markers *gata4*, *gata5*, *gata6* and *ets1* did not indicate early mesodermal defects (Fig 4.19).

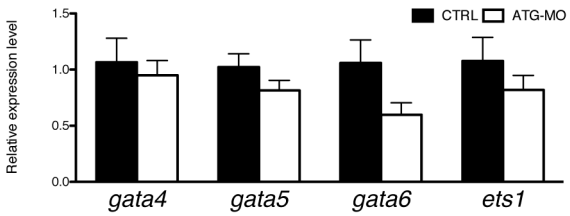

Figure 4.19: *smoc2* morphants do not present early mesodermal defects
qPCR analysis of the early mesodermal markers *gata4*, *gata5*, *gata6* and *ets1*.

To assess possible defects in cardiovascular development, we examined the effect of reducing *smoc2* levels on the expression of vascular and cardiac markers (Fig 4.20A-R'). Consistent with our morphological observations, no ectopic or loss of expression was seen in the expression pattern of the cardiac marker *nkx2.5* at 12 ss and 20 ss (Fig 4.20A-D) or the vascular markers (*fli*, *vegfc*, *flt4*, *flk1*, *dll4*) at 12 ss, 20 ss and at the onset of blood cell circulation (Fig 4.20E-R') (Chen and Fishman, 1996; Thompson et al., 1998; Ober et al., 2004; Hofmann and Luisa Iruela-Arispe, 2007). Also, the analysis of the vascular *Tg(fli:eGFP)*^{y1} and the cardiac *Tg(myl7:GFP)* reporter line at 24 and 50 hpf, respectively, did not indicate a defect in cardiac or vascular development (Fig 4.20Q-R' and data not shown) (Lawson and Weinstein, 2002; Huang et al., 2003).

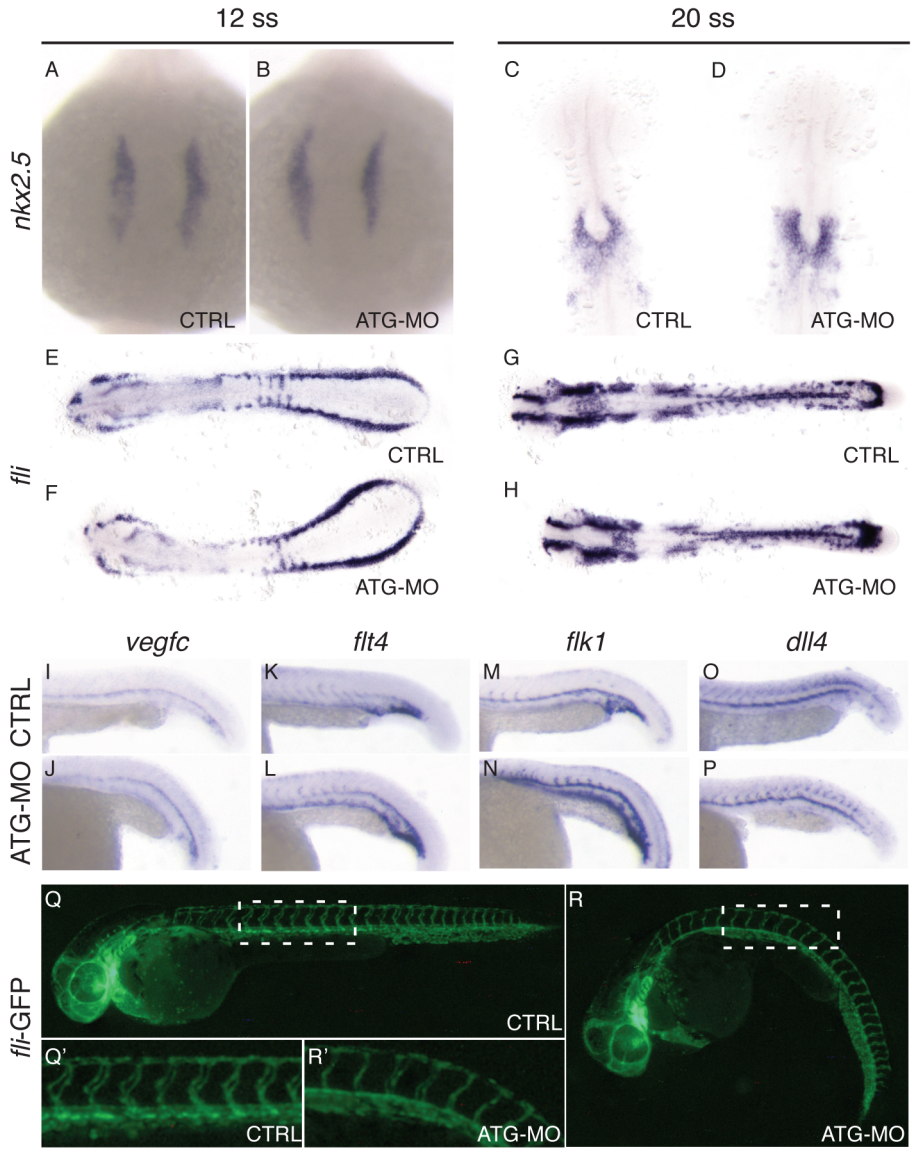

Figure 4.20: *smoc2* morphants do not display cardiovascular defects

Dorsal (A-D: anterior to the top; E-H: anterior to the left) and lateral view (I-P; anterior to the left) of embryos at 12 ss (A-B, E-F), 20 ss (C-D, G-H), the onset of circulation (I-P) and 50 hpf (Q-R'). Analysis of the expression pattern of the early cardiac marker *nkx2.5* (A-D), the vascular marker *fli* (E-H), the dorsal aorta marker *vegfc* (I-J), the marker for all venous and arterial cells *flt4* (K-L), the endothelial marker *flk1* (M-N) and the arterial marker *dll4* (O-P) (n≥14).. (Q-R') Vasculature in *fli* reporter embryos (*Tg(fli:eGFP)*^{y1}) at 50 hpf (n≥11).

In summary, Smoc2 deficiency did not influence the differentiation or outgrowth of the cardiovascular system.

4.3.6 *smoc2* affects the expression of Bmp target genes in the ALPM during embryonic myelopoiesis

It has been reported that Alk8-mediated Bmp signaling is required for rostral *spi1b* expression and the subsequent specification of myeloid progenitor cells in the RBI (Hogan et al., 2006). Therefore we performed a qPCR analysis on the ALPM at 12 ss to evaluate the effect of *smoc2* knockdown on members of the Bmp signaling cascade (Fig 4.21A). The expression level of the ligands *bmp2b* and *bmp4* did not change significantly. Neither did the expression of extracellular Bmp inhibitor, *chd*, nor the Bmp type I receptor *alk8*. However, the expression of the Bmp target genes *vox* and *ved*, was significantly downregulated in the *smoc2* morphants (Imai et al., 2001; Gilardelli et al., 2004). This reduction was partially rescued by co-injection of *smoc2* mRNA supporting the observation that *smoc2* knockdown could affect Bmp signaling without affecting the expression of the ligands, the receptor or its extracellular inhibitors. To confirm the qPCR result, we performed a WISH analysis for *vox* (Fig 4.21B-C). At 12 ss, the expression of *vox* in the anterior, and medial structures appeared to be reduced upon injection with the *smoc2* ATG-MO. Furthermore, the gradient at the posterior end of the embryo appears to be steeper when compared to the control condition (Fig 4.21B).

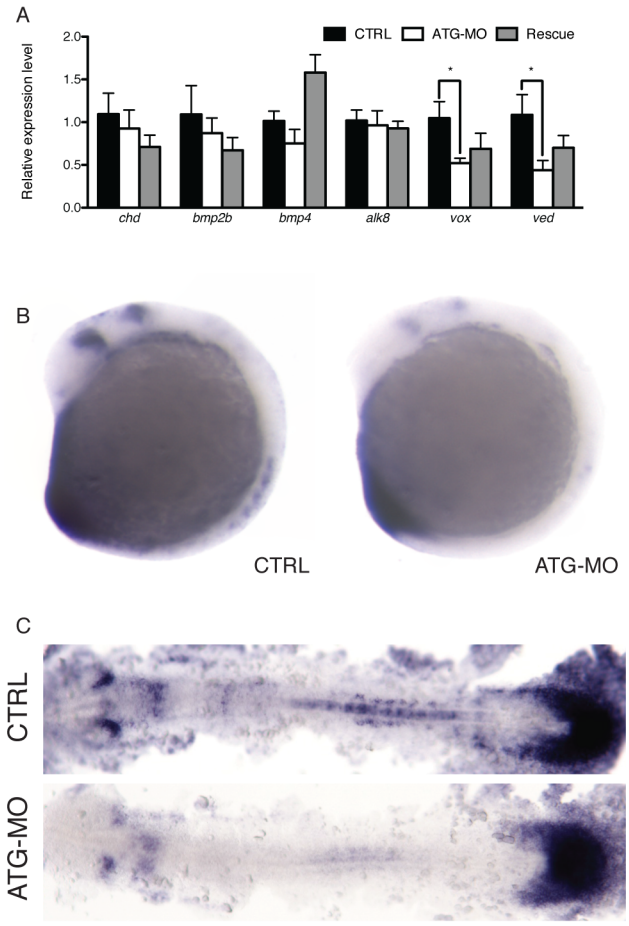

Figure 4.21: *smoc2* modulates Bmp signaling in the ALPM at 12 ss

A. qPCR analysis of members of the Bmp signaling cascade in the anterior lateral plate mesoderm of *smoc2* morphants. Values plotted as mean ± SEM; n=4; * $p<0.05$. B-C. WISH analysis of *vox* expression at 12 ss. Lateral views, anterior to the top (B); dorsal views, anterior to the left (C) (n≥25).

In summary, our results suggest that Smoc2 functions as a modulator of Bmp signaling as the expression levels and domains of Bmp target genes appears to be altered upon injection with a *smoc2* morpholino.

4.3.7 *smoc2* does not affect the expression of genes involved in osteoclastogenesis

In a recent publication, the level of C/EBPα, related to C/EBP1 and also involved during myelopoiesis, was shown to regulate the commitment to the osteoclast lineage in mice. Additionally, the transcription factors involved in the transition from the macrophage/monocyte lineage to the osteoclast lineage, *Spi1b*, *C-fos*, *Ctsk* and *Nfatc1*, were shown to be downregulated in the *C/ebpα* $^{-/-}$ mice (Chen et

al., 2013). Similarly, our analysis indicated a decrease in the expression levels of *spi1b* in the *smoc2* morphants. Therefore we wanted to investigate the effect of *smoc2* on the expression of *c/ebpα*, *c-fos*, *ctsk* and *nfatc1* in zebrafish embryos by qPCR. Importantly, at the stage at which the zebrafish were analyzed (the onset of blood cell circulation), no cartilage or bone tissue is formed yet. However, these genes are present in different tissues, like the brain and the heart among others, which enables us to still evaluate the effect of *smoc2* on the expression of *c/ebpα*, *c-fos*, *ctsk* and *nfatc1* albeit in a different tissue context. Using this approach, we could shed new light on the function of *smoc2* in the context of the joint, articular cartilage, and/or subchondral bone. However, none of the investigated genes showed a significant change in expression level at the onset of blood cell circulation upon injection of the *smoc2* MO (Fig 4.22).

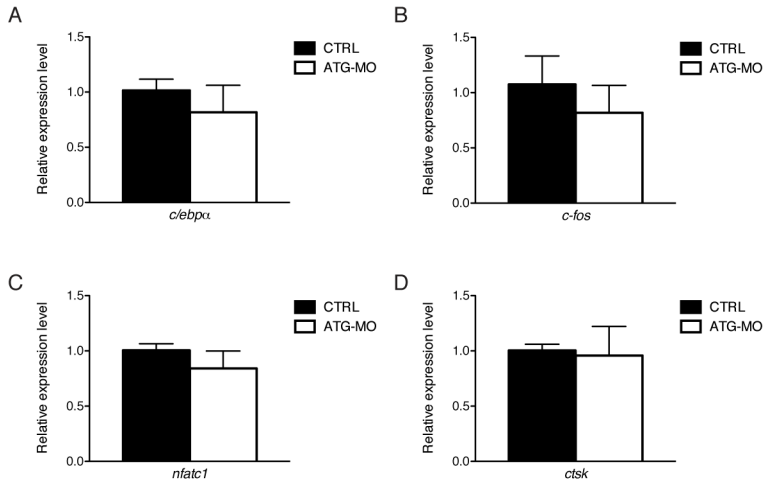

Figure 4.22: qPCR analysis of osteoclast related transcription factors *c/ebpα*, *c-fos*, *nfatc1* and *ctsk* at the onset of blood cell circulation.

4.3.8 *smoc2* loss-of-function influences cartilage and bone development

In an attempt to compare our results with the previously published data on *smoc2* morphants, we performed a skeletal staining of 6 days old control and *smoc2* morphant zebrafish embryos. Of the few morphants that survived until that stage, the majority presented defects in the skeletal elements (Fig 4.23A-D). The cartilagenous elements of both the viscerocranium and the neurocranium were smaller and appeared to contain less proteoglycans as the intensity of the Alcian Blue staining was reduced. However, the patterning and the development

of the different elements was unaltered. Furthermore, the reduction in Alizarin Red staining indicated that the ossification of the bones was reduced. The pharyngeal teeth were barely detectable, and other structures of both the viscerocranium (cleithrum, opercle and posterior branchiostegal ray) and the neurocranium (notochord and parasphenoid) also appeared less ossified. The reduced development of the pharyngeal teeth is in line with the publications on the importance of *smoc2* during craniofacial development. In contrast however, our study indicates that the maturation of the cartilage is affected whereas the data from the Melvin study suggested a patterning defect.

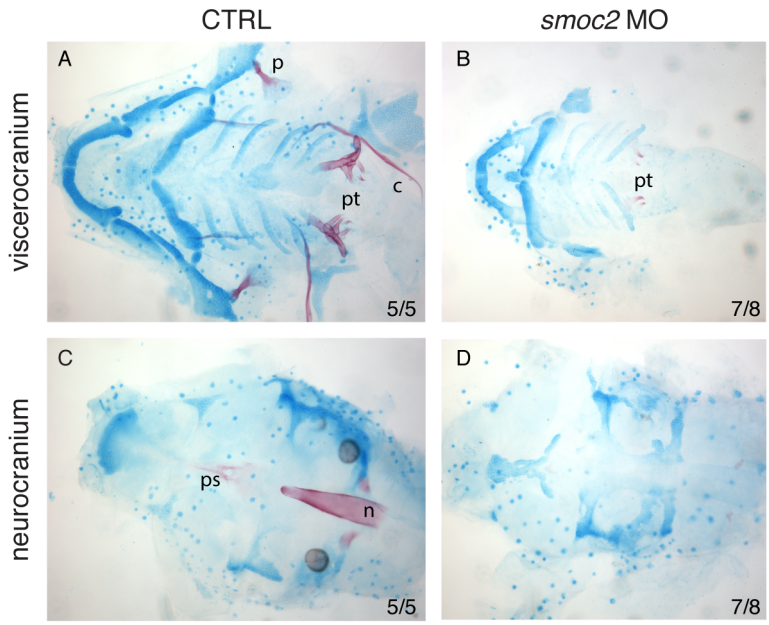

Figure 4.23: *smoc2* affects skeletal development at 6 dpf

A-D. Ventral view, anterior to the left. Cartilagenous elements are stained with Alcian Blue, ossified endogenous and dermal bones by Alizarin Red. p: posterior branchiostegal ray, c: cleithrum, pt, pharyngeal teeth, ps: parasphenoid, n: notochord.

4.4 *smoc2* gain of function

All the data presented in this section were initially obtained using the clone with the incomplete 3' end resulting in an incorrect very C-terminal protein sequence. Once the correct clone was generated, experiments were repeated and resulted in the same phenotypes indicating that the C-terminal sequence error did not contribute to the observable phenotype. Camila Esguerra initially performed all work on this gain of function approach. When she left the lab, I adopted the

project and reproduced all results. All presented data were collected and submitted for publication by Camila Esguerra with me as a shared first author.

4.4.1 *smoc2* overexpression results in dorso-ventral patterning defects

In order to further investigate the function of *smoc2* during zebrafish development, in vitro transcribed *smoc2* mRNA was injected into the yolk of one-cell stage zebrafish embryos. Injection with 200pg *smoc2* mRNA resulted in a range of dorsalized phenotypes at 24 hpf (class I-V, with class V being the most severe phenotype) and 48 hpf (Fig 4.24) (Little and Mullins, 2004). The incidence of the different classes was dose dependent, as even with low doses class V dorsalized embryos could be detected.

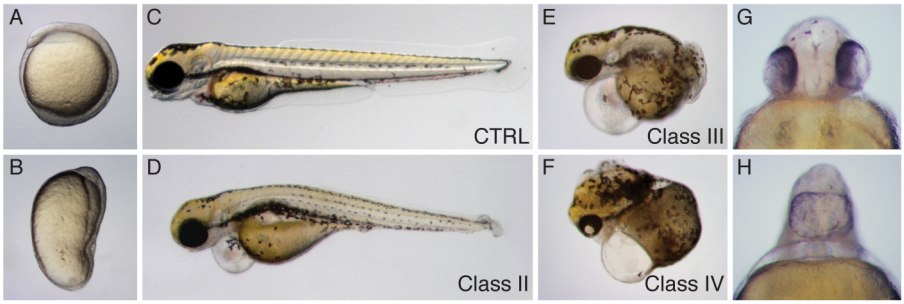

Figure 4.24: *smoc2* overexpression induced dorsalization

A-B. During somitogenesis, zebrafish injected with *smoc2* mRNA acquire an elongate egg shape (B). C-F. At 48 hpf, different classes of dorsalizations can be seen (n≥135). G-H. A subset of the embryos injected with *smoc2* mRNA develop cyclopia and synophtalmia. Injections and processing by C. Esguerra.

During somitogenesis the injected zebrafish embryos displayed an elongated egg shape, indicative of a defective dorso-ventral patterning (Fig 4.24A-B). At later stages, overexpression of *smoc2* mRNA resulted in defects in the caudal part of the zebrafish embryo, with loss of the ventral fin, shortening, curling or even loss of the trunk and tail structures (Fig 4.24C-F). Anteriorly, the fish presented malformed brain structures and in some severe cases a fusion of the eye fields resulting in synophthalmia at later stages of development (Fig 4.24G-H).

For the molecular characterization of the phenotype we analyzed the expression pattern of the mesodermal markers *ntl*, *myoD* and *pcdh8* (Fig 4.25) (Schulte-Merker et al., 1994; Weinberg et al., 1996; Yamamoto et al., 1998). All marker genes indicated a lateral expansion of the expression domain, wider axial

structures and somites stretching around the embryo. This all in combination with a defect in the anterior-posterior extension of the embryo. Both of these defects are typically indicative of defective convergence and extension movements (CE movements) during gastrulation stages. Note also the elongated shape of the embryos upon injection with *smoc2* mRNA.

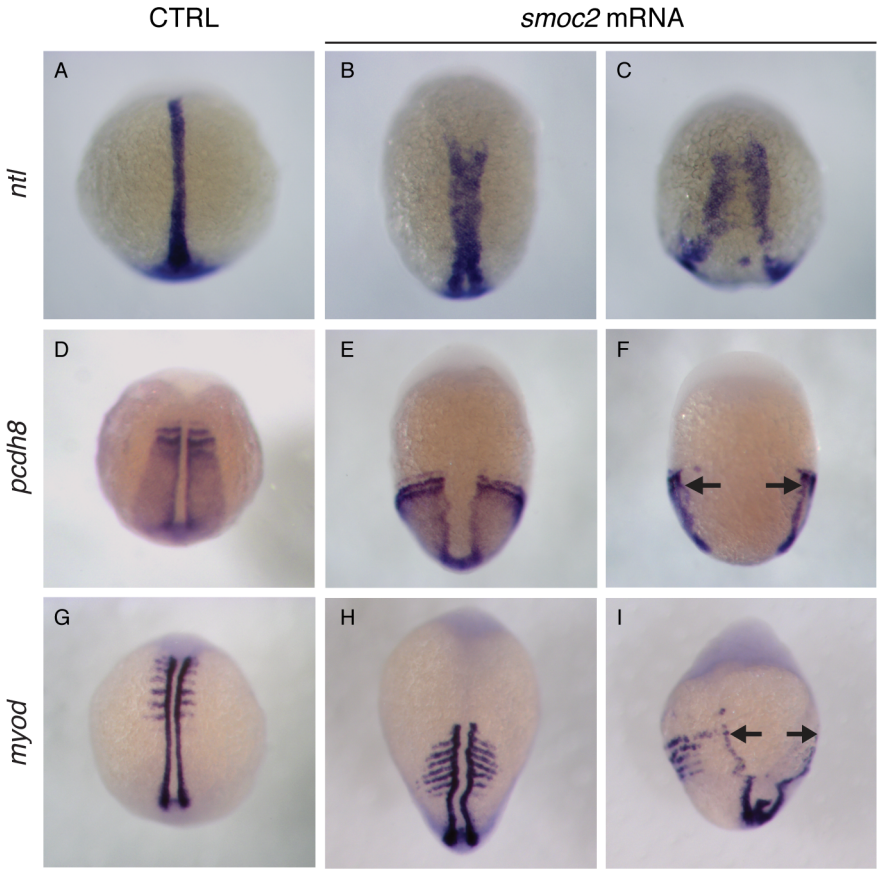

Figure 4.25: Mesodermal patterning defects when *smoc2* is overexpressed

WISH analysis of the expression pattern at 5-9 ss of mesodermal markers (*ntl*: axial mesoderm, *pcdh8*: paraxial mesoderm, *myod*: adaxial mesoderm) illustrates the conversion defect, with somites stretching all around the embryo; and the elongation defect with the failure of the mesoderm to migrate towards the anterior part of the embryo (n≥52). Injections and processing by C. Esguerra.

4.4.2 *smoc2* modulates Bmp mediated signaling

In an attempt to analyze the dorso-ventral patterning defects, we performed WISH analysis for the predominant Bmp inhibitor during pre-gastrula stages, *chordin* and for the Bmp target gene, *gata2* (Maeno et al., 1996; Schulte-Merker et al., 1997).

A mild, but apparent increase in *chd* expression, without a change in the expression domain, was detected in the embryos that were injected with *smoc2*

mRNA at shield stage. Two hours later, at 70% epiboly, this small difference could not be detected anymore. Concomitant with the increase in *chd* expression at shield stage, a discrete reduction in the expression of the *gata2* was seen (Fig 4.26).

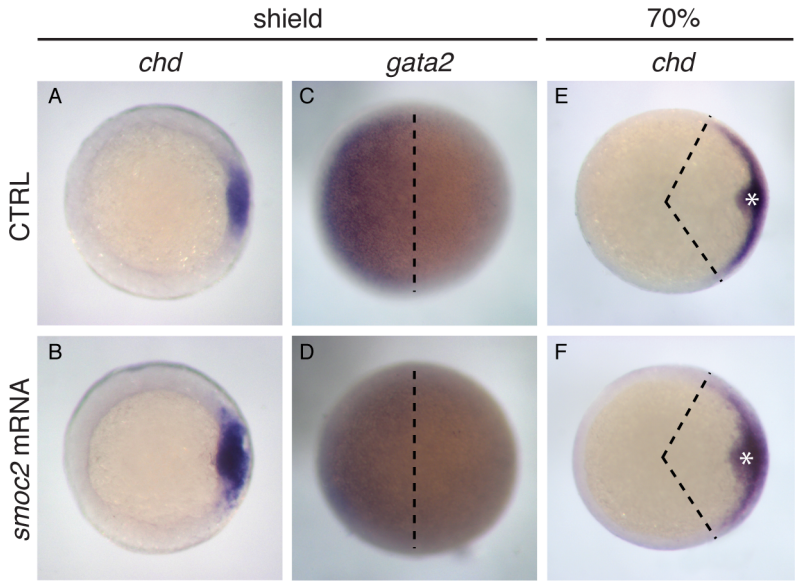

Figure 4.26: *smoc2* overexpression mildly affects dorso-ventral patterning

A-F Animal view, dorsal to the right. A-D. Shield stage; E-F 70% epiboly. WISH analysis for *chordin* (A-B, E-F) and *gata2* (C-D) (n≥30). Injections and processing by C. Esguerra.

Since the *chordin* expression analysis indicated a discrete increase in expression, we attempted to rescue the *smoc2* mRNA induced phenotypes by reducing the levels of *chordin*, using a *chd* MO. Molecular analysis of the embryos, using the paraxial mesodermal marker *pcdh8*, indicated that the dorso-ventral patterning defect was rescued upon co-injection with *chd* MO. The CE defects however appeared to be still present (Fig 4.27). Co-injection of *smoc2* mRNA with *chd* MO, was therefore unable to fully rescue the *smoc2* mRNA induced phenotype.

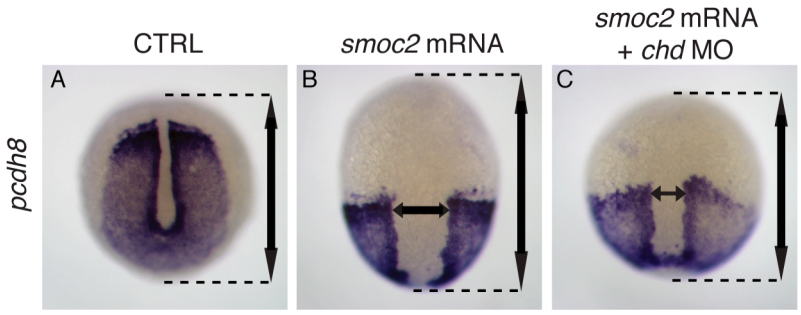

Figure 4.27: *smoc2* overexpression is partially rescued by injection with *chd* MO

A-C. Dorsal view, anterior to the top. WISH analysis for *pcdh8* at the 5-9 ss in control, *smoc2* mRNA injected and *smoc2* mRNA, *chd* MO injected embryos (n≥20). Injections and processing by C. Esguerra.

4.4.3 *smoc2* modulates *wnt5b* mediated signaling

Since CE movements are mainly regulated by the non-canonical Wnt signaling pathway we investigated the effect of co-injecting *smoc2* mRNA with the mRNA of different Wnt ligands (Rauch et al., 1997; Heisenberg et al., 2000; Kilian et al., 2003).

Injection of *wnt5b* resulted in a ventralized embryo with severe anterior defects, a loss of head structures, an enlarged yolk sac extension and a compressed tail (Fig 4.28A, C) (similar to (Westfall et al., 2003). In contrast, the *smoc2* gain-of-function resulted in a loss of the dorsal structures (Fig 4.28A-B). Co-injection of *smoc2* and *wnt5b* rescued these defects (Fig 4.28D-I). 50% of the embryos were fully rescued whereas the other 50% were class I or class II dorsalization phenotypes.

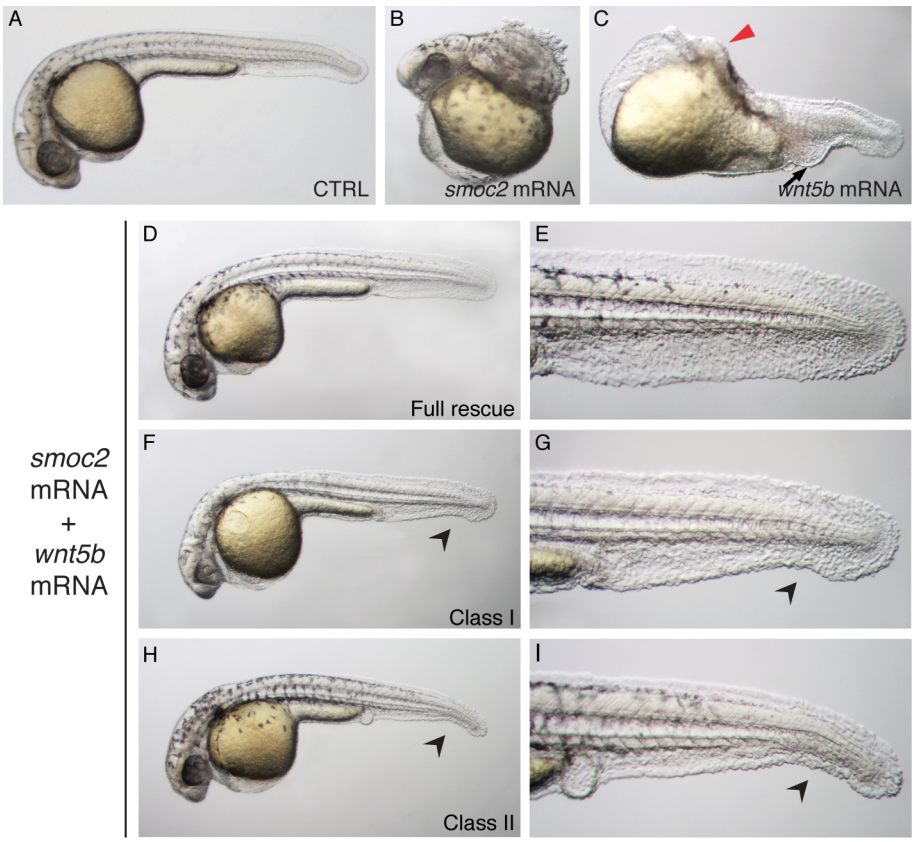

Figure 4.28: Co-injection of *wnt5b* mRNA rescues the *smoc2* mRNA induced phenotype

Injection with *smoc2* mRNA or *wnt5b* mRNA results in opposite defects with the loss of posterior structures and the loss of anterior structures respectively. Upon co-injection of *smoc2* and *wnt5b* mRNA, 50% of the

zebrafish appeared normal at 24 hpf, while the other 50% only displayed a mild dorsalization with (partial) loss of the ventral fin (n≥101). Injections and processing by C. Esguerra.

The *wnt5b*-mediated rescue was shown to be specific as co-injection with another non-canonical *wnt* (*wnt11*) or a canonical *wnt* (*wnt8*) did not rescue the morphological defects of *smoc2* overexpressing embryos (Fig 4.29). Co-injection of *smoc2* mRNA with *wnt8.1* or *wnt11* resulted in a similar distribution of dorsalized phenoytpes, indicating *wnt11* and *wnt8.1* do not interfere with the *smoc2* mediated signaling events.

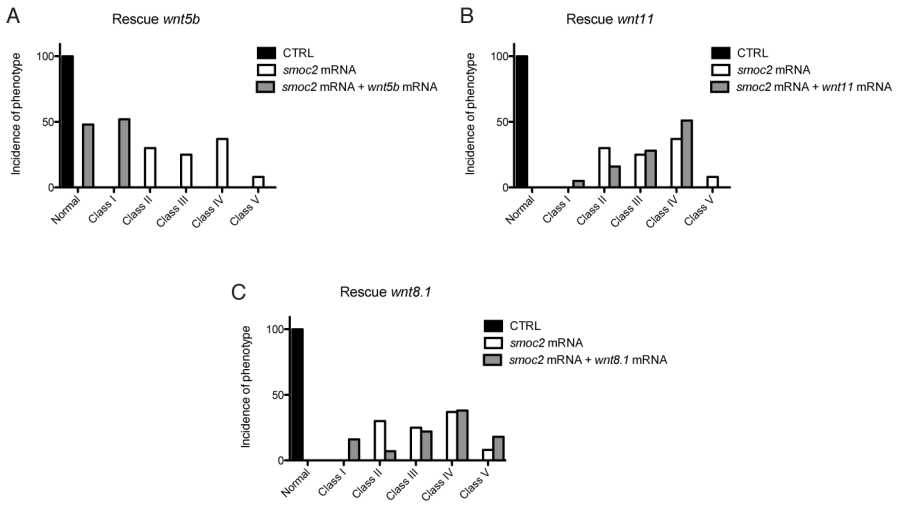

Figure 4.29: The rescue of *smoc2* dorsalized phenotypes is specific for *wnt5b*

The distribution of dorsalized phenotypes induced by *smoc2* mRNA shifts to less severe phenotypes when coinjected with *wnt5b* (n≥101). Co-injection with *wnt11* (n≥100) or *wnt8.1* (n≥45) does not have the same effect as similar distribution of the phenotypes can be seen as with single *smoc2* injection. Injections and processing by H. Mommaerts.

Molecular analysis of this rescue was done by performing a WISH analysis using the mesodermal marker *pcdh8,* which confirmed our observation that the *smoc2* mediated phenotype could be rescued by overexpressing *wnt5b* mRNA (Fig 4.30). Both the dorsalization of the embryo and the convergence and extension defects were rescued, as the embryo lost its egg shape and the expression pattern of paraxial mesodermal cells (*pcdh8*) appeared normal.

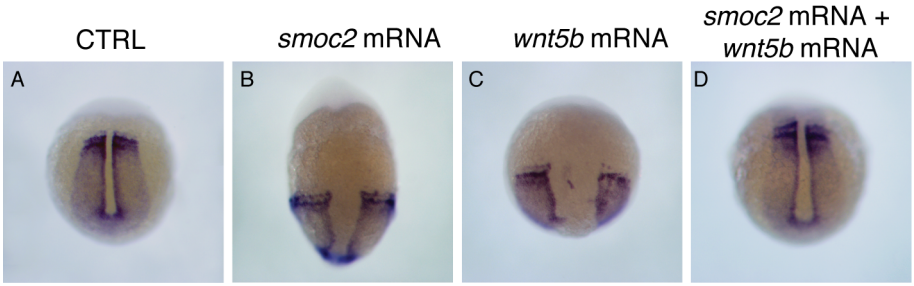

Figure 4.30: *wnt5b* rescues the *smoc2* induced dorssalization and conversion and extension defects

WISH analysis of *pcdh8* expression, 1-3 somite stage, dorsal view, anterior to the top. Co-injection of *smoc2* and *wnt5b* results in the rescue of the dorsalization and a rescue of the paraxial *pcdh8* expression pattern (n≥25). Injections and processing by C. Esguerra.

4.5 Generation of tools to study the function of Smoc2 domains in zebrafish

As moc2 is a secreted protein, it is likely to interact through its domain(s) with matrix molecules, ligands, receptors or cofactors. The first step in unraveling the function of the different domains is the generation of mutant clones of *smoc2* in which the domain of interest is deleted. We systematically generated clones in which the EC domain, the SMOC domain or the FS domain was absent. Based on the amino acid sequence, primers were generated to perform a series of PCRs to remove the region flanked by the middle primers (Fig 4.31).

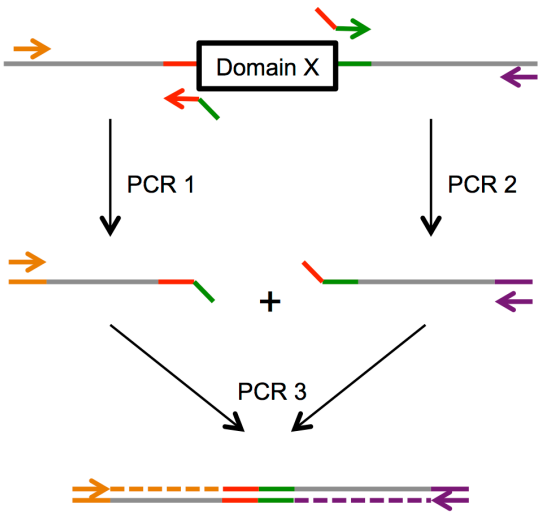

Figure 4.31: Schematic representation of PCR strategy

Subsequent PCRs, with partially overlapping primers, induce the amplification of a fragment in which domain X is removed.

We generated 3 PCR fragments of the *smoc2* ORF each lacking a specific domain (Fig 4.31, 4.32). Subcloning them in pCS2+ allowed us to generate capped and polyadenylated mRNA in vitro, suitable for injection in the zebrafish.

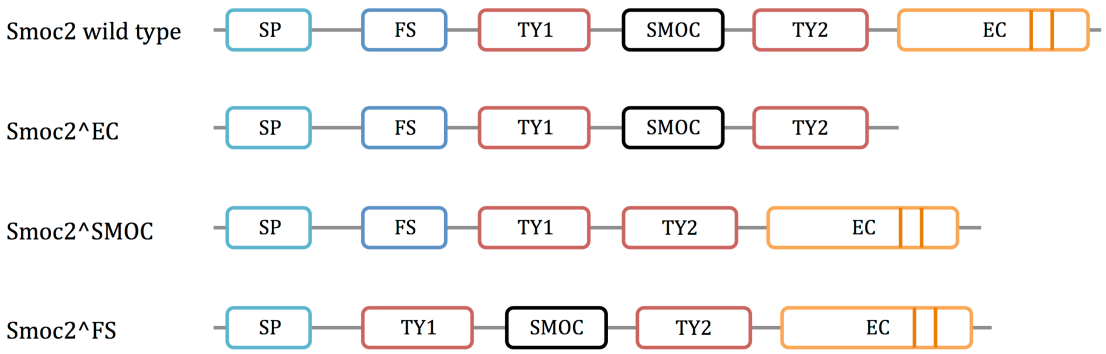

Figure 4.32: Schematic representation of the different Smoc2 mutants

Preliminary injections with these mutant constructs (Fig 4.33) and scoring at 1 dpf indicated that the loss of these domains did not affect the function of Smoc2. Injected embryos still displayed a range of dorsalized phenotypes, similar to the *smoc2* wild type overexpression phenotypes. Interestingly, the incidence of severely dorsalized embryos was reduced when the FS mutant was overexpressed (Fig 4.33). Whether this is due to a decreased mRNA stability or due to a disturbed function of the protein is yet to be determined. In addition, further studies are necessary to investigate the effect of the loss of these domains on the rescue of the morphant phenotype, allowing us to determine the role of that specific domain in the absence of endogenous *smoc2*.

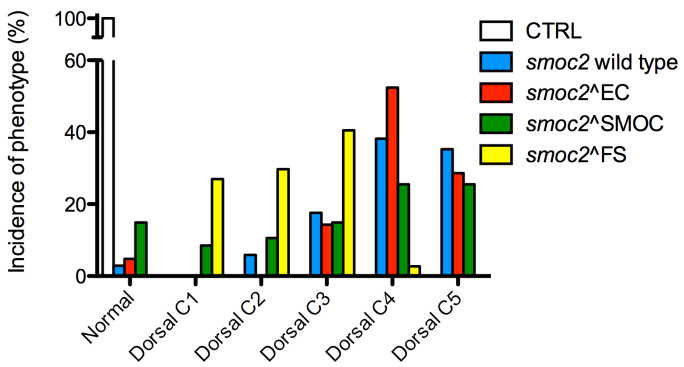

Figure 4.33: Scoring of the phenotypes after overexpressing *smoc2* mutants

Chapter 5:

Functional study of SMOC2 using the chicken limb model

The function of Smoc2 in the joint cannot be investigated in the zebrafish for the obvious reason that the zebrafish does not have limbs and joints, similar to human limbs and joints. So in order to investigate the effect of SMOC2 on the development of cartilage, bone and joints we turned to the chicken limb model. These data were included in the master thesis of Laura-An Guns (supervised by H.M.).
Previously, gain of function approaches by means of electroporation, retroviral infection or transgenics have shown that the chicken model provides powerful tools for embryologists (Mozdziak and Petitte, 2004; Funahashi and Nakamura, 2008; Gordon et al., 2009). The chicken model system and the RCAS delivery system were fully optimized in the lab by Nathalie Brison and have resulted in a few successful publications (Fantini et al., 2009; Brison et al., 2012).

We cloned chicken *SMOC2* ORF by PCR using primers that were based on online available ESTs. The resulting fragment was cloned in the pSLAX12 shuttle vector and subsequently in the RCASBPA viral vector. Care was taken to ensure that the chicken *SMOC2* ORF was in frame with the rest of the viral genes. Next, we transfected DF1 cells in vitro to produce and collect the virus. Similar steps were undertaken to clone the *GFP* ORF into the RCASBPB vector. Using the RCAS specific 3C2 monoclonal antibody the titer of the viruses was determined to be at least 1x10^8 cfu. RCASBPA-*SMOC2* and RCASBPB-*GFP* were mixed in a 70:30 ratio and injected in the prospective hindlimb of a HH10 stage chicken embryo. The embryos were incubated until stage HH22-24 when they were harvested for further analysis of the phenotype. Successful injections were selected based on the presence of a unilateral GFP signal.

Preliminary morphological comparison of the green, infected limb with its contralateral control indicated an outgrowth defect of the limb in 10% of the injected embryos (Fig 5.1).

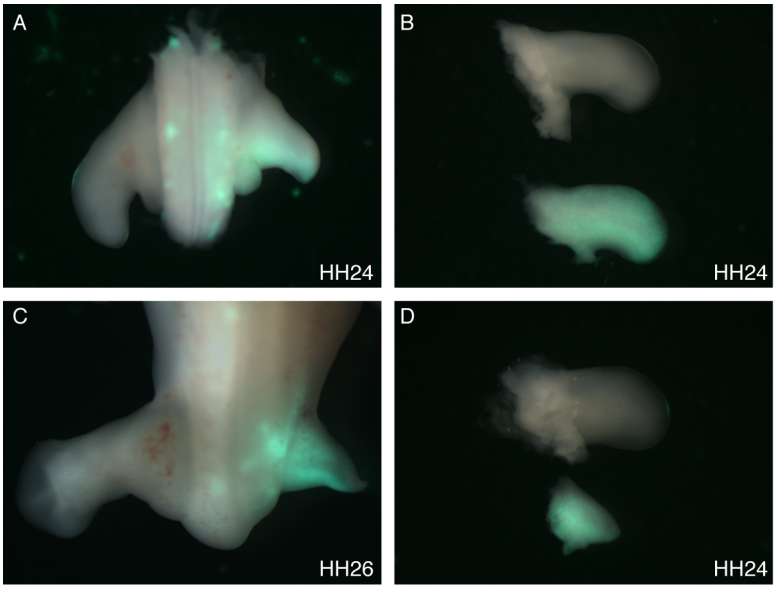

Figure 5.1: Morphology of RCASBPA-*SMOC2* and RCASBPB-*GFP* injected embryos

Dorsal view, anterior to the top. 10% of the limbs injected at HH10 present an outgrowth defect at HH24-26. The severity of the defect depends on the titer of the virus and on the rate of infection with the RCASBPA-*SMOC2* virus.

The harvested limbs were further processed for molecular analysis by means of WISH for genes that are known to regulate the outgrowth of the limb (Fig 5.2). Using in-house probes, we could detect a change in the expression of *FGF8,* a marker of the apical ectodermal ridge, in the RCASBPA-*SMOC2* injected limb as compared to the uninjected contralateral control (Fig 5.2D). Although WISH cannot be used for the quantification of expression, the pattern appears to be less intense. Furthermore, the domain of expression appears to be reduced, potentially explaining the reduced size of the limb.

The expression domains of the other available probes (*SHH* for the ZPA and *BMP2* and *dHAND* for posterior mesenchyme) were unaltered when *SMOC2* was overexpressed in the chicken limb (Fig 5.2A-C).

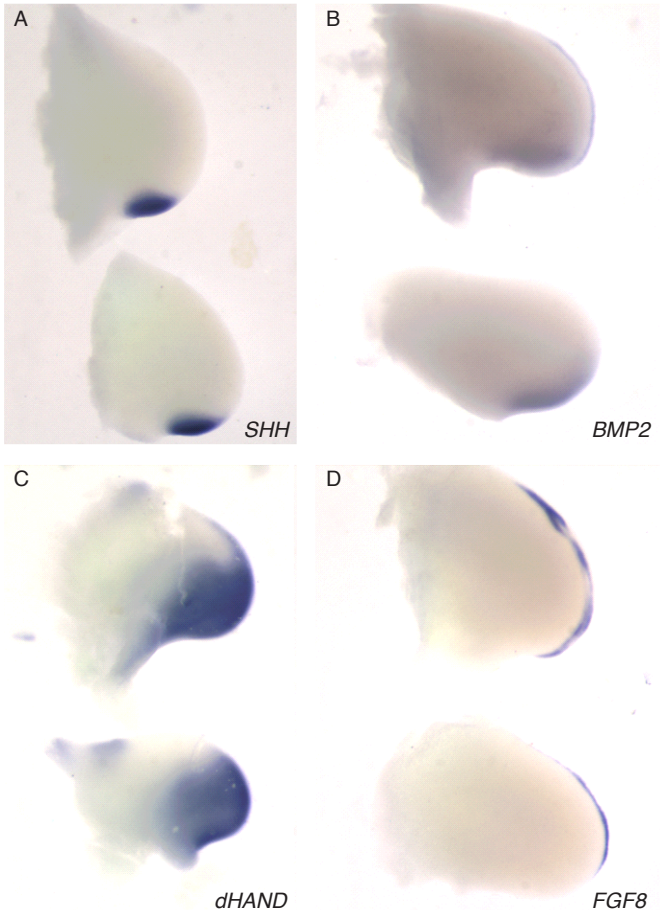

Figure 5.2: *SMOC2* overexpression induces a decrease in the expression of *FGF8* in the AER

Dorsal view, anterior to the top. Expression analysis using WISH for *SHH*, *BMP2*, *dHAND* and *FGF8*. Top limbs are the uninjected contralateral control, bottom limbs are the RCASBPA-*SMOC2* injected limbs.

In summary, we have generated the tools to investigate SMOC2 function in the developing chick limb. Our preliminary analysis indicated that the ectopic application of *SMOC2* resulted in a defective outgrowth of the embryonic limb. This defect could be attributed to the reduced expression of *FGF8*, one of the key molecules to regulate limb outgrowth.

Chapter 6:

Preliminary characterization of *Smoc2* null mice

To further clarify the role of SMOC2 during embryonic development, we used the mouse model to create a *Smoc2* null mouse. The generation of heterozygous animals was outsourced to the Texas A&M Institute for Genomic Medicine (www.tigm.org). The first exon of *Smoc2* was replaced by a LacZ cassette, thereby removing the translation start site and preventing the proper translation of the protein (Fig 6.1A). Additional downstream translation start sites could give rise to a truncated protein. However, the secretion of a potential protein is prevented as the signal peptide is lost. Long range PCR was performed to confirm the replacement of exon 1 with the LacZ cassette (personal communication with Andrei Golovko, TIGM) and indicated that in all samples the recombination event has taken place (Fig 6.1B)

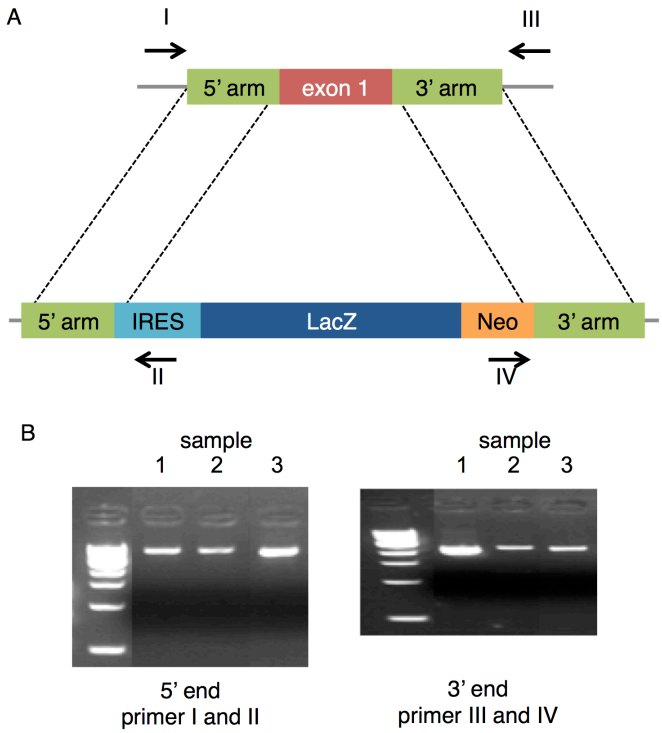

Figure 6.1: *Smoc2* targeting strategy

A. Schematic representation of the *Smoc2* targeting strategy. B. Long-range PCR as a control for the recombination with the primers indicated in A.

Heterozygote adult mice appeared healthy and were fertile. Crossing of *Smoc2* heterozygotes resulted in small litters (7-9 pups) with a normal morphology. Genotyping of these pups indicated that only wild type (±30%) and heterozygous mice were born. To screen for subtle differences, limbs of *Smoc2* wild type and

Smoc2 heterozygous embryos were isolated at birth and processed for skeletal staining and H&E staining (Fig 6.2). No differences in size, patterning or staining intensity were detected.

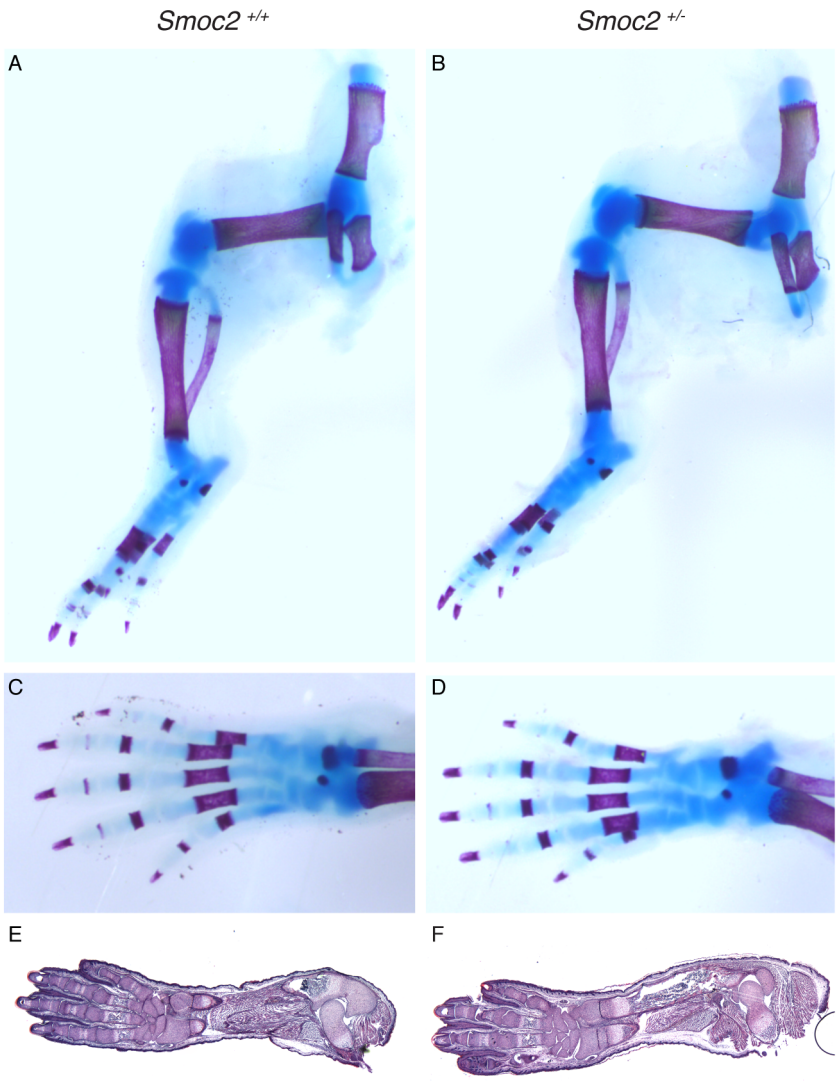

Figure 6.2: Morphological analysis of *Smoc2*$^{+/+}$ and *Smoc2*$^{+/-}$ embryos

A-D. Lateral view (A-B), Dorsal view (C-D). Skeletal staining of *Smoc2*$^{+/+}$ (A, C) and *Smoc2*$^{+/-}$ (B-D) hindlimbs at birth (n≥3 per genotype). E-F. Dorsal view. H&E staining of paraffin sections of *Smoc2*$^{+/+}$ (E) and *Smoc2*$^{+/-}$ (F) forelimbs (n≥2 per genotype).

In an attempt to investigate *Smoc2* null embryos, embryos were collected during earlier stages of development. Systematic screening indicated that the embryos died between 8 and 9.5 dpc. Genotyping was performed on the yolk sacs of these early stage embryos and confirmed the presence of *Smoc2* null mice. These embryos displayed a clear delay in development, associated with defects in the

outgrowth of anterior and cardiac structures. Furthermore, whereas the wild type embryos underwent axial rotation at 8.5 dpc, the *Smoc2* null mice did not. Once the *Smoc2* null embryos were isolated from the surrounding amnion, they stretched out unlike the wild type embryos that retained their typical embryonic position (Fig 6.3A-E).

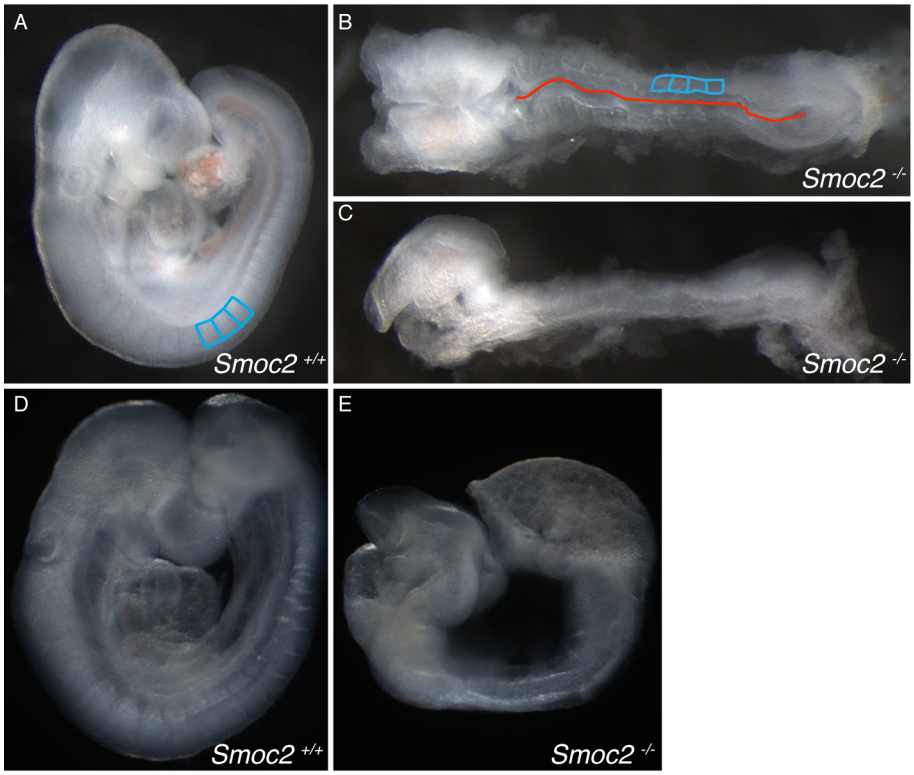

Figure 6.3: Morphology of *Smoc2*$^{+/+}$ and *Smoc2*$^{-/-}$ embryos at 8.5 dpc

A, D. Lateral view of *Smoc2*$^{+/+}$ embryos. B, C, E. *Smoc2*$^{-/-}$ embryos; dorsal view, anterior to the left (B); lateral view, anterior to the left (C, E). *Smoc2*$^{-/-}$ embryos were clearly reduced in size, did not undergo axial rotation, failed to close the head folds, formed irregularly shaped somites (blue delineation) and had misshapen axial structures (red line).

In addition, at 8.5 dpc the development of the blood could be seen in the *Smoc2* wild type embryos, while in the *Smoc2* null embryos, no red blood pools were detected. This is probably caused by the developmental delay, and at this point cannot be attributed to the loss of SMOC2 (Fig 6.3A-E).

The *Smoc2* wild type and knock-out embryos were further processed for paraffin embedding and H&E staining. Sagittal sections of both genotypes confirmed the observation of anterior defects, the failure to undergo axial rotation and the

delay in growth. Other structures like the somites, and axial structures seemed to develop properly, although these structures appeared misshapen (Fig 6.3A-B and Fig 6.4A-B).

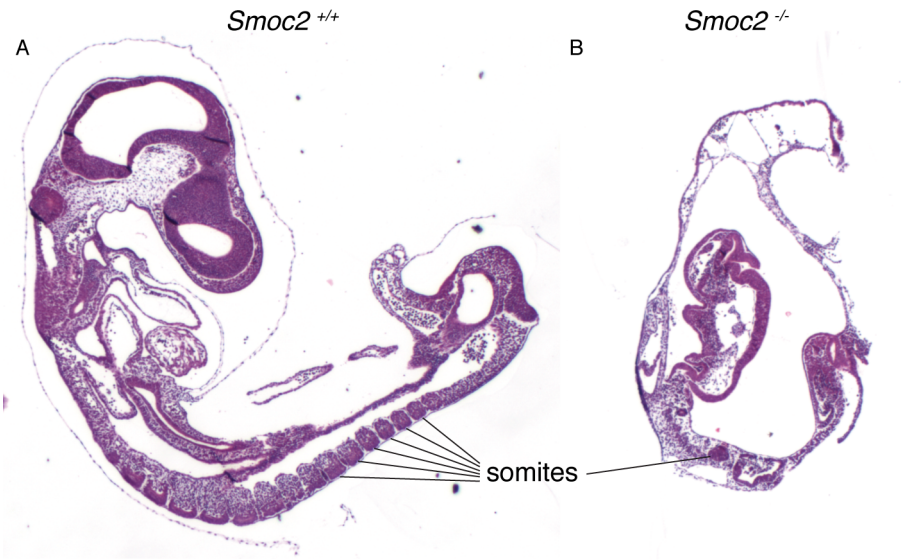

Figure 6.4: Sagittal sections of *Smoc2*$^{+/+}$ and *Smoc2*$^{-/-}$ embryos at 8.5 dpc

A, B. Lateral view, anterior to the top of *Smoc2*$^{+/+}$ embryo (A) and *Smoc2*$^{+/+}$ embryo (B).

In conclusion, we have shown for the first time the embryonic lethal phenotype of a *Smoc2* null embryo. Our first analysis indicated that the *Smoc2* null embryos were embryonic lethal and might present mesendodermal defects. Further research is however required to investigate the underlying cause of this defect.

Chapter 7:

Discussion

There are over 230 moveable and semi-moveable joints in the human body. The development and homeostasis of each and every one of them requires an accurate spatio-temporal control of signaling events and tissue interactions. Over the past decades, the joint has been intensely studied since a malfunctioning joint can result in progressive joint damage, discomfort and a reduced quality of life. Despite all the efforts, the development, homeostasis and the onset and progression of joint degeneration are far from being completely understood. Therefore, our lab analyzed a protein extract from bovine articular cartilage, and isolated among others, a novel protein called SMOC2. Over the years multiple groups have associated *SMOC2* with many developmental and disease processes but this work failed to identify a clear biological function of the protein.

In an attempt to clarify the biological role of SMOC2, we took advantage of different well-established animal models and used them to investigate the function of SMOC2 in a simpler and better-described context. By identifying the associated signaling pathway and assigning a function to the protein, our data will allow further research in the context of the joint.

In this thesis, we focused on the identification of pathways modulated by *smoc2* using the zebrafish model. Additionally, we performed preliminary analysis of the function of SMOC2 in the chicken limb bud and the mouse model.

7.1 Smoc2 in zebrafish

7.1.1 *smoc2* loss of function

Up to date, zebrafish *smoc2* was shown to be associated with tooth and craniofacial defects (Bloch-Zupan et al., 2011; Melvin et al., 2013). We reproduced some aspects of these reported defects, like the reduction in pharyngeal teeth. However, other defects like the ceratohyal defect could not be reproduced. Considering the severe defects and the bad shape of the embryos, we were puzzled by the discrete phenotypes at the stages presented in the previously published papers and the absence of earlier phenotypes. Especially since we observed *smoc2* transcripts during earlier stages of development. Careful analysis revealed new and important defects caused by silencing of

smoc2 transcript during these earlier stages. The fact that we were able to reproduce some of the late defects but discovered new ones in our morphants is not completely unexpected. The key reason may lie in the silencing technology used. While the morpholino technology has been essential to uncover function of many zebrafish genes, it is known to produce variable results due to the target sequence dependent efficiency and non-specific effects like p53-mediated apoptosis and edema. Since our target sequences differ from those of the groups of Bloch-Zupan and Melvin, we might expect phenotypic differences (Bloch-Zupan et al., 2011; Melvin et al., 2013). The problem is so widely known that several journals now include a checklist for the experiments involving morpholinos and define the specific controls required (http://cdn.elsevier.com/promis_misc/ydbioguidelinesmorpholinostudies.pdf).

It is our opinion that the target sequences chosen by Bloch-Zupan and Melvin are suboptimal. In the study of Bloch-Zupan et al. two different MOs were designed against either the splice donor site of exon 10 or a splice variant with only the C-terminal EC domain of full-length *smoc2* and in the study of Melvin et al. against the splice donor site of exon 11 (3' of the dominant donor splice site) or the 5' UTR (Bloch-Zupan et al., 2011; Melvin et al., 2013). Except for the latter, these strategies might produce a truncated, partially functional protein. Such a protein might have various changes in its activity/specificity resulting in aberrant phenotypes. In our analysis, we limited this possibility by designing the ATG-MO against the ATG translation start site of full-length *smoc2* and the SPLICE-MO against the first intron-exon boundary of the full-length *smoc2.* In addition, when assuming all studies were performed with an injection volume of 1 nl, the used amount of MO differs in all studies. Interestingly, the amount of injected MO in the paper of Bloch-Zupan et al is almost 45% higher for the MO targeting the splicing of exon 11 as compared to our study (5 ng vs. 3.5-3.6 ng). For Melvin et al, the differences were even bigger with an amount that was almost 3 times higher compared to our study (10 ng vs. 3.5-3.6 ng). Taking under consideration the typical non-specific effects of a MO and the fact that we needed to co-inject *p53* MO to prevent head necrosis, it is interesting to notice that in both papers none of those were reported.

Recently and in accordance with mouse models, a better alternative to morpholinos was developed: the targeted inactivation of genes of interest in zebrafish. Although the zebrafish genome is partially duplicated, making genomic modifications more complicated than in rodents, the recent technology can circumvent this problem. There are several strategies available at this moment with the most promising using endonucleases to induce DNA double-strand breaks and activate the error-prone non-homologous end joining (NHEJ) or homology-directed repair at specific genomic locations. Zinc-finger nucleases (ZFNs) and transcription activator-like effector nucleases (TALENs) have the Fok1 enzyme bound to the target sequence, while the CRISPR/CAS9 system requires the co-injection of the mRNA of the target sequence and the mRNA encoding the Cas9 enzyme (Doyon et al., 2008; Clark et al., 2011; Hwang et al., 2013). The latter system was suggested to be superior as the generation of the target mRNA sequence is much simpler and cheaper than the engineering and production of the ZFNs or TALENs, which require the enzyme to be physically bound to the target sequence. Yet the main advantage of the morpholino is the phenotypic analysis a few hours after injection. This advantage is lost as the screening for a germ-line transmitting chimaera and the breeding of a stable mutant takes at least six months, similar to mouse models. However, once a viable stable mutant line is generated, no more injections are required. In addition, the small housing costs of the zebrafish and the high yield of embryos from a single mating provides an additional benefit as compared to the mouse. While we have the TALEN constructs ready to introduce into the fish, the time and funding limitations did not allow us to embark on this strategy.

7.1.1.1 *smoc2* morphants present a mild ventralization and defects in myelopoiesis

Our analysis revealed that morphant embryos displayed a reduced axial length, somite defects, and a mild ventralization of the posterior tissues, among others. Molecular analysis indicated that there was an anterior defect in the development of the hemangioblast (*scl, gata2, lmo2*) and the myeloid progenitor cells (*spi1b*). As a result, the expression of both macrophage- and neutrophil-specific marker genes was affected at later stages of development. Concomitant

with the loss of the myeloid progenitor marker *spi1b,* we showed a decrease in the expression level of Bmp target genes.

It has been reported that the reduction of hemangioblast markers, *tal1* and *lmo2*, resulted in cardiovascular and hematopoietic defects (Dooley et al., 2005; Patterson et al., 2005). In contrast, *spi1b* morphants presented only myelopoiesis defects, without cardiovascular abnormalities (Rhodes et al., 2005; Patterson et al., 2007). We showed that *smoc2* morphants did not present cardiovascular defects, despite the loss of early *tal1* and *lmo2* expression in the ALPM. Potentially, the restoration of the *tal1* levels at 20 ss in *smoc2* morphants could compensate for the early loss of *tal1* expression and therefore ensure proper cardiovascular differentiation at later stages of development. In case this is indeed some sort of compensatory mechanism that ensures the proper cardiovascular development of the *smoc2* morphants, it appears to be unable to rescue the *spi1b* expression and the myeloid defects in the *smoc2* morphants. This hypothesis could be tested by co-injecting the *smoc2* morphants with sub-phenotypic doses of *tal1* or *lmo2* MO.

As *spi1b* expression was downregulated in the *smoc2* morphants and *spi1b* and *smoc2* morphants present comparable myeloid phenotypes, we hypothesize that the *smoc2*-associated myelopoietic defects could be attributed to the reduced *spi1b* mRNA levels.

7.1.1.2. *smoc2* affects Bmp signaling in the anterior lateral plate mesoderm

Previous studies have shown that the induction of *spi1b* in the hemangioblasts was dependent on *alk8*-mediated Bmp signaling (Hogan et al., 2006; Sumanas et al., 2008). The maternal zygotic mutant for *alk8*, *lost-a-fin*, displays a strong dorsalized phenotype (Mintzer et al., 2001). However, despite the caudal embryonic tissues being the primary affected tissue in the *lost-a-fin* mutants and the *smoc2* morphants, the expression of hematopoietic marker genes in the PLPM appeared unaltered during early developmental stages. Similar to the *smoc2* morphant, the *lost-a-fin* mutant had a reduced expression of *spi1b*, *runx1* and *c-myb* in the ALPM during somitogenesis. As development progressed, both the loss of *smoc2* and the loss of Alk8 resulted in a reduction of macrophage- and

neutrophil-specific markers, suggesting that Smoc2 might influence the Alk8-mediated induction of myeloid specific genes (Hogan et al., 2006).

Furthermore, studies of Smad proteins in zebrafish indicated that the hemangioblast markers, *tal1* and *lmo2*, were transcriptional targets of the Bmp signaling pathway and were redundantly regulated by *smad1* and *smad5* (McReynolds et al., 2007). The reduction of the expression level of *tal1* and *lmo2* in the *smoc2* morphants might therefore be a result of the reduced expression of Bmp target genes. Yet, the *lost-a-fin* mutant did not present a reduction in the expression level of *tal1,* indicating that the induction of *tal1* happens independently of Alk8-mediated Bmp signaling, in contrast to the induction of *spi1b* (Hogan et al., 2006).

Together, this suggests that Smoc2 might function, during early zebrafish development, as a specific modulator of the development of the hemangioblast in the ALPM (potentially by modulating Alk8-independent Bmp signaling) and initiation of the myelopoietic program in the ALPM (potentially by modulating Alk8-dependent Bmp signaling). Co-injection of sub-phenotypic doses of *alk8* MO and *smoc2* MO or co-injection of the *smoc2* MO with *caAlk8* mRNA could test for the dependency of the *smoc2* morphant phenotype on Alk8-mediated Bmp signaling.

Investigation of the Bmp signaling pathway during pregastrula stages did not indicate apparent defects in the expression level or the expression domain of Bmp target genes *vox* and *vent* or the Bmp antagonist *chd*. While at 12 ss, we could show a downregulation of the Bmp target genes *vox* and *ved* in the ALPM of the *smoc2* morphants. Our qPCR analysis indicated that this reduction in expression could not be attributed to changes in the expression levels of the Bmp ligands, *bmp2b* and *bmp4*, although it was reported previously that the expression of *bmp2b* in the pharyngeal teeth was reduced in the *smoc2* morphants at 56 hpf (Bloch-Zupan et al., 2011). Furthermore, no change in expression was detected for the extracellular inhibitor *chd* and the receptor *alk8*. Similar to the qPCR data, our WISH analysis indicated a reduction of anterior *vox* expression at 12 ss. Consequently, the reduction in Bmp signaling in the ALPM of *smoc2* morphants and the associated anterior myeloid defect is in line with the reported role for Bmp signaling in mediating myeloid development in the ALPM.

As modulation of the Bmp signaling pathway was shown to result in severe dorso-ventral patterning defects prior to somitogenesis stages, the effect of the silencing of *smoc2* is surprisingly late and discrete. A possible explanation is that the morpholino approach is not 100% efficient. This implies that some maternal *smoc2* mRNA will be able to be translated into Smoc2 proteins during the initial critical stages. Studies on murine SPARC, a SMOC2 family member, have shown that *Sparc* mRNA has a half-life of over 24 hours (Delany and Canalis, 1998). The half-life of Smoc2 is unknown, but it is possible that, although *smoc2* morpholinos are able to silence most of the *smoc2* mRNA, the fraction of proteins that is translated in the morphants could persist for much longer and ensures the proper initial development. This potentially also explains the lack of phenotypes as seen in embryos with altered levels of Bmp signaling (Lieschke et al., 2002). As we have shown that the dorso-ventral patterning in pregastrulation morphants is unchanged, it is unlikely that the pregastrulation fate map, as suggested by Lieschke is altered (Lieschke et al., 2002). We are however aware of the fact that the techniques used in this study have their limits and might not be sensitive enough to detect subtle differences that can alter cell fates. Another possibility is the compensation of the loss of Smoc2 by its closet family member, Smoc1. However, this is unlikely as during initial dorsoventral patterning stages *smoc1* could not be detected (our unpublished data and (Maier, 2006).

Through what mechanism the expression of the Bmp target genes is affected by Smoc2 remains to be determined. However, Pentagone (Pent), a protein found in D. melanogaster and a member of the SPARC family, has a highly similar domain organization to Smoc1 and Smoc2 (Vuilleumier et al., 2010; Vuilleumier et al., 2011). Despite the reversed order of the second TY domain and the first EF-hand, Pentagone was shown to be the closest Smoc2 homologue in D. melanogaster (Vuilleumier et al., 2010; Vuilleumier et al., 2011). Overexpression of *pent* mRNA in zebrafish embryos resulted in similar dorsalizations as in *smoc2* mRNA injected embryos. Studies have shown that *pent* regulates the gradient of Bmp signaling by competing with the Bmp ligand Dpp, for binding to Dally, a heparan sulphate proteoglycan (HSPG). By doing so, Pent was suggested to promote ligand distribution, antagonize the co-receptor function of Dally, or

regulate the interaction of Dpp and Dally (Vuilleumier et al., 2010; Vuilleumier et al., 2011). Bearing this in mind, one could interpret the *smoc2* morphant WISH analysis for the players of the Bmp signaling pathway in a similar way. As there is no difference in the expression of the Bmp ligands, or the Bmp antagonist *chd* and yet a decrease in the Bmp target gene expression is apparent, one could hypothesize that the distribution of the ligand might be altered. With *bmp2b* and *bmp4* being expressed in both the anterior and the posterior lateral plate mesoderm during somitogenesis stages, a gradient of Bmp signaling is established towards the middle of the embryo. Our WISH analysis indicated that the extent of the anterior and especially the posterior signal was reduced. Knowing that the expression of the Bmp ligands, *bmp2b* and *bmp4*, did not change and if there was indeed a reduction of the Bmp ligand diffusion, this could mean that an increased Bmp signaling is possible in the posterior part of the embryo, explaining the ventralized phenotype we see in the *smoc2* morphants at 24 hpf.

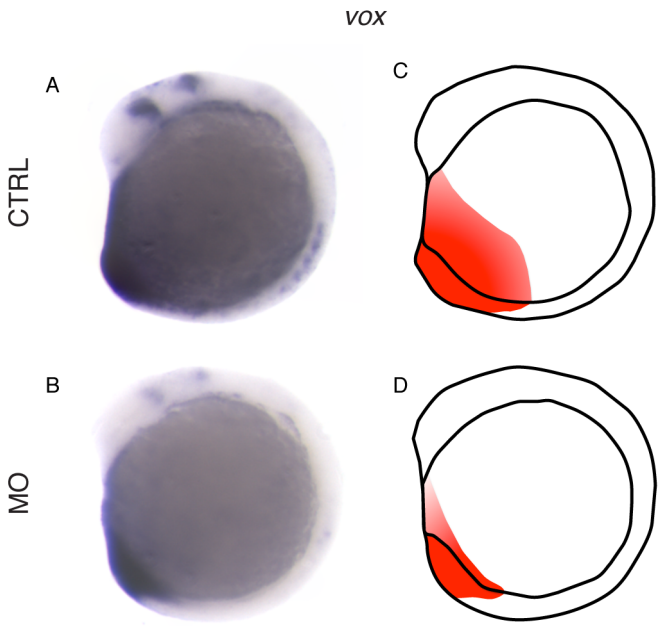

Figure 7.1: *smoc2* morphants display a reduced extent of *vox* expression

A-D. Lateral views, anterior to the top; 12 ss embryos. A-B. WISH analysis for the Bmp target gene *vox.* C-D. Schematic representation of embryos in A and B with posterior *vox* expression indicated in red.

In addition, SMOC1 was previously shown to interact with heparan sulphate proteoglycans (HSPG) in mice, thereby regulating cell adhesion (Klemencic et al.,

2013). Similar HSPG binding sites have been found in mouse and zebrafish Smoc2. This suggests that interaction of HSPG and Smoc2 in zebrafish and competition with Bmp ligands for HSPG could be possible (Klemencic et al., 2013; (Vuilleumier et al., 2010; Vuilleumier et al., 2011).

This hypothesis is further supported by the fact that Pent was suggested to function upstream of the Alk8 receptor as the overexpression of *pent* could rescue the *bmp2b*- but not the *alk8*-mediated ventralization. Interestingly, zebrafish *smoc2* gain of function resulted in similar dorsalized phenotypes, suggesting a functional conservation between *pent* and *smoc2* (Vuilleumier et al., 2010).

Furthermore, the X. laevis orthologue, *xsmoc1*, was shown to act as a Bmp antagonist possibly through Mapk-mediated phosphorylation of the R-Smads. The phenotype in the *xsmoc1* morphants was shown to be rescued after co-injecting zebrafish *smoc2* mRNA (Thomas et al., 2009) suggesting a functional conservation of the gene. Since there is only one *smoc* gene in X. laevis, and two paralogues in zebrafish, chickens, mice and humans, it is difficult to make statements on conservation of function. It must however be noted that the phenotype of *smoc1* morphant zebrafish is very different than that of *smoc2* morphants, which are more similar to the ventralized *xsmoc1* morphant defects (Thomas et al., 2009; Abouzeid et al., 2011; Rainger et al., 2011). In addition, gain of function of *xsmoc1* and *smoc2* result in similar dorsalized phenotypes as well (Vuilleumier et al., 2010).

In summary, our analysis shows that *smoc2* affects myelopoiesis in the anterior lateral plate mesoderm of developing zebrafish embryos, potentially through the modulation of Bmp signaling. It is tempting to speculate on how Smoc2 regulates embryonic myelopoiesis in the anterior lateral plate mesoderm during zebrafish development. One possibility is that by binding to the same sidechains of the HSPG present on the cell membrane, Smoc2 competes with Bmp ligands for these interactions and therefore promotes the diffusion of Bmp molecules further away from the source. Thereby Smoc2 ensures a widened Bmp gradient, with a shallower slope as compared to the natural Bmp gradient. In the absence of Smoc2, the gradient of the Bmp signaling is limited to the intrinsic diffusion

properties of the Bmp ligands itself. Therefore a steeper gradient can be seen, with cells more distant from the source of Bmp ligands not responding to the signal. The cells closest to the source, however, will have more ligands available as these cannot diffuse away further. When Smoc2 is abundantly available, the Smoc2 proteins outcompete the Bmp ligands for the HSPG binding sites. This results in an even further spreading of the Bmp ligands and a reduction of the overall Bmp signaling.

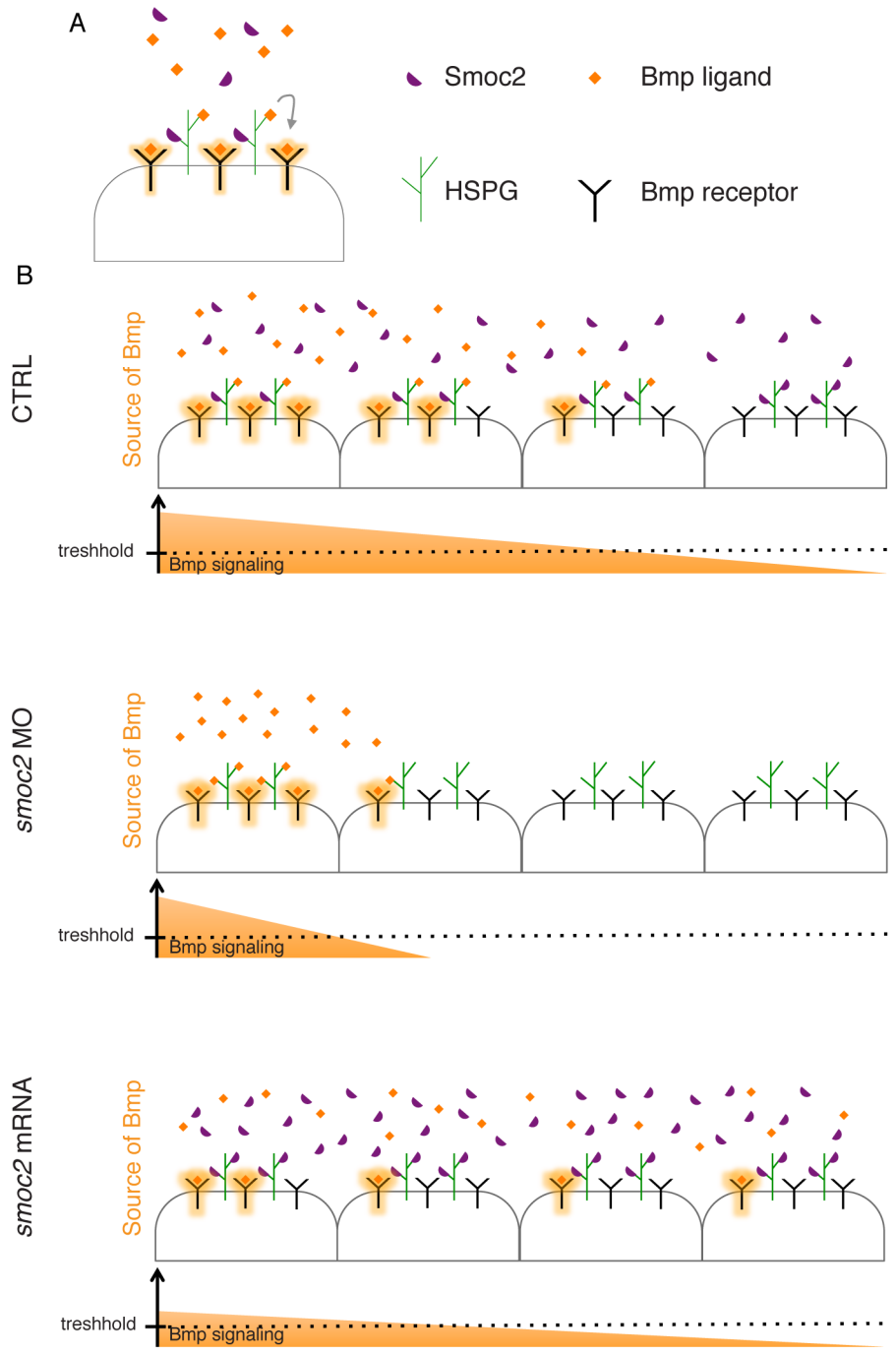

Figure 7.2: Hypothetical mechanism of action of Smoc2 based on the data of the zebrafish morphants

A. Binding of Bmp ligands to the receptor is mediated by the recruiting action of HSPGs. Bmp ligands bind the sidechains of these HSPG and thereby get recruited towards the cell membrane and the Bmp receptors. B. Bmp proteins diffuse away from their source. Smoc2 affects the diffusion of the Bmp ligands and shapes the extent of Bmp signaling.

Therefore Smoc2 affects the diffusion of the Bmp ligands and, just like in D. melanogaster, shapes the gradient of Bmp signaling that is required for proper specification of the hemangioblasts during early stages and the activation of the myeloid progenitor specific program at later stages of zebrafish development.

More research is however needed to investigate the relation between Smoc2 and Bmp, and to assess if there is a direct interaction, or if a secondary partner, like proteoglycans is involved.

7.1.2. *smoc2* gain of function

7.1.2.1 Smoc2 modulates Wnt5b mediated non-canonical Wnt signaling

The overexpression of *smoc2* mRNA in the zebrafish embryo resulted in a range of phenotypes at the initial stages of somitogenesis. Together with dorso-ventral patterning defects (DV), the injected embryos presented convergence and extension defects (CE). These DV and CE defects are traditionally the result of a defective Bmp and non-canonical Wnt signaling, respectively.

At the shield stage, a subtle increase in *chd* expression and a subtle decrease in *gata2* expression were detected. Although this could explain the DV patterning defect, the difference in *chd* expression at 70% epiboly was even smaller. In embryos with similar DV patterning defects at late stages, the changes in the expression of *chd* were reported to be more severe than upon injection with *smoc2* mRNA (Ghiselli and Farber, 2005; Seebald and Szeto, 2011; Wu et al., 2012). We therefore conclude that additional factors must be contributing to the DV pattering defects of the *smoc2* mRNA injected embryos or that at later stages the Bmp signaling is disturbed more severely. In addition, the *smoc2* mRNA injected embryos also presented CE movement defects, which are typically regulated by the non-canonical Wnt signaling pathway. Analysis of the latter indicated that a full and specific rescue of the *smoc2* mRNA induced phenotype

could be obtained upon co-injection with *wnt5b* mRNA. This indicates that Smoc2 modulates Wnt5b mediated signaling, but whether this is a through a direct interaction, or indirectly through other binding partners, receptors or cofactors or through other signaling pathways remains to be investigated.
The full rescue upon co-injection with *wnt5b* mRNA only suggests that Wnt5b is involved. It is important to mention that manipulation of Wnt5b-mediated non-canonical Wnt signaling was not reported to result in similar dorso-ventral defects as were seen after injection with *smoc2* mRNA (Hammerschmidt et al., 1996; Kilian et al., 2003; Marlow et al., 2004). In contrast, Bmp mutants like *snailhouse (snh; bmp7*), *swirl* (*swr; bmp2b*) and *somitabun* (*sbn; smad5*) displayed, next to dorso-ventral patterning defects, typical CE defects such as wider axial structures and somites all around the embryo (Mullins et al., 1996). Since non-canonical Wnt mutants do not display DV defects, and as Bmp mutants do display CE defects, one might suggest that the Bmp signaling pathway lies upstream of the Wnt signaling pathway (Hammerschmidt et al., 1996; Heisenberg et al., 2000; Kilian et al., 2003). This was further supported by the data on the reduced expression levels of non-canonical Wnts in *bmp* mutant zebrafish (Myers et al., 2002). However, which pathway regulates which is still an issue in both the zebrafish and the cartilage and bone research community and further research is needed to investigate this relation.

Yet if the primary target of Smoc2 is to be the non-canonical Wnt signaling pathway, one could hypothesize about the function that Smoc2 has within that pathway. As Smoc2 was shown to mediate the progression of the cell cycle by associating with Integrin-like kinase (ILK) through an unknown factor and as ILK has been associated with Wnt signaling (Mulholland et al., 2006; Oloumi et al., 2006; Yamabi et al., 2006), one could speculate that a Wnt ligand or (co-)receptor might be that unknown factor. In addition, changes in the DV patterning were shown to affect the expression of *wnt5b* and *wnt11* and therefore co-injection of *wnt5b* mRNA might restore the non-canonical Wnt balance resulting in a rescue of the *smoc2* mRNA induced phenotypes (Myers et al., 2002).

However, to test if any of these hypotheses stand, further research is needed to clarify the role of all these players and their interactions during the different stages of zebrafish development.

7.1.2.2. The FS-domain is essential for the function of Smoc2

Besides the full size Smoc2, we began testing the biological importance of the different Smoc2 domains. Our data indicated that none of the domains, besides the FS domain, contributed to the *smoc2* mRNA induced phenotype. The FS domain appeared to influence the severity of the phenotype. The name follistatin-like domain, is somewhat misleading as this immediately suggests that this domain has a similar function as Follistatin, an extracellular Tgfβ/Bmp/Gdf antagonist (Esch et al., 1987; Balemans and Van Hul, 2002). However, no proof has been provided, in this study or in any other that the FS domain can bind any of these ligands.

More likely, the loss of the FS domain interferes with the structure of the protein. In SPARC, the adjacent FS and EC domains were shown to interact and regulate the conformation of the protein (Hohenester et al., 1997; Busch et al., 2000). In Smoc2, however, the FS and EC domains are separated by two TY domains that flank a putative SMOC domain, which could alter the interaction between the FS and the EC domain. Surprisingly, the loss of the EC domain does not interfere with the severity of the phenotype, which indicates that the difference caused by removing the FS domain is unlikely to originate from changes in the conformation of Smoc2. Given the reported interaction of the EC domain with i

Integrin and the suggested interaction of the EC doman with HSPGs, the absence of a phenotypic difference upon injection with the *smoc2*^EC indicated that these interaction partners do not contribute to the development of the gain of function phenotype (Maier et al., 2008; Klemencic et al., 2013).

More importantly, the FS domain harbors a Kazal domain, which functions as a serine protease inhibitor (Hohenester et al., 1997). The loss of the FS domain, but not the loss of the EC or SMOC domain, could therefore result in a Smoc2 protein that is more prone to proteases. One could imagine that the window of activity of a protein, with a changed half-life, is smaller and that overexpression of such a less stable protein might result in milder phenotypes. Remarkably,

zebrafish injected with the FS mutant still present defects, which indicates that the FS domain alone is not responsible for the defect. We suggest that other domains like the TY1 or TY2 domain, although being reported to prevent proteolytic degradation (Molina et al., 1996; Lenarcic and Bevec, 1998), or other stretches of amino acids are more important for the induction of the phenotype. Additional mutant studies are therefore required to determine which part of Smoc2 causes the phenotype.

7.2 SMOC2 in the chicken limb model

7.2.1. *SMOC2* overexpression results in a suppression of *FGF8* expression

Processing of successfully injected limbs by means of WISH analysis indicated an apparent change in the expression of *FGF8*, essential for the proximodistal outgrowth of the limb (Niswander et al., 1993; Ohuchi et al., 1997; Saunders, 1998). *FGF8* is expressed in the apical ectodermal ridge that regulates the proximo-distal outgrowth of the limb. Previously it was shown that Bmp signaling controls the dorso-ventral patterning by regulating the expression of EN-1 but also the proximo-distal outgrowth of the limb bud by inducing the AER and the associated FGF signal. Once the AER is induced in the limb bud, the Bmp signaling exerts the opposite effect: it negatively regulates the maintenance of the AER (Pizette and Niswander, 1999; Pizette et al., 2001). Therefore, it is tempting to hypothesize that SMOC2 interferes with the expression of *FGF8* through modulation of BMP signaling, similar to its role in D. rerio and D. melanogaster.

7.3 SMOC2 in mice

Crossing *Smoc2*$^{+/-}$ mice resulted in mendelian distributed *Smoc2*$^{-/-}$ mice, which presented an embryonic lethal phenotype. Our preliminary analysis indicated that the embryos die around 8 dpc, suggesting that SMOC2 has a crucial function during the process of embryonic development. The strong conservation of the regulatory components of the hematopoietic molecular machinery across species would suggest that SMOC2, just as in zebrafish, regulates hematopoiesis in mice.

Indeed, TGFβ/BMP signaling was reported to influence the formation of the mesoderm and subsequently induction of hemangioblasts (Dzierzak and Medvinsky, 1995; Baron, 2001). However, the developmental delay of the *Smoc2*$^{-/-}$ embryos does not allow us to make any statement on the relation of the apparent reduction in blood formation in the *Smoc2*$^{-/-}$ embryos and the zebrafish loss of function data. Interestingly, the expression pattern of *SMOC2* in mouse embryos appears from embryonic day 7.5 onwards in the Reichert's membrane, a tissue found only in rodents, that separates the embryonic endoderm from the throphoblast cells (Maier et al., 2008). No additional expression was detected until 10.5 days post coitus, a stage at which the *Smoc2*$^{-/-}$ embryo has died already. This could indicate that the expression of SMOC2 in the Reichert's membrane is crucial for the development of the mouse embryo either by influencing the development of the embryo itself or by affecting the integrity of the Reichert's membrane. The Reichert's membrane was purported to influence the materno-embryonic exchange (Jollie, 1968; Jensen et al., 1975) and it was suggested that a defective Reichert's membrane could result in wasting and death of the embryos (Williamson et al., 1997).

Our *Smoc2*$^{-/-}$ phenotype differs greatly from the homozygous *Smoc2* knock-in mice of the group of Hans Clevers (Munoz et al., 2012). They inserted an EGFP-ires-CreERT2 cassette at the translational start site of *Smoc2* and reported that these mice do not present an embryonic lethal phenotype. Homozygous mice were apparently viable and did not show any defects. We can only speculate on the underlying reason for this major difference in phenotypes. This could be due to the difference in strategy, or strain of mice used to generate the knockout. It is not uncommon to see a difference in phenotypes when a gene is targeted in different strains or using different approaches. For example, *Noggin*$^{-/-}$ mice were shown to display different defects depending on the strain that was used (Tylzanowski et al., 2006). Furthermore, it was reported that the approach used to knock out *Smoc1* resulted in a different phenotype (Okada et al., 2011; Rainger et al., 2011). In our analysis, we replaced the first intron with the LacZ casette, while in the study of Munoz, they targeted their cassette at the translation start site of *Smoc2*. No further evidence was provided in their paper on whether the translation start site is therefore still active and a modified, potentially active

protein is still present (Munoz et al., 2012). It is therefore unclear whether the published *Smoc2* knock-in mouse is a full *Smoc2* null mouse.

Chapter 8:
Concluding remarks & future perspectives

To investigate the complexity of human biology and its associated pathological conditions we use animal models with comparable genetics, anatomy and/or physiology. In this project we used multiple animal models, each with their strengths and limitations, and best suited for the specific question we wanted to answer. Nevertheless, the findings presented in this thesis emphasize the fact that the intricate nature of the extracellular matrix puts forward a major challenge, animal models notwithstanding. The data indicate that changing the expression of just one single component results in a complex combination of tissue specific phenotypes. Using the zebrafish model, we have shown that Smoc2 is associated with Bmp and Wnt5b signaling. In addition, using the chicken limb bud model, we associated SMOC2 with *FGF8* expression which is regulated by BMP signaling. Furthermore, our preliminary analysis of the *Smoc2*$^{-/-}$ mouse indicated that SMOC2 is a crucial matricellular protein during the early stages of embryonic development.

In zebrafish, further research is required to identify the interaction partner(s) of Smoc2, which could be a signaling ligand, a cofactor or coreceptor. As we only report on the downstream changes induced by the manipulation of Smoc2 levels, we can only hypothesize on the function of Smoc2 and the level at which Smoc2 is interfering with a particular signaling cascade. Our analysis indicated that Bmp and/or Wnt ligands, cofactors or receptors are the primary candidates to have such a role. One could therefore start speculating that Smoc2 affects the ligand distribution, ligand-receptor interaction or co-factor availability to mention a few. As this are just speculations, the identification of the binding partner(s) of Smoc2 will assist to determine the primary target of Smoc2, distinguish primary from secondary defects and eventually clarify the function of Smoc2. This becomes relevant as our gain and loss of function analysis indicate different targets for Smoc2. With *wnt5b* also expressed in the ALPM and loss of Bmp signaling also resulting in CE defects, both mechanisms are amongst the possibilities.

Furthermore, a thorough dorso-ventral patterning analysis of the overexpression phenotype during pregastrula and segmentation stages and is

required, especially in light of the reduced expression of the Bmp target genes in the *smoc2* morphants.
Additionally, the domain analysis will have to be extended to other different domains. The identification of binding partners will help narrowing down what SMOC2 domain and what peptide sequence is involved in the interaction.

In the chicken limb bud, all tools were generated for the investigation of the outgrowth defect seen in the RCASBPA-*SMOC2* injected limbs. Analysis of the expression of additional molecular markers (Bmp target genes like *EN-1* or *VOX* and *VENT*, and other *FGF* and *WNT* related genes) will add valuable information for the interpretation of the induced defect. In addition, injection at later stages of development, could also be interesting, especially as it was shown that Bmp blocks the expression of *FGF* ligands once the AER is induced. (Pizette and Niswander, 1999; Pizette et al., 2001).
For the *Smoc2*$^{-/-}$ mouse, earlier stages of development (5.5-7.5 dpc) will have to be analyzed morphologically and molecularly (WISH, IHC) in order to investigate the dramatic effect of the loss of *Smoc2* on the development of the embryo. Experts in field of mouse embryonic development advised us to use mesenodermal probes as defects in the mesendoderm could explain the phenotype. Furthermore, the results of the zebrafish and chicken studies should be taken under consideration when choosing the probes of interest. In addition, valuable information could be added when investigating a tissue specific knockout. As our lab is interested in the development of the joint and as Smoc2 was isolated from the articular cartilage and shown to be expressed in the joint interzone, crossing a *Smoc2*$^{fl/fl}$ mouse with a mouse with joint interzone specific (*Gdf5*; (Buxton et al., 2001)) or cartilage specific (*Col2*; (Seyer and Vinson, 1974)) Cre expression should prevent early lethal phenotypes and might shed new light on the role of SMOC2 in the context of the joint.

Chapter 9:

Summary

Musculoskeletal conditions are the leading cause of morbidity and disability, resulting in enormous healthcare costs and working disability. About 150 diseases, syndromes and disorders are grouped in the musculoskeletal conditions, each being progressive and associated with pain (http://www.who.int). One of them is OA, a chronic and progressive joint disorder that is caused by degradation of the articular cartilage and associated defects of the subchondral bone. Although many research groups have investigated the onset and progression of this disabling condition, the underlying cause or mechanism is far from completely understood.

Therefore our lab analyzed a protein extract from bovine articular cartilage with in vivo chondrogenic activity and isolated the SMOC2 protein. In addition, *Smoc2* was shown to be expressed in the joint interzone of mouse embryonic digits. Recent evidence indicated that signaling pathways, which are known to regulate the embryonic stages of development, are reactivated during the onset and progression of multiple conditions, including musculoskeletal diseases. Therefore, we used developmental models to analyze the function of SMOC2.

To investigate the SMOC2 associated signaling pathway(s), we used the zebrafish model system and performed loss and gain of function experiments.

Our loss of function analysis indicated that Smoc2 affected myeloid development by reducing the number of macrophages and neutrophils during the primitive wave of zebrafish hematopoiesis. This defect could be traced back to the reduced expression of the myeloid progenitor specific gene *spi1b* at earlier stages of development. In addition, we detected a reduction in Bmp signaling, which was previously shown to regulate *spi1b* expression. This suggests that Smoc2 affects Bmp signaling in the ALPM, potentially by manipulation of the Bmp gradient.

Our gain of function analysis indicated that Smoc2 affects the DV patterning and CE movements during the gastrulation and subsequent segmentation stages of zebrafish development. In addition, Smoc2 appeared to mediate the Wnt5b mediated non-canonical Wnt signaling pathway.

Although Smoc2 could affect both the Bmp and the Wnt pathway directly, it is as likely that Smoc2 affects just one of them, which subsequently affects the other one. Obviously, the interaction and modulation of these signaling pathways all

depend on the specific microenvironment and the spatio-temporal context of the *smoc2* expressing cells.

In order to relate the function of SMOC2 to the homeostasis of the joint, the zebrafish model is less suited. Therefore, we opted for the chicken limb model, as the joints in these limbs are more equal to human joints. To overexpress *SMOC2* in the chicken limb bud, we cloned *SMOC2* into the RCAS viral vector that allows for infection of the chicken cells. Localized injection of this RCASBPA-*SMOC2* virus resulted in an outgrowth defect along the proximo-distal axis. Our preliminary analysis of the injected limbs indicated a reduced *FGF8* expression in the AER, which is known to regulate the outgrowth of the limb. However, it remains unclear whether SMOC2 directly affects FGF transcription or affects the expression through a secondary partner, like BMP.

As a third animal model, we have used the mouse model to analyze the phenotype upon loss of SMOC2. *Smoc2*$^{-/-}$ mouse embryos presented a lethal phenotype during early stages of development. As *Smoc2* is only reported to be expressed in the Reichert's membrane at those stages, potentially a defect in the Reichert's membrane underlies the lethal phenotype.

In conclusion, our work revealed new insights in the essential function of SMOC2 during zebrafish, chicken and mouse embryonic development, which allows further research to determine the role of SMOC2 within the intricate network of signaling cascades.

Chapter 10:

Samenvatting

Musculoskeletale aandoeningen zijn de primaire oorzaak van ziekte en ongemak die resulteren in enorme medische kosten en werkverlet. Ongeveer 150 progressieve en met pijn geassocieerde ziekten, syndromen en aandoeningen worden gegroepeerd onder de musculoskeletale aandoeningen (http://www.who.int). Eén daarvan is osteoarthritis, een chronische en progressieve aandoening van de gewrichten die veroorzaakt wordt door de afbraak van het gewrichtskraakbeen en defecten van het onderliggende subchondrale bot. Ondanks het intense onderzoek van verschillende groepen naar de initiatie en de progressie van deze invaliderende aandoening is de onderliggende oorzaak en het mechanisme van de aandoening nog niet duidelijk. Om die reden heeft ons labo een proteine extract met kraakbeeninducerende activiteit in vivo, afkomstig van het gewrichtskraakbeen van een rund, onderzocht en het SMOC2 proteïne geïsoleerd. Daarenboven werd aangetoond dat *Smoc2* tot expressie komt in de gewrichtsinterzone van de embryonale muis digit. Recent onderzoek heeft uitgewezen dat de signaalcascades, die de embryonale ontwikkeling regelen, gereactiveerd kunnen worden tijdens de beginfasen en de verdere onwikkeling van verschillende aandoeningen. Om de functie van SMOC2 te verklaren hebben we daarom gekozen om model organismen in hun embryonaal stadium te analyseren.

We hebben het zebravis model aangewend om uit te zoeken met welke signaalcascade Smoc2 geassocieerd is. Daartoe werden loss en gain of function analyses uitgevoerd.
Volgens de data uit onze loss of function studie beïnvloedde Smoc2 de myeloïde ontwikkeling door het aantal macrofagen en neutrofielen te reduceren tijdens de primaire ontwikkeling van het hematopoïetisch systeem in de zebravis. Dit defect bleek veroorzaakt te worden door een verlaagde expressie van *spi1b* tijdens voorafgaande stadia. Bovendien konden we een reductie van de Bmp signalisatie aantonen, waarvan voorheen aangetoond was dat die de inductie van *spi1b* medieert. Hieruit kunnen wij suggereren dat Smoc2 een effect heeft op de Bmp signaal cascade in het ALPM, mogelijks door de gradiënt van Bmp signalisatie te beïnvloeden.

Uit de gain of function experimenten bleek dat Smoc2 een effect heeft op de ontwikkeling van de dorsale en ventrale weefsels en de regulatie van de gecoördineerde celmigratie tijdens gastrulatie en segmentatie fasen beïnvloedt. Daarenboven bleek dat Smoc2 de Wnt5b gemedieerde non-canonical Wnt signaalcascade reguleert. Hoewel Smoc2 zowel de Bmp als de Wnt signaalcascade zou kunnen reguleren, is het evengoed mogelijk dat Smoc2 slechts één van de twee beïnvloedt en dat die op zijn beurt de andere cascade treft. Uiteraard is de interactie and de beïnvloeding van deze signallcascades afhankelijk van de specifieke micro-omgeving en de ruimtelijke en tijdelijke context van de cellen die *smoc2* tot expressie brengen.

Om binnen de context van een gewricht de functie van Smoc2 te bepalen, is het zebravis model minder geschikt. Aangezien de gewrichten van de kip meer gelijkenissen vertonen met die van de mens is het kippen ledemaat model een betere optie. Opdat we Smoc2 tot overexpressie zouden kunnen brengen in het lidmaat van het kippenembryo, hebben we Smoc2 in de virale RCAS vector gekloneerd. De gelokaliseerde injectie van het RCASBPA-*SMOC2* virus resulteerde in een verstoorde uitgroei van het lidmaat. Onze preliminaire analyse wees op een gereduceerde *FGF8* expressie in de AER, waarvan geweten is dat het de uitgroei van het ledemaat controleert. Onze analyse laat niet toe om uit te maken of SMOC2 de transcriptie van *FGF8* rechtstreeks, al dan niet via een secundaire interactie partner beïnvloed.

In een derde proefdiermodel, hebben we het phenotype van de *Smoc2*$^{-/-}$ muis bestudeerd. De afwezigheid van het SMOC2 proteïne resulteerde in een lethaal defect tijdens de vroege fasen van embryonale ontwikkeling. Mogelijks is dit het resultaat van een defect in het membraan van Reichert, waar Smoc2 tijdens deze stadia tot expressie komt.

Samengevat heeft ons werk bijgedragen tot nieuwe inzichten in de essentiële functie van SMOC2 tijdens de embryonale ontwikkeling van zebravis, kip en muis. Deze data laat verdere onderzoeksprojectentoe om een rol te bepalen voor SMOC2 binnen het ingewikkelde netwerk van signaal cascades.

Addendum:

Molecular analysis of the muscle phenotype of *Noggin* null mice

Our laboratory has a longstanding interest in the molecular and genetic events regulating BMP signaling in the developing limb. One of such novel candidate regulators could be SMOC2. Another one, NOGGIN, has also been a subject of research interest of the host lab and was also investigated during this PhD thesis. Specifically, we pursued hitherto undescribed embryonic muscle phenotype present in *Noggin* null mice.

A.1 Introduction

A.1.1 NOGGIN

NOGGIN is a glycosylated, secreted 64kDa protein homeodimer and one of the many extracellular antagonists of the BMP signaling pathway. Similar to *Chordin*, *Chordin-like*, *Follistatin*, *Fsrp* and *Cerberus*, *Noggin* encodes a protein that directly binds to the BMP (BMP2, BMP4, BMP5, BMP7) and GDF (GDF5, GDF6) ligands with various affinities, but in a picomolar range for BMP2 and BMP4 (Zimmerman et al., 1996; Merino et al., 1999; Gazzerro and Canalis, 2006). By preventing interaction of the ligands with their receptor, NOGGIN interferes with the downstream activation of the signaling cascade.

Noggin was first identified in *X. laevis* based on its ability to induce secondary axis formation (Smith et al., 1993; Brunet et al., 1998; McMahon et al., 1998). During later developmental stages, *Noggin* is expressed in the Spemann organizer where it regulates the development of dorsal tissues (Smith et al., 1993; McMahon et al., 1998). In the mouse model, *Noggin* was shown to be initially expressed in the node and later restricted to the notochord, the floor and roof plates of the neural tube and the dermomyotome. The presence of NOGGIN is required for the development of the ectodermal derived neural tube, hair follicles, teeth, lens and retina and the mesodermal derived tissues like the bone, cartilage, joints and somites (reviewed in (Balemans and Van Hul, 2002).

Loss of NOGGIN in mice resulted in an embryonic lethal phenotype that is characterized by different developmental defects such as exencephaly, axial outgrowth defects with a loss of the caudal vertebrae, failure of neural tube

closure, excessive cartilage formation and fused joints to mention a few (Fig A1) (Brunet et al., 1998). In addition, our lab has discovered a late onset muscle defect.

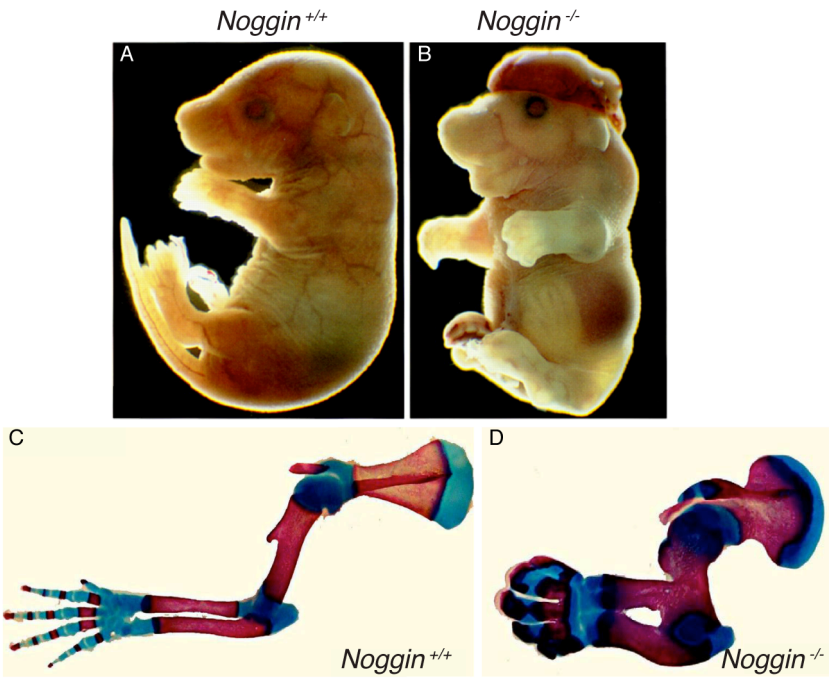

Fig A1: *Noggin* null mice present multiple developmental defect

A-B. Newborn littermates of a *Noggin*$^{+/-}$ mating. The *Noggin*$^{-/-}$ embryo presents hemorrhages, shorter and thicker limbs, exencephaly, and loss of caudal vertebrae. C-D: Skeletal staining of the forelimb of 18 dpc embryos displayed joint fusions and excessive cartilage and bone formation

A.1.2 Mouse embryonic muscle development

During embryonic development, the lateral plate mesoderm segments into bilaterally organized somites. This temporary tissue further differentiates into a ventral-medial part, called the sclerotome, and a dorsal-lateral part, called the dermomyotome. The sclerotome gives rise to the cartilage and the bone of the vertebral column, while the dermomyotome develops into muscle, endothelia, cartilage, connective tissue and dermis (Fig A3).

At 9.5 dpc, PAX3 positive cells at the epaxial and the hypaxial lip of the dermomyotome delaminate and migrate inwards to form an underlying cell population, the myotome (Fig A3). This cell population will eventually give rise to the muscles of the back and the trunk. At the limb level however, the cells

from the hypaxial dermomyotome delaminate and migrate into the developing limb bud, where they will start differentiating into the muscles of the limb.

At 10.5-12.5 dpc, the first wave of myogenesis (embryonic myogenesis) takes place (Fig A2). Embryonic myoblasts fuse with each other and differentiate into a large primary myofibers. As most of the myoblasts remain in a committed and undifferentiated state, the number of myofibers produced in this first wave is limited. These primary myofibers serve to form the basic muscle pattern. These primary fibers will then trigger the proliferation of the fetal myoblasts, which will give rise to many smaller secondary myofibers during the secondary wave of myogenesis (14.5-16.5 dpc), or fetal myogenesis (Fig A2).

Next to these types of myoblasts and myofibers, some cells stay PAX7 positive and stay in an undifferentiated state (Fig A2). These cells are present from early stage onwards and give rise to fetal myoblasts. However, when PAX7 positive cells can be morphologically identified as mononucleated cells residing between the myofiber plasma membrane and the basal lamina (17,5 dpc), they are called satellite cells. These cells form the stem cell niche of the muscle and are responsible for the growth and restoration of the muscle following triggers like trauma or physical exercise during postnatal stages.

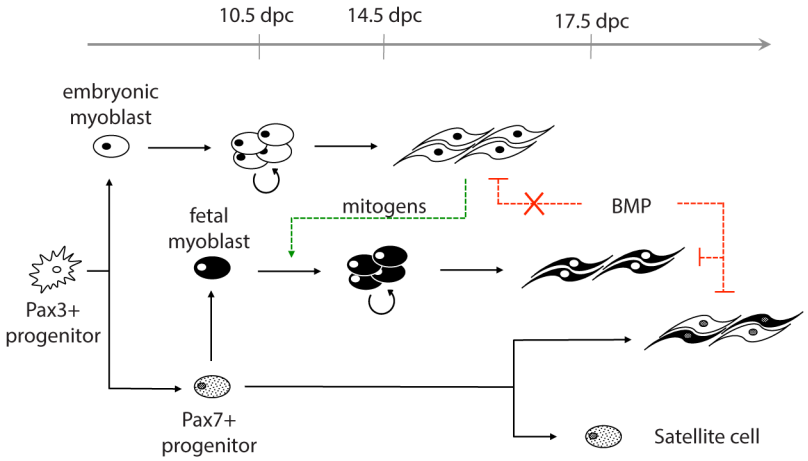

Figure A2: Timing of differentiation of different muscle cell populations
Embryonic myoblasts give rise to large primary fibers, while fetal myoblasts differentiate into small secondary fibers. Mitogens, secreted by the embryonic myoblasts, promote the proliferation of fetal myoblasts. Further differentiation of these fetal myoblasts is regulated by BMP signaling. A third cell population of Pax7 positive cells is able to develop into both primary and secondary fibers or satellite cells.

A.1.3 Molecular regulation of myogenesis.

One of the earliest indications of myogenic commitment is the expression of *Pax3* and *Pax7* in the dermomyotome (Fig A3). PAX3 is required for somite segmentation, (dermo)myotome formation and limb musculature development, whereas PAX7 is necessary for the maintenance of adult satellite cells (Bober et al., 1994; Goulding et al., 1994; Seale et al., 2000; Tajbakhsh and Buckingham, 2000; Schubert et al., 2001; Oustanina et al., 2004; Relaix et al., 2004; Relaix et al., 2005; Relaix et al., 2006; Frantz et al., 2010).

During the process of differentiation, the myogenic cells lose their *Pax3/7* expression and begin expressing myogenic regulatory factors (MRF) like *MyoD, Myf5, Myf6*, and *Myogenin* (Fig A3). These are helix-loop-helix proteins that regulate the further development of the skeletal muscle (Sabourin and Rudnicki, 2000; Bentzinger et al., 2012). Upon association with the ubiquitously expressed E-proteins, the MRFs can bind to specific DNA motifs (E-boxes) to activate the transcription of their target genes. Using knockout mouse models, it was shown that not all MRFs are required for normal muscle development and individual MRFs are unable to completely substitute for each other. Single knockouts for *MyoD*, *Myf5* and *Myf6* were able to develop normal muscle although with some delays, while the loss of *Myogenin* resulted in perinatal lethal phenotypes with severe muscle defects. Double knockouts however, resulted in more dramatic defects (Braun et al., 1992; Rudnicki et al., 1992; Hasty et al., 1993; Nabeshima et al., 1993; Rudnicki et al., 1993; Braun and Arnold, 1995; Arnold and Braun, 1996; Rawls et al., 1998). Furthermore, MYOD and MYF5 appeared to regulate the early stages of myoblast determination, while MYF6 and MYOGENIN were required for the further differentiation.

Once the progenitor population is determined and differentiation is initiated, post-mitotic myoblasts will adhere, align and fuse in order to generate multinucleated myofibers. In addition, the expression of *Myosin heavy chain* (MHC), *Actin* and *Desmin* among others contributes to the development of a fully differentiated muscle with a functional contractile apparatus.

The dermomyotomal and sclerotomal somitic populations are subject to the crosstalk of WNT, SHH, and BMP signaling cascades, which ensures an intricate

balance that allows for a regulated differentiation of these lineages (Fig A3) (http://www.rndsystems.com/resources/images/5834.pdf). WNT signaling from the overlying epidermis and the roof plate of the neural tube induces the expression of dermomyotome specific genes, while SHH signaling from the notochord and the floor plate of the neural tube induces sclerotomal gene expression. In addition, *Bmp* expression in the epidermis, the roof plate of the neural tube and the lateral plate mesoderm prevents the differentiation of myogenic precursors while NOGGIN, present in the roof and floor plate of the neural tube, blocks this BMP action and therefore allows for the myogenic precursors to differentiate (Yusuf and Brand-Saberi, 2006). This balance between multiple signaling pathways results in the restricted expression of MRFs and *Pax* genes in the proper cell populations (Fig A2).

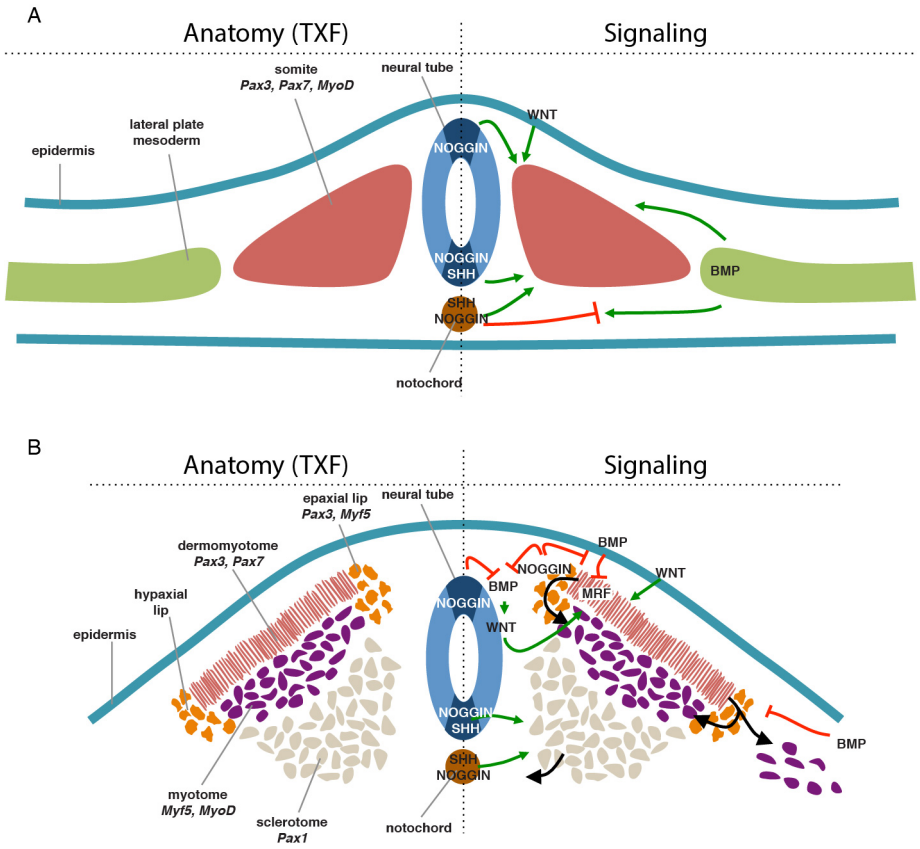

Figure A3: Overview of the anatomy and signaling events in the somite

Schematic representation of transversal section of embryonic myogenic induction at early (A) and late stage (B) of myogenic induction.

Besides its role during the patterning of the somite, BMP signaling also affects the differentiation of myofibers. The effect of BMP signaling was shown to

depend on the developmental stage and the progression along the myogenic program. The differentiation of embryonic myoblasts was shown to be insensitive to BMP signals, whereas the fetal myoblasts and the PAX7 positive precuresors require a decrease of the BMP signaling in order to allow further myogenic differentiation (Fig A2).

One of the tissues severely affected in *Noggin*$^{-/-}$ mice is the developing muscle. This phenotype has not been reported to date and this part of my thesis focused on the molecular basis of this defect.

A.2 Results

A.2.1 Muscle phenotype in *Noggin*$^{-/-}$ embryos

The *Noggin*$^{-/-}$ mice presented a muscle defect during the final stages of in utero development. As the embryos display an excessive chondrogenesis, the size of the muscles in the *Noggin*$^{-/-}$ embryos is reduced from early stages onwards. At 18.5 dpc, the *Noggin*$^{-/-}$ embryos displayed a dramatic muscle phenotype characterized by disorganized myofibers that failed to align. In addition, the number of multinucleated myofibers appeared reduced, more mononucleated myoblasts were found (arrowheads in Fig A3D) and the nuclei failed to migrate towards the plasma membrane in the *Noggin* null muscles. When tracing back the defect at earlier stages of development, we could not detect any of these defects at 16.5 dpc, indicating that between 16.5 dpc and 18.5 dpc (fetal myogenesis) the loss of *Noggin* had a dramatic effect.

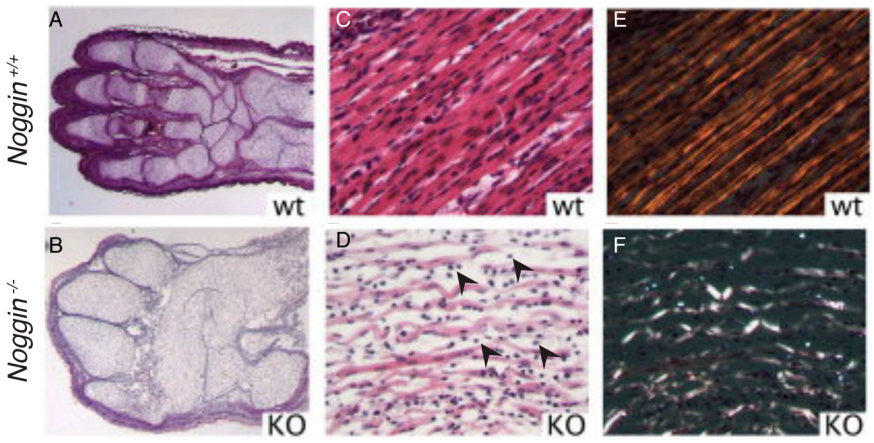

Figure A3: *Noggin*$^{-/-}$ embryos display a dramatic muscle defect

A-F. Newborn littermates of a *Noggin*$^{+/-}$ mating. H&E staining on sagittal sections through the limb shows the excessive chondrogenesis and the disorganization of the muscle fibers in the *Noggin*$^{-/-}$ embryos (A-D). Same section of C and D under polarized light (E-F). Adapted from (Tylzanowski et al., 2006)

A.2.2 Selection of a muscle

To be able to correctly compare *Noggin* null muscles with their wild type littermates, we needed to select anatomically the same muscle in both genotypes. Therefore we performed H&E stainings and compared the anatomy of the limbs. As the limbs of the *Noggin* null mouse were shorter and thicker and had an excess of cartilage, the identification of the different muscles was not evident. Using the Jatlasviewer (www.emage.org), we could identify the same muscle (musculus flexor carpi ulnaris) identifiable in the control and the *Noggin*$^{-/-}$ limbs (Fig A4). We focused on three different stages of fetal myogenesis as the defect developed during this phase of muscle development. Specifically, we isolated limbs at the stage at which there was no apparent defect (16.5 dpc), a dramatic defect (18.5 dpc) and the stage in between (17.5 dpc).

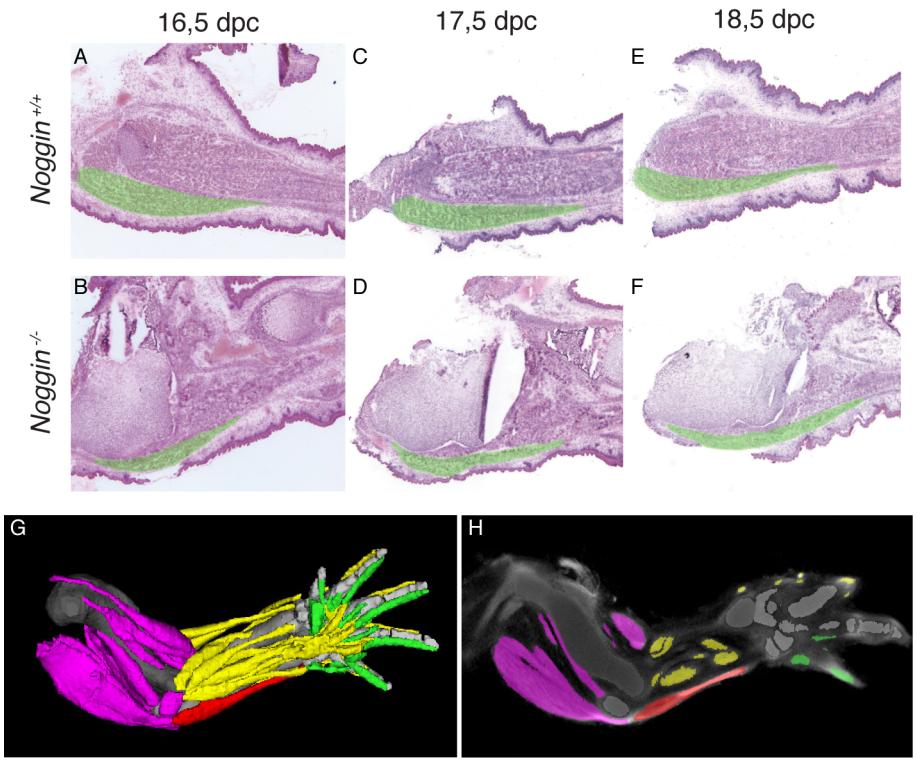

Figure A4: Identification of the musculus flexor carpi ulnaris

A-F: H&E staining on sagittal sections of the limbs at the indicated stages and genotype. The musculus flexor carpi ulnaris is digitally indicated in green. H-I. The limb at 15-16 dpc using Jatlasviewer. The musculus flexor carpi ulnaris is colored in red.

A.2.3 Morphological analysis

To further visualize the difference in the myofiber morphology, we performed an Actin staining using Phalloidin and measured the thickness of the myofibers. As indicated before, no difference in the overall morphology of the muscle could be detected at 16.5 dpc. During later stages however, a decrease in the thickness of the muscle fiber was apparent (Fig A5).

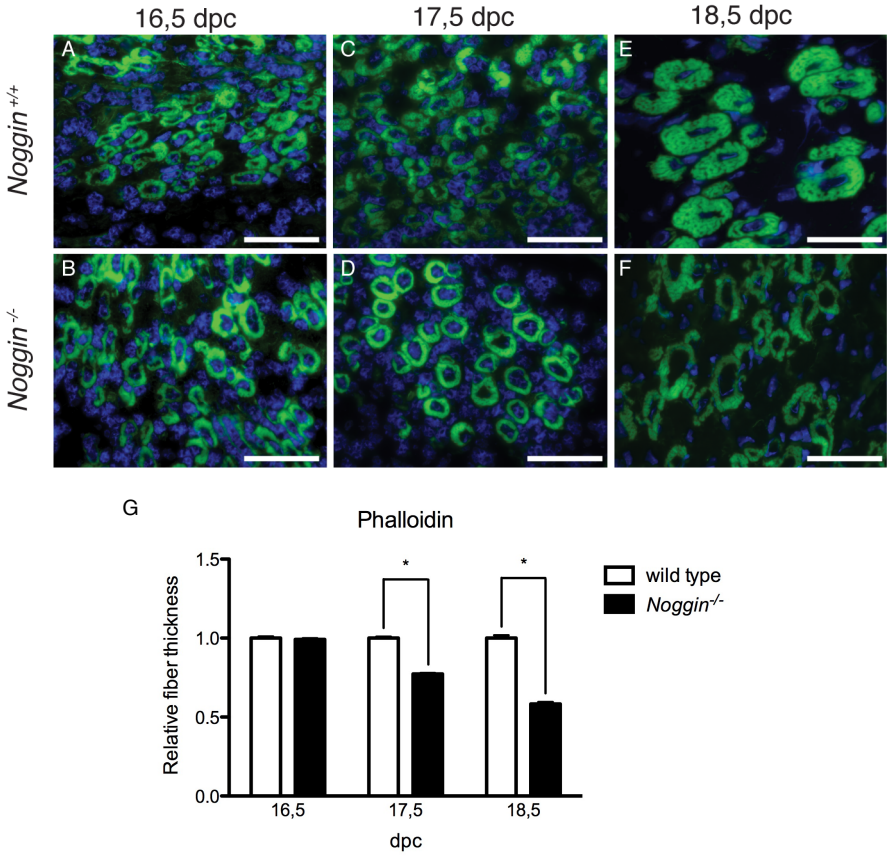

Figure A5: Analysis of the muscle fiber thickness

A-F: Actin immunofluorescence on cross-sections of muscles at the indicated stages. G: Quantification using ImageJ of the thickness of the fiber. Values plotted as mean ± SEM; over 100 fibers of at least 3 different mice embryos were analyzed per condition; *p<0.05

A.2.4 BMP signaling

As NOGGIN is a BMP antagonist, we hypothesized that this phenotype could result in an overactivation of the BMP signaling. Therefore we investigated the activation of the SMAD 1/5/8 proteins and the expression level of different

immediate BMP target genes in the developing limbs with the focus on the developing muscle.

The immunohistochemical analysis for the phosphorylated SMAD 1/5/8 showed an apparent increase of SMAD activation from 16.5 dpc onwards. Interestingly, the morphological muscle defects could only be detected from 17.5 dpc onwards (Fig A6A). The expression of immediate BMP target genes was analyzed using qPCR at 16.5 dpc and indicated that two of them, *Id3* and *Msx1*, were significantly upregulated (Fig A6B).

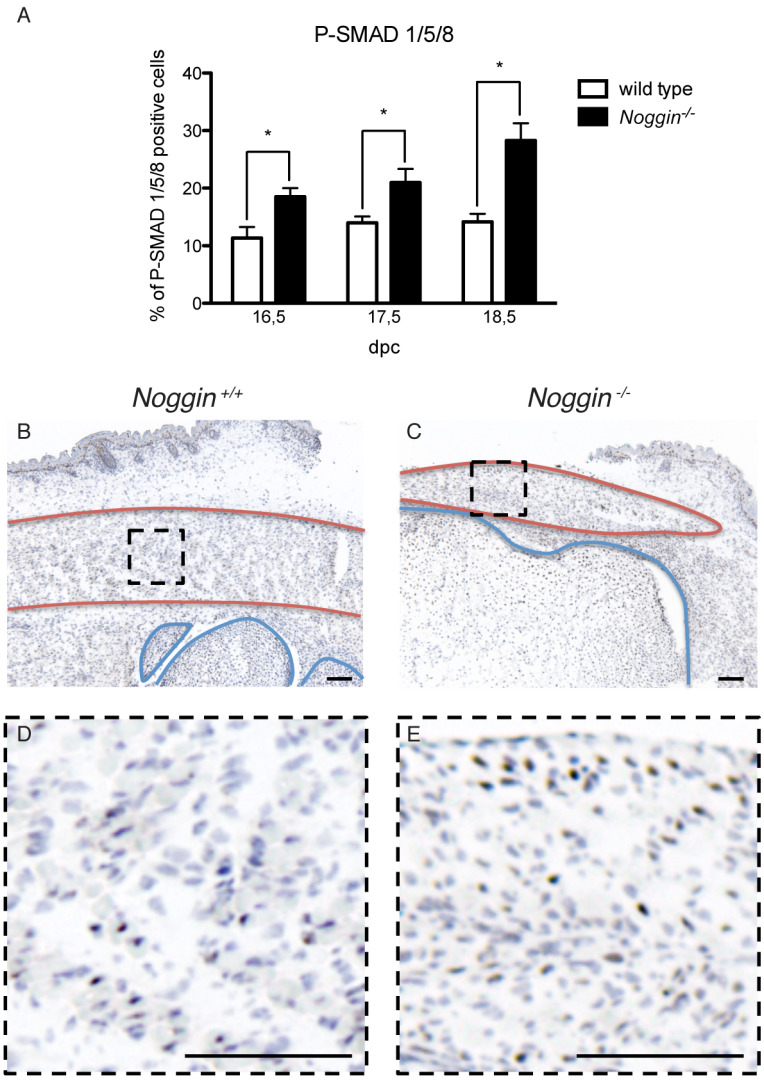

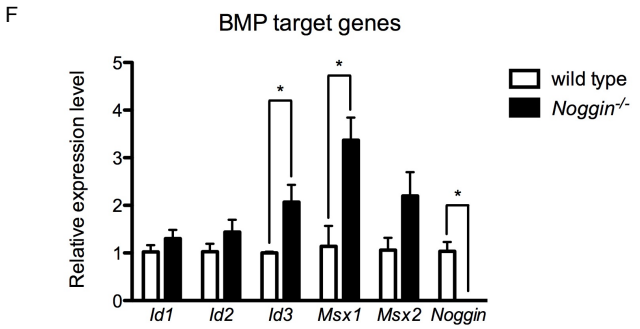

Figure A6: Analysis of the BMP signaling pathway

A. Quantification of P-SMAD 1/5/8 immunohistochemistry on sagittal sections. B-E. Immunohistochemistry for P-SMAD1/5/8 in *Noggin*$^{+/+}$ and *Noggin*$^{-/-}$ 16.5 dpc limbs. Muscle is delineated in red, cartilage and bone in blue. D-E. Blowout of muscle area delineated in black in B and C. Scale bar: 100 µm. F. qPCR analysis of BMP target genes at E16.5. Values plotted as mean ± SEM; n=5; *p<0.05

A.2.5 Proliferation

Since a decrease in the size of the muscle could have been caused by a change in the rate of proliferation and it was shown previously that BMP signaling can change the rate of proliferation (Wang et al., 2010), we analyzed the cell mitotic activity using a KI67 antibody. Despite the difference in size of the muscle and thickness of the fibers, no significant difference in the cell proliferation could be detected in the *Noggin* null muscle (Fig A7).

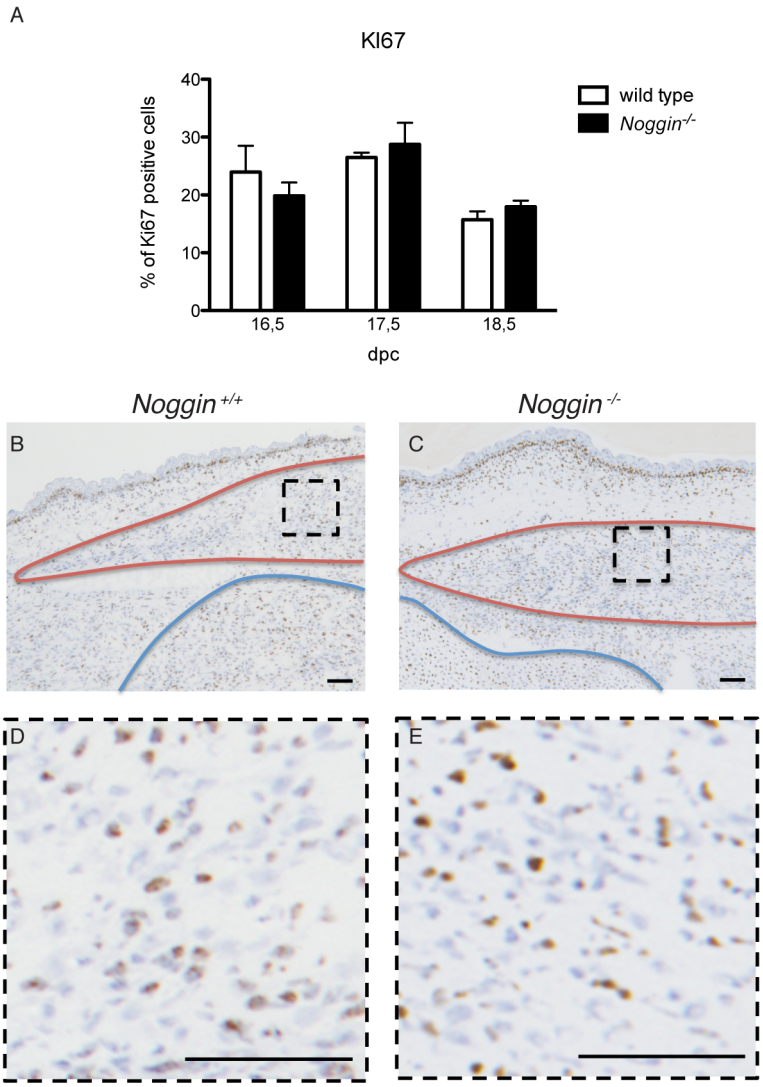

Figure A7: Analysis of the mitotic activity

A Quantification of KI67 immunohistochemistry on sagittal sections. Values plotted as mean ± SEM; n=5; *p<0.05. B-E: Immunohistochemistry for KI67 in *Noggin*$^{+/+}$ and *Noggin*$^{-/-}$ 16.5 dpc limbs. Muscle is delineated in red, cartilage and bone in blue. D-E. Blowout of muscle area delineated in black in B and C. Scale bar: 100 µm.

A.2.6 PAX7 positive progenitor cells

Next to the contribution of the embryonic and the fetal myoblast, a third type of cells, the PAX7 positive cells, contributes to the development of a muscle. During postnatal stages, they were shown to be responsible for further muscle growth and regeneration upon trauma, but also during embryonic stages they contribute significantly to the development of muscle (Kassar-Duchossoy et al., 2005; Relaix et al., 2005). Therefore we decided to investigate this cell population. Interestingly, the number of PAX7 positive cells was progressively reduced in *Noggin*$^{-/-}$ muscles (Fig A8).

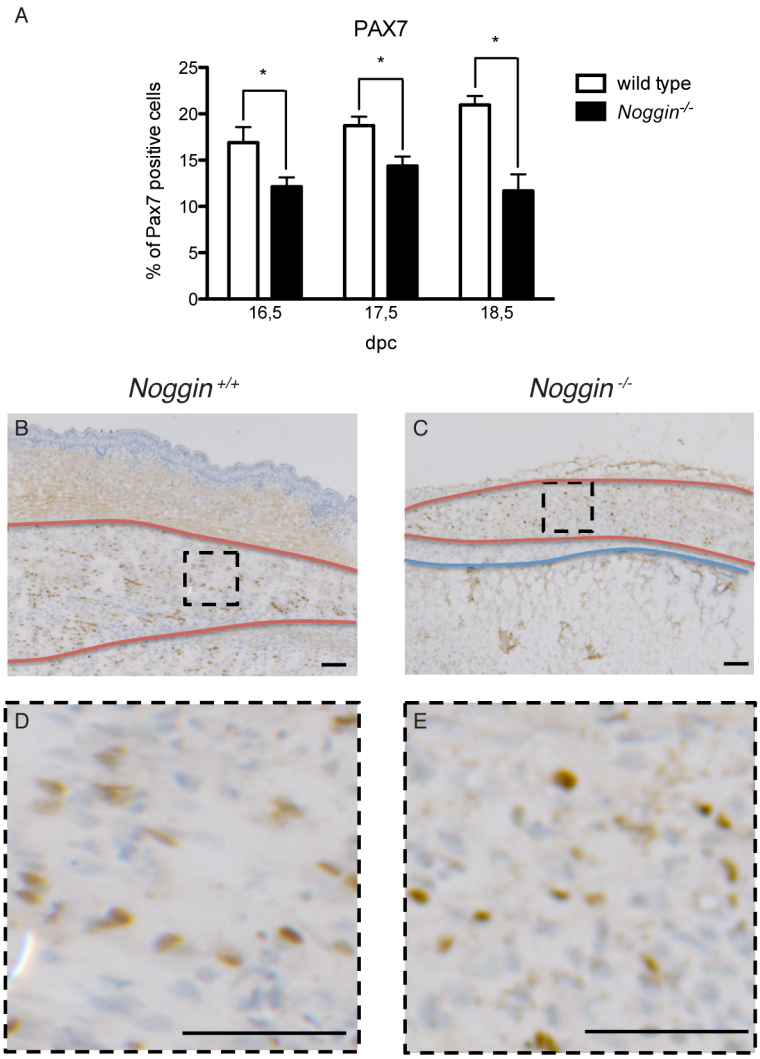

Figure A8: Analysis of the satellite cells

A. Quantification of PAX7 immunohistochemistry on sagittal sections. Values plotted as mean ± SEM; n≤5; *p<0.05. B-E. Immunohistochemistry for PAX7 in *Noggin*$^{+/+}$ and *Noggin*$^{-/-}$ 18 dpc limbs. Muscle is delineated in red, cartilage and bone in blue. D-E. Blowout of muscle area delineated in black in B and C. Scale bar: 100 µm.

A.3 Discussion

While analyzing the *Noggin* null phenotype, we discovered a hitherto unreported muscle defect. Interestingly, the defect reported here has a late onset, indicating that the initial muscle induction and formation occurs normally. At the later stages however, when the muscle acquire more mass, it becomes sensitive to the absence of NOGGIN. Our analysis indicated that the loss of NOGGIN in the mouse embryonic muscle resulted in an increased BMP signaling together with a decrease in the relative number of PAX7 positive cells.

A.3.1 The effect of BMP signaling

Our analysis indicated that the loss of NOGGIN during embryonic stages resulted in an increased Bmp signaling. Molecularly, the inhibitory effect of BMP signaling on the myogenic program was suggested to be a result of the sequestering of the E-proteins by the immediate BMP target genes (*Id1, 2, 3*) (Clever et al., 2010). Thereby the ID proteins block the MRF-mediated activation of the myogenic program, which is dependent on the binding of the MRFs to these E-proteins. Furthermore, MSX1 was shown to block celullar differentiation by preventing cell cycle exit and to antagonize the myogenic activity of PAX3 in migrating limb muscle precursors (Bendall et al., 1999; Hu et al., 2001; Hughes, 2001; Perk et al., 2005). Since the BMP target genes are upregulated in the *Noggin* null mice, the sequestering of the E-proteins, the inhibition of cell cycle exit and/or the loss of differentiation of the migrating limb precursors are all potential mechanisms underlying the *Noggin* null muscle phenotype.

The BMP signaling was shown to regulate the patterning of the somite and the myogenic program, thus a muscle defect in BMP antagonist mutants could have been anticipated. However, the extent of the muscle defect in the *Noggin* null mice was far greater than reported for other BMP antagonist mutants (Matzuk et al., 1995). Reshef et al did suggest that the epaxial musculature in the *Noggin* null mice was largely absent in the posterior of the embryo, but next to a suggestion that NOGGIN plays an important role in muscle formation no further research was conducted on the muscles of the *Noggin* null mice (Reshef et al., 1998). Yet our study is the first one to investigate the muscle defect in *Noggin* null mice and our data show that the *Noggin* null mouse models the numerous in vitro data on the inhibitory effect of BMP signaling on fetal myoblast and satellite cell differentiation in an in vivo setting.

A.3.2 The importance of timing the BMP signaling

In vitro, BMP signaling was shown to balance the proliferation and differentiation of satellite cells. Upon differentiation, BMP signaling is downregulated resulting in the activation of the myogenic program and formation of myofibers (Friedrichs et al., 2011; Ono et al., 2011). In contrast,

when BMP was applied ectopically in the chicken wing, the number of muscle fibers and PAX7 positive cells increased (Amthor et al., 1999; Wang et al., 2010). However, when BMP was applied during earlier stages of chicken development, similar chondrogenesis and myogenesis defects were seen as in the *Noggin* null mice (Duprez et al., 1996a; Duprez et al., 1996b). Potentially the timing of the application of the ectopic signal determines the response and explains the different results.

A.3.3 Intrinsic differences within the myogenic lineage

It was suggested that cells in the same somitic environment could have different intrinsic properties as they respond differently to the same signals (Biressi et al., 2007). For example, embryonic myoblasts were shown to be insensitive to BMP signaling allowing them to stop proliferating and differentiate into the primary myofibers. For fetal myoblasts and satellite cells, however, it was shown that the level of BMP signaling has to be reduced, by either reducing the expression of BMP ligands, or antagonizing the signaling, in order to let differentiation and fusion into secondary fibers occur. This potentially explains our phenotype as the increased Bmp signaling in the *Noggin*$^{-/-}$ muscle would have no effect on the differentiation of the primary fibers, but inhibits the generation of the secondary fibers. Therefore the fetal myoblasts, which normally give rise to the secondary fibers maintain their committed but undifferentiated state. Indeed, we observed numerous mononucleated myoblasts in the *Noggin* null muscle, concomittant with a reduction of multinucleated myofibers. The limited number of primary fibers that is formed might therefore be unable to compensate for the loss of secondary myofibers resulting in a muscle that fails to maintain its organization.
Alternatively, as in vitro evidence indicated that addition of BMP proteins to the medium of C2C12 cells, a rodent myoblast cell lineage, resulted in the transdifferentiation of muscle cells into cells of the chondrogenic and osteogenic lineages one could hypothesize that a number of muscle progenitor cells are drawn into the chondrogenic lineage in the *Noggin* null limb (Murray et al., 1993; Katagiri et al., 1994). This would deplete the pool of muscle precursors in a way that initially enough cells are left to maintain the muscle organization, but at

later stages, when the muscles grow rapidly, there are not enough cells to supply the muscle with cells.

Taken together, the loss of NOGGIN induces a SMAD-dependent increase in BMP signaling that results in an inhibition of fetal myoblast differentiation and a reduction in the number of satellite cells, which causes a severe late onset muscle defect.

A.4 Materials and Methods

A.4.1 Embryo processing

Mice were sacrificed and embryos were collected at 16.5, 17.5 and 18 days post coitus. Forelimbs were isolated using forceps and subsequently embedded in Tissue-Tek (Laborimpex), snap frozen in liquid nitrogen and stored at -80°C. Hindlimbs were processed for LacZ genotyping. Frozen sections (5µm) for immunological staining and histological staining (Haematoxylin and eosin; standard protocol) were made using a cryostat (Prosan).

A.4.2 LacZ genotyping

Hindlimbs were fixed in 4%PFA/PBS for 10 minutes and washed twice with LacZ1 solution (PBS, 2mM $MgCl_2$, 5mM EGTA) for 10 minutes at RT, followed by another washing step with LacZ2 (PBS, 0.1M Na_3PO_4, 2mM $MgCl_2$, 0.01% sodium deoxycholate, 0.02% NP-40; pH 7.2-7.4) for 5 minutes at RT. Staining was performed by applying staining solution (5mM $K_3Fe(CN)_6$, 5mM $K_4Fe(CN)_6$, 0.5mg/ml, X-gal in LacZ2 buffer for 2-3 hours at 37°C or ON at RT. After washing steps with PBS and clearing with 2% KOH, limbs were treated with an increasing gradient of glycerol/KOH before storage.

A.4.3 Immunohistochemistry

Phalloidin

Staining was performed using manufacturers protocol.

P-SMAD

Frozen sections were fixed with methanol for 10 minutes at -20°C. After quenching in 3% H202/MQ and washing in TBST, antigen retrieval was performed with sodium citrate buffer (pH6), followed by additional washing with TBST. Sections were blocked with Normal Goat Serum (Millipore) (1/5 in TBST) and O/N incubated with the primary antibody (P-SMAD 1/5/8, Cell Signaling, 9511S; 1/100) at 4°C. After washing, the biotinylated secondary antibody was applied for 30 minutes at RT. The signal was amplified with the ABC reagent (Vectastain, dilution according to manufacturers protocol) for 30

minutes at RT. After washing, the color was developed using DAB (DAKO, dilution according to manufacturers protocol) and sections were mounted using Pertex.

Ki67 and PAX7

The P-SMAD protocol was used with following modifications. Frozen sections were fixed with ethanol and methanol for 5 minutes and quenched in 0.5% H202/MeOH. Washing steps were performed with PBS, a KI67 antibody (DAKO TEC3; 1/100) or PAX7 antibody (DSHB, Kawakami Atushi, Yokohama, Japan; 1/400) was used and blocking was done with 10%NGS/PBS.

Quantification

ImageJ software was used for measuring the muscle fiber thickness and the quantification of the percentage of P-SMAD, KI67 or PAX7 positive cells. The significance of the difference in expression was analyzed using the Student's T-test.

A.4.4 qPCR

RNA was isolated by scraping the muscles of at least 10 frozen sections 16.5 dpc embryonic limbs using the High Pure RNA Isolation Kit (Roche Applied Science). At least three RNA isolations were performed per condition and subsequently reverse transcribed using Primescript RT Reagent (Takara; manufacturers protocol). Real-time PCR was performed in duplicate with gene specific primers (Table A1) with SYBR Premix Ex Taq II (Takara; manufacturers protocol) using Rotor-gene 6000 detection system (Corbett Research, Westburg). Gene expression was normalized to the housekeeping gene *Hprt1* and presented as a ratio to control embryos. The significance of the difference in expression was analyzed using the Student's T-test.

Gene	Primer sense 5'-3'	Primer antisense 5'-3'
Hprt1	TGCTGACCTGCTGGATTACA	TATGTCCCCCGTTGACTGAT
Id1	GAGTCTGAAGTCGGGACCAC	AACACATGCCGCCTCGG
Id2	CCTGCATCACCAGAGACCTG	GGGAATTCAGATGCCTGCAA
Id3	TGCAGCGTGTCATAGACTACA	TGAGCTCAGCTGTCTGGATCG
Msx1	GCCAGAAGATGCTCTGGTGA	TCAGCCGTCTGGCTGGG
Msx2	GCCTCGGTCAAGTCGGAAAA	GGCTCATATGTCTGGGCGG
Noggin	GGGGCGAAGTAGCCATAAAG	GGGGCGAAGTAGCCATAAAG

Table A1: Primer sequences used for qPCR

References

Abouzeid H, Boisset G, Favez T, Youssef M, Marzouk I, Shakankiry N, Bayoumi N, Descombes P, Agosti C, Munier FL, Schorderet DF. 2011. Mutations in the SPARC-related modular calcium-binding protein 1 gene, SMOC1, cause waardenburg anophthalmia syndrome. Am J Hum Genet 88:92-98.
Alkhateeb A, Al-Dain Marzouka N, Qarqaz F. 2010. SMOC2 gene variant and the risk of vitiligo in Jordanian Arabs. Eur J Dermatol 20:701-704.
Alkhateeb A, Marzouka NA, Tashtoush R. 2013. Variants in PTPN22 and SMOC2 genes and the risk of thyroid disease in the Jordanian Arab population. Endocrine 44:702-709.
Amaya E. 2013. The hemangioblast: a state of competence. Blood 122:3853-3854.
Amthor H, Christ B, Patel K. 1999. A molecular mechanism enabling continuous embryonic muscle growth - a balance between proliferation and differentiation. Development 126:1041-1053.
Arnold HH, Braun T. 1996. Targeted inactivation of myogenic factor genes reveals their role during mouse myogenesis: a review. Int J Dev Biol 40:345-353.
Balemans W, Van Hul W. 2002. Extracellular regulation of BMP signaling in vertebrates: a cocktail of modulators. Dev Biol 250:231-250.
Baron MH. 2001. Molecular regulation of embryonic hematopoiesis and vascular development: a novel pathway. J Hematother Stem Cell Res 10:587-594.
Bendall AJ, Ding J, Hu G, Shen MM, Abate-Shen C. 1999. Msx1 antagonizes the myogenic activity of Pax3 in migrating limb muscle precursors. Development 126:4965-4976.
Bentzinger CF, Wang YX, Rudnicki MA. 2012. Building muscle: molecular regulation of myogenesis. Cold Spring Harb Perspect Biol 4.
Biressi S, Molinaro M, Cossu G. 2007. Cellular heterogeneity during vertebrate skeletal muscle development. Dev Biol 308:281-293.
Birlea SA, Gowan K, Fain PR, Spritz RA. 2010. Genome-wide association study of generalized vitiligo in an isolated European founder population identifies SMOC2, in close proximity to IDDM8. J Invest Dermatol 130:798-803.
Bloch-Zupan A, Jamet X, Etard C, Laugel V, Muller J, Geoffroy V, Strauss JP, Pelletier V, Marion V, Poch O, Strahle U, Stoetzel C, Dollfus H. 2011. Homozygosity mapping and candidate prioritization identify mutations, missed by whole-exome sequencing, in SMOC2, causing major dental developmental defects. Am J Hum Genet 89:773-781.
Bober E, Franz T, Arnold HH, Gruss P, Tremblay P. 1994. Pax-3 is required for the development of limb muscles: a possible role for the migration of dermomyotomal muscle progenitor cells. Development 120:603-612.
Bolli N, Payne EM, Grabher C, Lee JS, Johnston AB, Falini B, Kanki JP, Look AT. 2010. Expression of the cytoplasmic NPM1 mutant (NPMc+) causes the expansion of hematopoietic cells in zebrafish. Blood 115:3329-3340.
Bornstein P. 2000. Matricellular proteins: an overview. Matrix Biol 19:555-556.
Bornstein P. 2009. Matricellular proteins: an overview. J Cell Commun Signal 3:163-165.
Bornstein P, Sage EH. 2002. Matricellular proteins: extracellular modulators of cell function. Curr Opin Cell Biol 14:608-616.
Bradshaw AD. 2009. The role of SPARC in extracellular matrix assembly. J Cell Commun Signal 3:239-246.
Bradshaw AD. 2012. Diverse biological functions of the SPARC family of proteins. Int J Biochem Cell Biol 44:480-488.
Bradshaw AD, Reed MJ, Sage EH. 2002. SPARC-null mice exhibit accelerated cutaneous wound closure. J Histochem Cytochem 50:1-10.
Bradshaw AD, Sage EH. 2001. SPARC, a matricellular protein that functions in cellular differentiation and tissue response to injury. J Clin Invest 107:1049-1054.
Braun T, Arnold HH. 1995. Inactivation of Myf-6 and Myf-5 genes in mice leads to alterations in skeletal muscle development. EMBO J 14:1176-1186.
Braun T, Rudnicki MA, Arnold HH, Jaenisch R. 1992. Targeted inactivation of the muscle regulatory gene Myf-5 results in abnormal rib development and perinatal death. Cell 71:369-382.
Brekken RA, Sage EH. 2001. SPARC, a matricellular protein: at the crossroads of cell-matrix communication. Matrix Biol 19:816-827.
Brison N, Debeer P, Fantini S, Oley C, Zappavigna V, Luyten FP, Tylzanowski P. 2012. An N-terminal G11A mutation in HOXD13 causes synpolydactyly and interferes with Gli3R function during limb pre-patterning. Hum Mol Genet 21:2464-2475.

Brown WR, Hubbard SJ, Tickle C, Wilson SA. 2003. The chicken as a model for large-scale analysis of vertebrate gene function. Nat Rev Genet 4:87-98.
Brownlie A, Donovan A, Pratt SJ, Paw BH, Oates AC, Brugnara C, Witkowska HE, Sassa S, Zon LI. 1998. Positional cloning of the zebrafish sauternes gene: a model for congenital sideroblastic anaemia. Nat Genet 20:244-250.
Brownlie A, Hersey C, Oates AC, Paw BH, Falick AM, Witkowska HE, Flint J, Higgs D, Jessen J, Bahary N, Zhu H, Lin S, Zon L. 2003. Characterization of embryonic globin genes of the zebrafish. Dev Biol 255:48-61.
Brunak S, Engelbrecht J, Knudsen S. 1991. Prediction of human mRNA donor and acceptor sites from the DNA sequence. J Mol Biol 220:49-65.
Brunet LJ, McMahon JA, McMahon AP, Harland RM. 1998. Noggin, cartilage morphogenesis, and joint formation in the mammalian skeleton. Science 280:1455-1457.
Busch E, Hohenester E, Timpl R, Paulsson M, Maurer P. 2000. Calcium affinity, cooperativity, and domain interactions of extracellular EF-hands present in BM-40. J Biol Chem 275:25508-25515.
Buxton P, Edwards C, Archer CW, Francis-West P. 2001. Growth/differentiation factor-5 (GDF-5) and skeletal development. J Bone Joint Surg Am 83-A Suppl 1:S23-30.
Ceinos RM, Torres-Nunez E, Chamorro R, Novoa B, Figueras A, Ruane NM, Rotllant J. 2013. Critical role of the matricellular protein SPARC in mediating erythroid progenitor cell development in zebrafish. Cells Tissues Organs 197:196-208.
Chang SC, Hoang B, Thomas JT, Vukicevic S, Luyten FP, Ryba NJ, Kozak CA, Reddi AH, Moos M, Jr. 1994. Cartilage-derived morphogenetic proteins. New members of the transforming growth factor-beta superfamily predominantly expressed in long bones during human embryonic development. J Biol Chem 269:28227-28234.
Chen JN, Fishman MC. 1996. Zebrafish tinman homolog demarcates the heart field and initiates myocardial differentiation. Development 122:3809-3816.
Chen W, Zhu G, Hao L, Wu M, Ci H, Li YP. 2013. C/EBPalpha regulates osteoclast lineage commitment. Proc Natl Acad Sci U S A 110:7294-7299.
Childs S, Weinstein BM, Mohideen MA, Donohue S, Bonkovsky H, Fishman MC. 2000. Zebrafish dracula encodes ferrochelatase and its mutation provides a model for erythropoietic protoporphyria. Curr Biol 10:1001-1004.
Clark KJ, Voytas DF, Ekker SC. 2011. A TALE of two nucleases: gene targeting for the masses? Zebrafish 8:147-149.
Clever JL, Sakai Y, Wang RA, Schneider DB. 2010. Inefficient skeletal muscle repair in inhibitor of differentiation knockout mice suggests a crucial role for BMP signaling during adult muscle regeneration. Am J Physiol Cell Physiol 298:C1087-1099.
Clevers H. 2006. Wnt/beta-catenin signaling in development and disease. Cell 127:469-480.
Corkery DP, Dellaire G, Berman JN. 2011. Leukaemia xenotransplantation in zebrafish--chemotherapy response assay in vivo. Br J Haematol 153:786-789.
Craven SE, French D, Ye W, de Sauvage F, Rosenthal A. 2005. Loss of Hspa9b in zebrafish recapitulates the ineffective hematopoiesis of the myelodysplastic syndrome. Blood 105:3528-3534.
Cumano A, Godin I. 2007. Ontogeny of the hematopoietic system. Annu Rev Immunol 25:745-785.
Dal-Pra S, Furthauer M, Van-Celst J, Thisse B, Thisse C. 2006. Noggin1 and Follistatin-like2 function redundantly to Chordin to antagonize BMP activity. Dev Biol 298:514-526.
Danen EH, Sonneveld P, Brakebusch C, Fassler R, Sonnenberg A. 2002. The fibronectin-binding integrins alpha5beta1 and alphavbeta3 differentially modulate RhoA-GTP loading, organization of cell matrix adhesions, and fibronectin fibrillogenesis. J Cell Biol 159:1071-1086.
Danilova N, Sakamoto KM, Lin S. 2008. Ribosomal protein S19 deficiency in zebrafish leads to developmental abnormalities and defective erythropoiesis through activation of p53 protein family. Blood 112:5228-5237.
Davidson AJ, Zon LI. 2004. The 'definitive' (and 'primitive') guide to zebrafish hematopoiesis. Oncogene 23:7233-7246.
Davidson LA, Marsden M, Keller R, Desimone DW. 2006. Integrin alpha5beta1 and fibronectin regulate polarized cell protrusions required for Xenopus convergence and extension. Curr Biol 16:833-844.
De A. 2011. Wnt/Ca2+ signaling pathway: a brief overview. Acta Biochim Biophys Sin (Shanghai) 43:745-756.

Del Vecchio GC, Giordani L, De Santis A, De Mattia D. 2005. Dyserythropoietic anemia and thrombocytopenia due to a novel mutation in GATA-1. Acta Haematol 114:113-116.
Delany AM, Amling M, Priemel M, Howe C, Baron R, Canalis E. 2000. Osteopenia and decreased bone formation in osteonectin-deficient mice. J Clin Invest 105:1325.
Delany AM, Canalis E. 1998. Basic fibroblast growth factor destabilizes osteonectin mRNA in osteoblasts. Am J Physiol 274:C734-740.
Desmet FO, Hamroun D, Lalande M, Collod-Beroud G, Claustres M, Beroud C. 2009. Human Splicing Finder: an online bioinformatics tool to predict splicing signals. Nucleic Acids Res 37:e67.
Donovan A, Brownlie A, Zhou Y, Shepard J, Pratt SJ, Moynihan J, Paw BH, Drejer A, Barut B, Zapata A, Law TC, Brugnara C, Lux SE, Pinkus GS, Pinkus JL, Kingsley PD, Palis J, Fleming MD, Andrews NC, Zon LI. 2000. Positional cloning of zebrafish ferroportin1 identifies a conserved vertebrate iron exporter. Nature 403:776-781.
Dooley KA, Davidson AJ, Zon LI. 2005. Zebrafish scl functions independently in hematopoietic and endothelial development. Dev Biol 277:522-536.
Doyon Y, McCammon JM, Miller JC, Faraji F, Ngo C, Katibah GE, Amora R, Hocking TD, Zhang L, Rebar EJ, Gregory PD, Urnov FD, Amacher SL. 2008. Heritable targeted gene disruption in zebrafish using designed zinc-finger nucleases. Nat Biotechnol 26:702-708.
Duprez D, Bell EJ, Richardson MK, Archer CW, Wolpert L, Brickell PM, Francis-West PH. 1996a. Overexpression of BMP-2 and BMP-4 alters the size and shape of developing skeletal elements in the chick limb. Mech Dev 57:145-157.
Duprez DM, Coltey M, Amthor H, Brickell PM, Tickle C. 1996b. Bone morphogenetic protein-2 (BMP-2) inhibits muscle development and promotes cartilage formation in chick limb bud cultures. Dev Biol 174:448-452.
Dzierzak E, Medvinsky A. 1995. Mouse embryonic hematopoiesis. Trends Genet 11:359-366.
Eib DW, Martens GJ. 1996. A novel transmembrane protein with epidermal growth factor and follistatin domains expressed in the hypothalamo-hypophysial axis of Xenopus laevis. J Neurochem 67:1047-1055.
Ellett F, Lieschke GJ. 2010. Zebrafish as a model for vertebrate hematopoiesis. Curr Opin Pharmacol 10:563-570.
Esch FS, Shimasaki S, Mercado M, Cooksey K, Ling N, Ying S, Ueno N, Guillemin R. 1987. Structural characterization of follistatin: a novel follicle-stimulating hormone release-inhibiting polypeptide from the gonad. Mol Endocrinol 1:849-855.
Fantini S, Vaccari G, Brison N, Debeer P, Tylzanowski P, Zappavigna V. 2009. A G220V substitution within the N-terminal transcription regulating domain of HOXD13 causes a variant synpolydactyly phenotype. Hum Mol Genet 18:847-860.
Frantz C, Stewart KM, Weaver VM. 2010. The extracellular matrix at a glance. J Cell Sci 123:4195-4200.
Friedrichs M, Wirsdoerfer F, Flohe SB, Schneider S, Wuelling M, Vortkamp A. 2011. BMP signaling balances proliferation and differentiation of muscle satellite cell descendants. BMC Cell Biol 12:26.
Funahashi J, Nakamura H. 2008. Electroporation in avian embryos. Methods Mol Biol 461:377-382.
Gao C, Chen YG. 2010. Dishevelled: The hub of Wnt signaling. Cell Signal 22:717-727.
Garrity DM, Childs S, Fishman MC. 2002. The heartstrings mutation in zebrafish causes heart/fin Tbx5 deficiency syndrome. Development 129:4635-4645.
Gazzerro E, Canalis E. 2006. Bone morphogenetic proteins and their antagonists. Rev Endocr Metab Disord 7:51-65.
Ghiselli G, Farber SA. 2005. D-glucuronyl C5-epimerase acts in dorso-ventral axis formation in zebrafish. BMC Dev Biol 5:19.
Gilardelli CN, Pozzoli O, Sordino P, Matassi G, Cotelli F. 2004. Functional and hierarchical interactions among zebrafish vox/vent homeobox genes. Dev Dyn 230:494-508.
Gilbert S. 2006. Developmental Biology Eighth edition. Sinauer.
Gilboa L, Nohe A, Geissendorfer T, Sebald W, Henis YI, Knaus P. 2000. Bone morphogenetic protein receptor complexes on the surface of live cells: a new oligomerization mode for serine/threonine kinase receptors. Mol Biol Cell 11:1023-1035.
Gilles C, Bassuk JA, Pulyaeva H, Sage EH, Foidart JM, Thompson EW. 1998. SPARC/osteonectin induces matrix metalloproteinase 2 activation in human breast cancer cell lines. Cancer Res 58:5529-5536.

Gordon CT, Rodda FA, Farlie PG. 2009. The RCAS retroviral expression system in the study of skeletal development. Dev Dyn 238:797-811.
Goulding M, Lumsden A, Paquette AJ. 1994. Regulation of Pax-3 expression in the dermomyotome and its role in muscle development. Development 120:957-971.
Gray C, Loynes CA, Whyte MK, Crossman DC, Renshaw SA, Chico TJ. 2011. Simultaneous intravital imaging of macrophage and neutrophil behaviour during inflammation using a novel transgenic zebrafish. Thromb Haemost 105:811-819.
Hamburger V, Hamilton HL. 1992. A series of normal stages in the development of the chick embryo. 1951. Dev Dyn 195:231-272.
Hammerschmidt M, Pelegri F, Mullins MC, Kane DA, Brand M, van Eeden FJ, Furutani-Seiki M, Granato M, Haffter P, Heisenberg CP, Jiang YJ, Kelsh RN, Odenthal J, Warga RM, Nusslein-Volhard C. 1996. Mutations affecting morphogenesis during gastrulation and tail formation in the zebrafish, Danio rerio. Development 123:143-151.
Hasty P, Bradley A, Morris JH, Edmondson DG, Venuti JM, Olson EN, Klein WH. 1993. Muscle deficiency and neonatal death in mice with a targeted mutation in the myogenin gene. Nature 364:501-506.
Heisenberg CP, Tada M. 2002. Zebrafish gastrulation movements: bridging cell and developmental biology. Semin Cell Dev Biol 13:471-479.
Heisenberg CP, Tada M, Rauch GJ, Saude L, Concha ML, Geisler R, Stemple DL, Smith JC, Wilson SW. 2000. Silberblick/Wnt11 mediates convergent extension movements during zebrafish gastrulation. Nature 405:76-81.
Hoang B, Moos M, Jr., Vukicevic S, Luyten FP. 1996. Primary structure and tissue distribution of FRZB, a novel protein related to Drosophila frizzled, suggest a role in skeletal morphogenesis. J Biol Chem 271:26131-26137.
Hofmann JJ, Luisa Iruela-Arispe M. 2007. Notch expression patterns in the retina: An eye on receptor-ligand distribution during angiogenesis. Gene Expr Patterns 7:461-470.
Hogan BM, Layton JE, Pyati UJ, Nutt SL, Hayman JW, Varma S, Heath JK, Kimelman D, Lieschke GJ. 2006. Specification of the primitive myeloid precursor pool requires signaling through Alk8 in zebrafish. Curr Biol 16:506-511.
Hohenester E, Maurer P, Timpl R. 1997. Crystal structure of a pair of follistatin-like and EF-hand calcium-binding domains in BM-40. EMBO J 16:3778-3786.
Horie M, Mitsumoto Y, Kyushiki H, Kanemoto N, Watanabe A, Taniguchi Y, Nishino N, Okamoto T, Kondo M, Mori T, Noguchi K, Nakamura Y, Takahashi E, Tanigami A. 2000. Identification and characterization of TMEFF2, a novel survival factor for hippocampal and mesencephalic neurons. Genomics 67:146-152.
Hu G, Lee H, Price SM, Shen MM, Abate-Shen C. 2001. Msx homeobox genes inhibit differentiation through upregulation of cyclin D1. Development 128:2373-2384.
Huang CJ, Tu CT, Hsiao CD, Hsieh FJ, Tsai HJ. 2003. Germ-line transmission of a myocardium-specific GFP transgene reveals critical regulatory elements in the cardiac myosin light chain 2 promoter of zebrafish. Dev Dyn 228:30-40.
Hughes SM. 2001. Muscle development: reversal of the differentiated state. Curr Biol 11:R237-239.
Hwang WY, Fu Y, Reyon D, Maeder ML, Tsai SQ, Sander JD, Peterson RT, Yeh JR, Joung JK. 2013. Efficient genome editing in zebrafish using a CRISPR-Cas system. Nat Biotechnol 31:227-229.
Imai Y, Gates MA, Melby AE, Kimelman D, Schier AF, Talbot WS. 2001. The homeobox genes vox and vent are redundant repressors of dorsal fates in zebrafish. Development 128:2407-2420.
Jagannathan-Bogdan M, Zon LI. 2013. Hematopoiesis. Development 140:2463-2467.
Jensen MA, Koszalka TR, Brent RL. 1975. Production of congenital malformations using tissue antisera. Dev Biol 42:1-12.
Jin H, Li L, Xu J, Zhen F, Zhu L, Liu PP, Zhang M, Zhang W, Wen Z. 2012. Runx1 regulates embryonic myeloid fate choice in zebrafish through a negative feedback loop inhibiting Pu.1 expression. Blood 119:5239-5249.
Jing L, Zon LI. 2011. Zebrafish as a model for normal and malignant hematopoiesis. Dis Model Mech 4:433-438.
Jollie WP. 1968. Changes in the fine structure of the parietal yolk sac of the rat placenta with increasing gestational age. Am J Anat 122:513-531.
Kane DA, Kimmel CB. 1993. The zebrafish midblastula transition. Development 119:447-456.

Kassar-Duchossoy L, Giacone E, Gayraud-Morel B, Jory A, Gomes D, Tajbakhsh S. 2005. Pax3/Pax7 mark a novel population of primitive myogenic cells during development. Genes Dev 19:1426-1431.
Katagiri T, Yamaguchi A, Komaki M, Abe E, Takahashi N, Ikeda T, Rosen V, Wozney JM, Fujisawa-Sehara A, Suda T. 1994. Bone morphogenetic protein-2 converts the differentiation pathway of C2C12 myoblasts into the osteoblast lineage. J Cell Biol 127:1755-1766.
Kawakami Y, Capdevila J, Buscher D, Itoh T, Rodriguez Esteban C, Izpisua Belmonte JC. 2001. WNT signals control FGF-dependent limb initiation and AER induction in the chick embryo. Cell 104:891-900.
Kawano Y, Kypta R. 2003. Secreted antagonists of the Wnt signalling pathway. J Cell Sci 116:2627-2634.
Kilian B, Mansukoski H, Barbosa FC, Ulrich F, Tada M, Heisenberg CP. 2003. The role of Ppt/Wnt5 in regulating cell shape and movement during zebrafish gastrulation. Mech Dev 120:467-476.
Kimelman D. 2006. Mesoderm induction: from caps to chips. Nat Rev Genet 7:360-372.
Klemencic M, Novinec M, Maier S, Hartmann U, Lenarcic B. 2013. The heparin-binding activity of secreted modular calcium-binding protein 1 (SMOC-1) modulates its cell adhesion properties. PLoS One 8:e56839.
Korchynskyi O, Dechering KJ, Sijbers AM, Olijve W, ten Dijke P. 2003. Gene array analysis of bone morphogenetic protein type I receptor-induced osteoblast differentiation. J Bone Miner Res 18:1177-1185.
Kulkeaw K, Sugiyama D. 2012. Zebrafish erythropoiesis and the utility of fish as models of anemia. Stem Cell Res Ther 3:55.
Langdon YG, Mullins MC. 2011. Maternal and zygotic control of zebrafish dorsoventral axial patterning. Annu Rev Genet 45:357-377.
Langenau DM, Traver D, Ferrando AA, Kutok JL, Aster JC, Kanki JP, Lin S, Prochownik E, Trede NS, Zon LI, Look AT. 2003. Myc-induced T cell leukemia in transgenic zebrafish. Science 299:887-890.
Lappin DW, McMahon R, Murphy M, Brady HR. 2002. Gremlin: an example of the re-emergence of developmental programmes in diabetic nephropathy. Nephrol Dial Transplant 17 Suppl 9:65-67.
Law SH, Sargent TD. 2013. Maternal pak4 expression is required for primitive myelopoiesis in zebrafish. Mech Dev 130:181-194.
Lawson ND, Weinstein BM. 2002. In vivo imaging of embryonic vascular development using transgenic zebrafish. Dev Biol 248:307-318.
Lees C, Howie S, Sartor RB, Satsangi J. 2005. The hedgehog signalling pathway in the gastrointestinal tract: implications for development, homeostasis, and disease. Gastroenterology 129:1696-1710.
Lenarcic B, Bevec T. 1998. Thyropins--new structurally related proteinase inhibitors. Biol Chem 379:105-111.
Lewandoski M, Sun X, Martin GR. 2000. Fgf8 signalling from the AER is essential for normal limb development. Nat Genet 26:460-463.
Li L, Jin H, Xu J, Shi Y, Wen Z. 2011. Irf8 regulates macrophage versus neutrophil fate during zebrafish primitive myelopoiesis. Blood 117:1359-1369.
Li Y, Tower J. 2009. Adult-specific over-expression of the Drosophila genes magu and hebe increases life span and modulates late-age female fecundity. Mol Genet Genomics 281:147-162.
Liao EC, Paw BH, Peters LL, Zapata A, Pratt SJ, Do CP, Lieschke G, Zon LI. 2000. Hereditary spherocytosis in zebrafish riesling illustrates evolution of erythroid beta-spectrin structure, and function in red cell morphogenesis and membrane stability. Development 127:5123-5132.
Lieschke GJ, Oates AC, Paw BH, Thompson MA, Hall NE, Ward AC, Ho RK, Zon LI, Layton JE. 2002. Zebrafish SPI-1 (PU.1) marks a site of myeloid development independent of primitive erythropoiesis: implications for axial patterning. Dev Biol 246:274-295.
Little SC, Mullins MC. 2004. Twisted gastrulation promotes BMP signaling in zebrafish dorsal-ventral axial patterning. Development 131:5825-5835.
Liu P, Lu J, Cardoso WV, Vaziri C. 2008. The SPARC-related factor SMOC-2 promotes growth factor-induced cyclin D1 expression and DNA synthesis via integrin-linked kinase. Mol Biol Cell 19:248-261.

Logan CY, Nusse R. 2004. The Wnt signaling pathway in development and disease. Annu Rev Cell Dev Biol 20:781-810.
Lories RJ. 2008. Joint homeostasis, restoration, and remodeling in osteoarthritis. Best Pract Res Clin Rheumatol 22:209-220.
Lories RJ, Luyten FP. 2005. Bone morphogenetic protein signaling in joint homeostasis and disease. Cytokine Growth Factor Rev 16:287-298.
Lories RJ, Peeters J, Bakker A, Tylzanowski P, Derese I, Schrooten J, Thomas JT, Luyten FP. 2007. Articular cartilage and biomechanical properties of the long bones in Frzb-knockout mice. Arthritis Rheum 56:4095-4103.
Luyten FP, Lories RJ, Verschueren P, de Vlam K, Westhovens R. 2006. Contemporary concepts of inflammation, damage and repair in rheumatic diseases. Best Pract Res Clin Rheumatol 20:829-848.
Maeno M, Mead PE, Kelley C, Xu RH, Kung HF, Suzuki A, Ueno N, Zon LI. 1996. The role of BMP-4 and GATA-2 in the induction and differentiation of hematopoietic mesoderm in Xenopus laevis. Blood 88:1965-1972.
Maier S. 2006. Analyse der Expression und Funktion von SMOC-1 und SMOC-2. In. Cologne: University of Cologne.
Maier S, Paulsson M, Hartmann U. 2008. The widely expressed extracellular matrix protein SMOC-2 promotes keratinocyte attachment and migration. Exp Cell Res 314:2477-2487.
Mao Y, Schwarzbauer JE. 2005. Fibronectin fibrillogenesis, a cell-mediated matrix assembly process. Matrix Biol 24:389-399.
Marlow F, Gonzalez EM, Yin C, Rojo C, Solnica-Krezel L. 2004. No tail co-operates with non-canonical Wnt signaling to regulate posterior body morphogenesis in zebrafish. Development 131:203-216.
Martin CS, Moriyama A, Zon LI. 2011. Hematopoietic stem cells, hematopoiesis and disease: lessons from the zebrafish model. Genome Med 3:83.
Massague J, Chen YG. 2000. Controlling TGF-beta signaling. Genes Dev 14:627-644.
Matzuk MM, Lu N, Vogel H, Sellheyer K, Roop DR, Bradley A. 1995. Multiple defects and perinatal death in mice deficient in follistatin. Nature 374:360-363.
McClung HM, Thomas SL, Osenkowski P, Toth M, Menon P, Raz A, Fridman R, Rempel SA. 2007. SPARC upregulates MT1-MMP expression, MMP-2 activation, and the secretion and cleavage of galectin-3 in U87MG glioma cells. Neurosci Lett 419:172-177.
McMahon JA, Takada S, Zimmerman LB, Fan CM, Harland RM, McMahon AP. 1998. Noggin-mediated antagonism of BMP signaling is required for growth and patterning of the neural tube and somite. Genes Dev 12:1438-1452.
McReynolds LJ, Gupta S, Figueroa ME, Mullins MC, Evans T. 2007. Smad1 and Smad5 differentially regulate embryonic hematopoiesis. Blood 110:3881-3890.
Melvin VS, Feng W, Hernandez-Lagunas L, Artinger KB, Williams T. 2013. A morpholino-based screen to identify novel genes involved in craniofacial morphogenesis. Dev Dyn 242:817-831.
Merino R, Macias D, Ganan Y, Economides AN, Wang X, Wu Q, Stahl N, Sampath KT, Varona P, Hurle JM. 1999. Expression and function of Gdf-5 during digit skeletogenesis in the embryonic chick leg bud. Dev Biol 206:33-45.
Mintzer KA, Lee MA, Runke G, Trout J, Whitman M, Mullins MC. 2001. Lost-a-fin encodes a type I BMP receptor, Alk8, acting maternally and zygotically in dorsoventral pattern formation. Development 128:859-869.
Molina F, Bouanani M, Pau B, Granier C. 1996. Characterization of the type-1 repeat from thyroglobulin, a cysteine-rich module found in proteins from different families. Eur J Biochem 240:125-133.
Monteiro R, Pouget C, Patient R. 2011. The gata1/pu.1 lineage fate paradigm varies between blood populations and is modulated by tif1gamma. EMBO J 30:1093-1103.
Morgan BA, Fekete DM. 1996. Manipulating gene expression with replication-competent retroviruses. Methods Cell Biol 51:185-218.
Mozdziak PE, Petitte JN. 2004. Status of transgenic chicken models for developmental biology. Dev Dyn 229:414-421.
Mulholland DJ, Dedhar S, Wu H, Nelson CC. 2006. PTEN and GSK3beta: key regulators of progression to androgen-independent prostate cancer. Oncogene 25:329-337.
Mullins MC, Hammerschmidt M, Kane DA, Odenthal J, Brand M, van Eeden FJ, Furutani-Seiki M, Granato M, Haffter P, Heisenberg CP, Jiang YJ, Kelsh RN, Nusslein-Volhard C. 1996. Genes

establishing dorsoventral pattern formation in the zebrafish embryo: the ventral specifying genes. Development 123:81-93.
Munoz J, Stange DE, Schepers AG, van de Wetering M, Koo BK, Itzkovitz S, Volckmann R, Kung KS, Koster J, Radulescu S, Myant K, Versteeg R, Sansom OJ, van Es JH, Barker N, van Oudenaarden A, Mohammed S, Heck AJ, Clevers H. 2012. The Lgr5 intestinal stem cell signature: robust expression of proposed quiescent '+4' cell markers. EMBO J 31:3079-3091.
Murray SS, Murray EJ, Glackin CA, Urist MR. 1993. Bone morphogenetic protein inhibits differentiation and affects expression of helix-loop-helix regulatory molecules in myoblastic cells. J Cell Biochem 53:51-60.
Myers DC, Sepich DS, Solnica-Krezel L. 2002. Bmp activity gradient regulates convergent extension during zebrafish gastrulation. Dev Biol 243:81-98.
Nabeshima Y, Hanaoka K, Hayasaka M, Esumi E, Li S, Nonaka I, Nabeshima Y. 1993. Myogenin gene disruption results in perinatal lethality because of severe muscle defect. Nature 364:532-535.
Nischt R, Wallich M, Reibetanz M, Baumann P, Krieg T, Mauch C. 2001. BM-40 and MMP-2 expression are not coregulated in human melanoma cell lines. Cancer Lett 162:223-230.
Niswander L. 2003. Pattern formation: old models out on a limb. Nat Rev Genet 4:133-143.
Niswander L, Tickle C, Vogel A, Booth I, Martin GR. 1993. FGF-4 replaces the apical ectodermal ridge and directs outgrowth and patterning of the limb. Cell 75:579-587.
Nohe A, Hassel S, Ehrlich M, Neubauer F, Sebald W, Henis YI, Knaus P. 2002. The mode of bone morphogenetic protein (BMP) receptor oligomerization determines different BMP-2 signaling pathways. J Biol Chem 277:5330-5338.
North TE, Goessling W, Walkley CR, Lengerke C, Kopani KR, Lord AM, Weber GJ, Bowman TV, Jang IH, Grosser T, Fitzgerald GA, Daley GQ, Orkin SH, Zon LI. 2007. Prostaglandin E2 regulates vertebrate haematopoietic stem cell homeostasis. Nature 447:1007-1011.
Novinec M, Kovacic L, Skrlj N, Turk V, Lenarcic B. 2008. Recombinant human SMOCs produced by in vitro refolding: calcium-binding properties and interactions with serum proteins. Protein Expr Purif 62:75-82.
Ober EA, Olofsson B, Makinen T, Jin SW, Shoji W, Koh GY, Alitalo K, Stainier DY. 2004. Vegfc is required for vascular development and endoderm morphogenesis in zebrafish. EMBO Rep 5:78-84.
Ohuchi H, Nakagawa T, Yamamoto A, Araga A, Ohata T, Ishimaru Y, Yoshioka H, Kuwana T, Nohno T, Yamasaki M, Itoh N, Noji S. 1997. The mesenchymal factor, FGF10, initiates and maintains the outgrowth of the chick limb bud through interaction with FGF8, an apical ectodermal factor. Development 124:2235-2244.
Okada I, Hamanoue H, Terada K, Tohma T, Megarbane A, Chouery E, Abou-Ghoch J, Jalkh N, Cogulu O, Ozkinay F, Horie K, Takeda J, Furuichi T, Ikegawa S, Nishiyama K, Miyatake S, Nishimura A, Mizuguchi T, Niikawa N, Hirahara F, Kaname T, Yoshiura K, Tsurusaki Y, Doi H, Miyake N, Furukawa T, Matsumoto N, Saitsu H. 2011. SMOC1 is essential for ocular and limb development in humans and mice. Am J Hum Genet 88:30-41.
Oloumi A, Syam S, Dedhar S. 2006. Modulation of Wnt3a-mediated nuclear beta-catenin accumulation and activation by integrin-linked kinase in mammalian cells. Oncogene 25:7747-7757.
Ono Y, Calhabeu F, Morgan JE, Katagiri T, Amthor H, Zammit PS. 2011. BMP signalling permits population expansion by preventing premature myogenic differentiation in muscle satellite cells. Cell Death Differ 18:222-234.
Oustanina S, Hause G, Braun T. 2004. Pax7 directs postnatal renewal and propagation of myogenic satellite cells but not their specification. EMBO J 23:3430-3439.
Parichy DM, Ransom DG, Paw B, Zon LI, Johnson SL. 2000. An orthologue of the kit-related gene fms is required for development of neural crest-derived xanthophores and a subpopulation of adult melanocytes in the zebrafish, Danio rerio. Development 127:3031-3044.
Patterson LJ, Gering M, Eckfeldt CE, Green AR, Verfaillie CM, Ekker SC, Patient R. 2007. The transcription factors Scl and Lmo2 act together during development of the hemangioblast in zebrafish. Blood 109:2389-2398.
Patterson LJ, Gering M, Patient R. 2005. Scl is required for dorsal aorta as well as blood formation in zebrafish embryos. Blood 105:3502-3511.

Paw BH, Davidson AJ, Zhou Y, Li R, Pratt SJ, Lee C, Trede NS, Brownlie A, Donovan A, Liao EC, Ziai JM, Drejer AH, Guo W, Kim CH, Gwynn B, Peters LL, Chernova MN, Alper SL, Zapata A, Wickramasinghe SN, Lee MJ, Lux SE, Fritz A, Postlethwait JH, Zon LI. 2003. Cell-specific mitotic defect and dyserythropoiesis associated with erythroid band 3 deficiency. Nat Genet 34:59-64.

Payne EM, Bolli N, Rhodes J, Abdel-Wahab OI, Levine R, Hedvat CV, Stone R, Khanna-Gupta A, Sun H, Kanki JP, Gazda HT, Beggs AH, Cotter FE, Look AT. 2011. Ddx18 is essential for cell-cycle progression in zebrafish hematopoietic cells and is mutated in human AML. Blood 118:903-915.

Pazin DE, Albrecht KH. 2009. Developmental expression of Smoc1 and Smoc2 suggests potential roles in fetal gonad and reproductive tract differentiation. Dev Dyn 238:2877-2890.

Perk J, Iavarone A, Benezra R. 2005. Id family of helix-loop-helix proteins in cancer. Nat Rev Cancer 5:603-614.

Peterkin T, Gibson A, Patient R. 2009. Common genetic control of haemangioblast and cardiac development in zebrafish. Development 136:1465-1474.

Pizette S, Abate-Shen C, Niswander L. 2001. BMP controls proximodistal outgrowth, via induction of the apical ectodermal ridge, and dorsoventral patterning in the vertebrate limb. Development 128:4463-4474.

Pizette S, Niswander L. 1999. BMPs negatively regulate structure and function of the limb apical ectodermal ridge. Development 126:883-894.

Pruvot B, Jacquel A, Droin N, Auberger P, Bouscary D, Tamburini J, Muller M, Fontenay M, Chluba J, Solary E. 2011. Leukemic cell xenograft in zebrafish embryo for investigating drug efficacy. Haematologica 96:612-616.

Rainger J, van Beusekom E, Ramsay JK, McKie L, Al-Gazali L, Pallotta R, Saponari A, Branney P, Fisher M, Morrison H, Bicknell L, Gautier P, Perry P, Sokhi K, Sexton D, Bardakjian TM, Schneider AS, Elcioglu N, Ozkinay F, Koenig R, Megarbane A, Semerci CN, Khan A, Zafar S, Hennekam R, Sousa SB, Ramos L, Garavelli L, Furga AS, Wischmeijer A, Jackson IJ, Gillessen-Kaesbach G, Brunner HG, Wieczorek D, van Bokhoven H, Fitzpatrick DR. 2011. Loss of the BMP antagonist, SMOC-1, causes Ophthalmo-acromelic (Waardenburg Anophthalmia) syndrome in humans and mice. PLoS Genet 7:e1002114.

Ramel MC, Hill CS. 2012. Spatial regulation of BMP activity. FEBS Lett 586:1929-1941.

Rao TP, Kuhl M. 2010. An updated overview on Wnt signaling pathways: a prelude for more. Circ Res 106:1798-1806.

Rauch GJ, Hammerschmidt M, Blader P, Schauerte HE, Strahle U, Ingham PW, McMahon AP, Haffter P. 1997. Wnt5 is required for tail formation in the zebrafish embryo. Cold Spring Harb Symp Quant Biol 62:227-234.

Rawls A, Valdez MR, Zhang W, Richardson J, Klein WH, Olson EN. 1998. Overlapping functions of the myogenic bHLH genes MRF4 and MyoD revealed in double mutant mice. Development 125:2349-2358.

Relaix F, Montarras D, Zaffran S, Gayraud-Morel B, Rocancourt D, Tajbakhsh S, Mansouri A, Cumano A, Buckingham M. 2006. Pax3 and Pax7 have distinct and overlapping functions in adult muscle progenitor cells. J Cell Biol 172:91-102.

Relaix F, Rocancourt D, Mansouri A, Buckingham M. 2004. Divergent functions of murine Pax3 and Pax7 in limb muscle development. Genes Dev 18:1088-1105.

Relaix F, Rocancourt D, Mansouri A, Buckingham M. 2005. A Pax3/Pax7-dependent population of skeletal muscle progenitor cells. Nature 435:948-953.

Reshef R, Maroto M, Lassar AB. 1998. Regulation of dorsal somitic cell fates: BMPs and Noggin control the timing and pattern of myogenic regulator expression. Genes Dev 12:290-303.

Rhodes J, Hagen A, Hsu K, Deng M, Liu TX, Look AT, Kanki JP. 2005. Interplay of pu.1 and gata1 determines myelo-erythroid progenitor cell fate in zebrafish. Dev Cell 8:97-108.

Riddle RD, Johnson RL, Laufer E, Tabin C. 1993. Sonic hedgehog mediates the polarizing activity of the ZPA. Cell 75:1401-1416.

Ridges S, Heaton WL, Joshi D, Choi H, Eiring A, Batchelor L, Choudhry P, Manos EJ, Sofla H, Sanati A, Welborn S, Agarwal A, Spangrude GJ, Miles RR, Cox JE, Frazer JK, Deininger M, Balan K, Sigman M, Muschen M, Perova T, Johnson R, Montpellier B, Guidos CJ, Jones DA, Trede NS. 2012. Zebrafish screen identifies novel compound with selective toxicity against leukemia. Blood 119:5621-5631.

Robu ME, Larson JD, Nasevicius A, Beiraghi S, Brenner C, Farber SA, Ekker SC. 2007. p53 activation by knockdown technologies. PLoS Genet 3:e78.

Rocnik EF, Liu P, Sato K, Walsh K, Vaziri C. 2006. The novel SPARC family member SMOC-2 potentiates angiogenic growth factor activity. J Biol Chem 281:22855-22864.
Rohde LA, Heisenberg CP. 2007. Zebrafish gastrulation: cell movements, signals, and mechanisms. Int Rev Cytol 261:159-192.
Rosier RN, O'Keefe RJ. 1998. Autocrine regulation of articular cartilage. Instr Course Lect 47:469-475.
Rosier RN, O'Keefe RJ, Hicks DG. 1998. The potential role of transforming growth factor beta in fracture healing. Clin Orthop Relat Res:S294-300.
Roxburgh SA, Murphy M, Pollock CA, Brazil DP. 2006. Recapitulation of embryological programmes in renal fibrosis--the importance of epithelial cell plasticity and developmental genes. Nephron Physiol 103:p139-148.
Rudnicki MA, Braun T, Hinuma S, Jaenisch R. 1992. Inactivation of MyoD in mice leads to up-regulation of the myogenic HLH gene Myf-5 and results in apparently normal muscle development. Cell 71:383-390.
Rudnicki MA, Schnegelsberg PN, Stead RH, Braun T, Arnold HH, Jaenisch R. 1993. MyoD or Myf-5 is required for the formation of skeletal muscle. Cell 75:1351-1359.
Sabourin LA, Rudnicki MA. 2000. The molecular regulation of myogenesis. Clin Genet 57:16-25.
Sala A, Capaldi S, Campagnoli M, Faggion B, Labo S, Perduca M, Romano A, Carrizo ME, Valli M, Visai L, Minchiotti L, Galliano M, Monaco HL. 2005. Structure and properties of the C-terminal domain of insulin-like growth factor-binding protein-1 isolated from human amniotic fluid. J Biol Chem 280:29812-29819.
Salsi V, Vigano MA, Cocchiarella F, Mantovani R, Zappavigna V. 2008. Hoxd13 binds in vivo and regulates the expression of genes acting in key pathways for early limb and skeletal patterning. Dev Biol 317:497-507.
Saunders JW, Jr. 1998. The proximo-distal sequence of origin of the parts of the chick wing and the role of the ectoderm. 1948. J Exp Zool 282:628-668.
Schier AF, Talbot WS. 2005. Molecular genetics of axis formation in zebrafish. Annu Rev Genet 39:561-613.
Schmid B, Furthauer M, Connors SA, Trout J, Thisse B, Thisse C, Mullins MC. 2000. Equivalent genetic roles for bmp7/snailhouse and bmp2b/swirl in dorsoventral pattern formation. Development 127:957-967.
Schubert FR, Tremblay P, Mansouri A, Faisst AM, Kammandel B, Lumsden A, Gruss P, Dietrich S. 2001. Early mesodermal phenotypes in splotch suggest a role for Pax3 in the formation of epithelial somites. Dev Dyn 222:506-521.
Schulte-Merker S, Lee KJ, McMahon AP, Hammerschmidt M. 1997. The zebrafish organizer requires chordino. Nature 387:862-863.
Schulte-Merker S, van Eeden FJ, Halpern ME, Kimmel CB, Nusslein-Volhard C. 1994. no tail (ntl) is the zebrafish homologue of the mouse T (Brachyury) gene. Development 120:1009-1015.
Seale P, Sabourin LA, Girgis-Gabardo A, Mansouri A, Gruss P, Rudnicki MA. 2000. Pax7 is required for the specification of myogenic satellite cells. Cell 102:777-786.
Seebald JL, Szeto DP. 2011. Zebrafish eve1 regulates the lateral and ventral fates of mesodermal progenitor cells at the onset of gastrulation. Dev Biol 349:78-89.
Seyer JM, Vinson WC. 1974. Synthesis of type I and type II collagen by embryonic chick cartilage. Biochem Biophys Res Commun 58:272-279.
Shafizadeh E, Paw BH, Foott H, Liao EC, Barut BA, Cope JJ, Zon LI, Lin S. 2002. Characterization of zebrafish merlot/chablis as non-mammalian vertebrate models for severe congenital anemia due to protein 4.1 deficiency. Development 129:4359-4370.
Shaw GC, Cope JJ, Li L, Corson K, Hersey C, Ackermann GE, Gwynn B, Lambert AJ, Wingert RA, Traver D, Trede NS, Barut BA, Zhou Y, Minet E, Donovan A, Brownlie A, Balzan R, Weiss MJ, Peters LL, Kaplan J, Zon LI, Paw BH. 2006. Mitoferrin is essential for erythroid iron assimilation. Nature 440:96-100.
Simmons DJ, Gilliam J. 1981. Articular cartilage repair in the avian quail-chick chimera model. Clin Orthop Relat Res:315-325.
Slack J. 2013. Essential Developmental Biology Third edition. Wiley-Blackwell.
Smith WC, Knecht AK, Wu M, Harland RM. 1993. Secreted noggin protein mimics the Spemann organizer in dorsalizing Xenopus mesoderm. Nature 361:547-549.
Solnica-Krezel L, Sepich DS. 2012. Gastrulation: making and shaping germ layers. Annu Rev Cell Dev Biol 28:687-717.

Stern CD. 2004. The chick embryo--past, present and future as a model system in developmental biology. Mech Dev 121:1011-1013.
Stern CD. 2005. The chick; a great model system becomes even greater. Dev Cell 8:9-17.
Sugimura R, Li L. 2010. Noncanonical Wnt signaling in vertebrate development, stem cells, and diseases. Birth Defects Res C Embryo Today 90:243-256.
Sumanas S, Gomez G, Zhao Y, Park C, Choi K, Lin S. 2008. Interplay among Etsrp/ER71, Scl, and Alk8 signaling controls endothelial and myeloid cell formation. Blood 111:4500-4510.
Tajbakhsh S, Buckingham M. 2000. The birth of muscle progenitor cells in the mouse: spatiotemporal considerations. Curr Top Dev Biol 48:225-268.
Thisse B, Pflumio, S., Fürthauer, M., Loppin, B., Heyer, V., Degrave, A., Woehl, R., Lux, A., Steffan, T., Charbonnier, X.Q., Thisse, C. . 2001. Expression of the zebrafish genome during embryogenesis (NIH R01 RR15402). ZFIN Direct Data Submission (http://zfin.org).
Thisse C, Thisse B. 2008. High-resolution in situ hybridization to whole-mount zebrafish embryos. Nat Protoc 3:59-69.
Thomas JT, Canelos P, Luyten FP, Moos M, Jr. 2009. Xenopus SMOC-1 Inhibits bone morphogenetic protein signaling downstream of receptor binding and is essential for postgastrulation development in Xenopus. J Biol Chem 284:18994-19005.
Thompson MA, Ransom DG, Pratt SJ, MacLennan H, Kieran MW, Detrich HW, 3rd, Vail B, Huber TL, Paw B, Brownlie AJ, Oates AC, Fritz A, Gates MA, Amores A, Bahary N, Talbot WS, Her H, Beier DR, Postlethwait JH, Zon LI. 1998. The cloche and spadetail genes differentially affect hematopoiesis and vasculogenesis. Dev Biol 197:248-269.
Tickle C. 2003. Patterning systems--from one end of the limb to the other. Dev Cell 4:449-458.
Tickle C. 2004. The contribution of chicken embryology to the understanding of vertebrate limb development. Mech Dev 121:1019-1029.
Tremble PM, Lane TF, Sage EH, Werb Z. 1993. SPARC, a secreted protein associated with morphogenesis and tissue remodeling, induces expression of metalloproteinases in fibroblasts through a novel extracellular matrix-dependent pathway. J Cell Biol 121:1433-1444.
Tylzanowski P, Mebis L, Luyten FP. 2006. The Noggin null mouse phenotype is strain dependent and haploinsufficiency leads to skeletal defects. Dev Dyn 235:1599-1607.
Uechi T, Nakajima Y, Chakraborty A, Torihara H, Higa S, Kenmochi N. 2008. Deficiency of ribosomal protein S19 during early embryogenesis leads to reduction of erythrocytes in a zebrafish model of Diamond-Blackfan anemia. Hum Mol Genet 17:3204-3211.
van Rooijen E, Voest EE, Logister I, Korving J, Schwerte T, Schulte-Merker S, Giles RH, van Eeden FJ. 2009. Zebrafish mutants in the von Hippel-Lindau tumor suppressor display a hypoxic response and recapitulate key aspects of Chuvash polycythemia. Blood 113:6449-6460.
Vannahme C, Gosling S, Paulsson M, Maurer P, Hartmann U. 2003. Characterization of SMOC-2, a modular extracellular calcium-binding protein. Biochem J 373:805-814.
Vannahme C, Smyth N, Miosge N, Gosling S, Frie C, Paulsson M, Maurer P, Hartmann U. 2002. Characterization of SMOC-1, a novel modular calcium-binding protein in basement membranes. J Biol Chem 277:37977-37986.
Vuilleumier R, Affolter M, Pyrowolakis G. 2011. Pentagone: patrolling BMP morphogen signaling. Fly (Austin) 5:210-214.
Vuilleumier R, Springhorn A, Patterson L, Koidl S, Hammerschmidt M, Affolter M, Pyrowolakis G. 2010. Control of Dpp morphogen signalling by a secreted feedback regulator. Nat Cell Biol 12:611-617.
Wakefield LM, Roberts AB. 2002. TGF-beta signaling: positive and negative effects on tumorigenesis. Curr Opin Genet Dev 12:22-29.
Wang H, Long Q, Marty SD, Sassa S, Lin S. 1998. A zebrafish model for hepatoerythropoietic porphyria. Nat Genet 20:239-243.
Wang H, Noulet F, Edom-Vovard F, Tozer S, Le Grand F, Duprez D. 2010. Bmp signaling at the tips of skeletal muscles regulates the number of fetal muscle progenitors and satellite cells during development. Dev Cell 18:643-654.
Wang M, Marin A. 2006. Characterization and prediction of alternative splice sites. Gene 366:219-227.
Weinberg ES, Allende ML, Kelly CS, Abdelhamid A, Murakami T, Andermann P, Doerre OG, Grunwald DJ, Riggleman B. 1996. Developmental regulation of zebrafish MyoD in wild-type, no tail and spadetail embryos. Development 122:271-280.

Westfall TA, Brimeyer R, Twedt J, Gladon J, Olberding A, Furutani-Seiki M, Slusarski DC. 2003. Wnt-5/pipetail functions in vertebrate axis formation as a negative regulator of Wnt/beta-catenin activity. J Cell Biol 162:889-898.
Williamson RA, Henry MD, Daniels KJ, Hrstka RF, Lee JC, Sunada Y, Ibraghimov-Beskrovnaya O, Campbell KP. 1997. Dystroglycan is essential for early embryonic development: disruption of Reichert's membrane in Dag1-null mice. Hum Mol Genet 6:831-841.
Wingert RA, Galloway JL, Barut B, Foott H, Fraenkel P, Axe JL, Weber GJ, Dooley K, Davidson AJ, Schmid B, Paw BH, Shaw GC, Kingsley P, Palis J, Schubert H, Chen O, Kaplan J, Zon LI, Tubingen Screen C. 2005. Deficiency of glutaredoxin 5 reveals Fe-S clusters are required for vertebrate haem synthesis. Nature 436:1035-1039.
Wu SY, Shin J, Sepich DS, Solnica-Krezel L. 2012. Chemokine GPCR signaling inhibits beta-catenin during zebrafish axis formation. PLoS Biol 10:e1001403.
Xu J, Du L, Wen Z. 2012. Myelopoiesis during zebrafish early development. J Genet Genomics 39:435-442.
Xu J, Orkin SH. 2011. The erythroid/myeloid lineage fate paradigm takes a new player. EMBO J 30:983-985.
Yamabi H, Lu H, Dai X, Lu Y, Hannigan G, Coles JG. 2006. Overexpression of integrin-linked kinase induces cardiac stem cell expansion. J Thorac Cardiovasc Surg 132:1272-1279.
Yamamoto A, Amacher SL, Kim SH, Geissert D, Kimmel CB, De Robertis EM. 1998. Zebrafish paraxial protocadherin is a downstream target of spadetail involved in morphogenesis of gastrula mesoderm. Development 125:3389-3397.
Yeh JR, Munson KM, Chao YL, Peterson QP, Macrae CA, Peterson RT. 2008. AML1-ETO reprograms hematopoietic cell fate by downregulating scl expression. Development 135:401-410.
Yeh JR, Munson KM, Elagib KE, Goldfarb AN, Sweetser DA, Peterson RT. 2009. Discovering chemical modifiers of oncogene-regulated hematopoietic differentiation. Nat Chem Biol 5:236-243.
Yusuf F, Brand-Saberi B. 2006. The eventful somite: patterning, fate determination and cell division in the somite. Anat Embryol (Berl) 211 Suppl 1:21-30.
Zimmerman LB, De Jesus-Escobar JM, Harland RM. 1996. The Spemann organizer signal noggin binds and inactivates bone morphogenetic protein 4. Cell 86:599-606.

Curriculum Vitae

Personalia

Name: Hendrik Mommaerts
Address: Notelarenweg 119/2
3020 Herent
Mobile phone: 0498/464968
E-mail: hendrik_mommaerts@hotmail.com
Date of Birth: December 15 1986
Place of Birth: Mechelen (Belgium)
Nationality: Belgian

Education

Oct 2009 - present PhD in Biomedical Sciences IWT scholarship
Skeletal Biology and Engineering Research Center, KU Leuven

Sep 2007 - Jun 2009 Master Biomedical Sciences (KU Leuven) Cum Laude
Laboratory of Skeletal Development and Joint Disorders, KULeuven

Sep 2004 - Jun 2007 Bachelor Biomedical Sciences (KU Leuven) Cum Fructu

Sep 1998 - Jun 2004 Latin-Science (H. Drievuldigheidscollege (Leuven))

Additional education & certificates

–	First Aid	KU Leuven	2004
–	Medical Technical skills (initiation)	KU Leuven	2007
–	Laboratory Animal Science (Module I)	KU Leuven	2007
–	Certificate for handling ionizing radiation	KU Leuven	2009
–	Managing my PhD	KU Leuven	2011
–	Ethics in Science	KU Leuven	2012
–	Laboratory Animal Science (Module II)	KU Leuven	2012
–	Member of British Society of Developmental Biology since 2012		

Extracurricular certificates

–	Supervisor in youthwork	Top Vakantie	2004
–	Physical Trainer ('Initiator' - Badminton)	Bloso	2008

Languages

- Dutch: native language
- English:fluent – daily active use
- French:good
- German: notions

Conference proceedings

Oct 2009: Ernst Klenk Symposium in Molecular Medicine (Koln):
Passive participation

Apr 2010: BSDB student meeting (Warwick):
Poster presentation: Muscle development in *Noggin* null mice

Apr 2011: BSDB student meeting (Kent):
Poster presentation: Muscle development in *Noggin* null mice

Jul 2011: European Zebrafish Meeting (Edinburgh):
Poster presentation: Smoc2 modulates Wnt5b/PCP mediated gastrulation and axial patterning

Apr 2012: BSDB student meeting (Warwick):
Poster presentation: Smoc2 modulates Wnt5b-mediated gastrulation in zebrafish

Jul 2013: European Zebrafish Meeting (Barcelona):
Poster presentation: Functional analysis of *smoc2*, a modulator of gastrulation and hematopoiesis

Oct 2013: IUAP meeting (Liege):
Oral presentation: The role of NOGGIN during embryonic myogenesis
Poster presentation: Muscle development in *Noggin* null mice
Poster presentation: *smoc2* is involved in hematopoietic differentiation in zebrafish

May 2014: State of the Art in Exercise Physiology (Leuven):
Oral presentation: The role of BMP signaling during myogenesis

Jun 2014: IUAP meeting (Jette):
Oral presentation: The role of *smoc2* during zebrafish myelopoiesis
Poster presentation: *smoc2* is involved in hematopoietic differentiation in zebrafish

Articles in international journals

Mommaerts H, Esguerra CV, Hartmann U, Luyten FP, Tylzanowski P. 2014 *Smoc2 modulates embryonic myelopoiesis during zebrafish development.* Dev Dyn

Mommaerts, H, Costamagna D, Sampaolesi M, Tylzanowski P. *The role of NOGGIN during embryonic myogenesis.* (in preparation)